Terms and Conditions of Use of Digitised Theses from Trinity College Library Dublin

Copyright statement

All material supplied by Trinity College Library is protected by copyright (under the Copyright and Related Rights Act, 2000 as amended) and other relevant Intellectual Property Rights. By accessing and using a Digitised Thesis from Trinity College Library you acknowledge that all Intellectual Property Rights in any Works supplied are the sole and exclusive property of the copyright and/or other IPR holder. Specific copyright holders may not be explicitly identified. Use of materials from other sources within a thesis should not be construed as a claim over them.

A non-exclusive, non-transferable licence is hereby granted to those using or reproducing, in whole or in part, the material for valid purposes, providing the copyright owners are acknowledged using the normal conventions. Where specific permission to use material is required, this is identified and such permission must be sought from the copyright holder or agency cited.

Liability statement

By using a Digitised Thesis, I accept that Trinity College Dublin bears no legal responsibility for the accuracy, legality or comprehensiveness of materials contained within the thesis, and that Trinity College Dublin accepts no liability for indirect, consequential, or incidental, damages or losses arising from use of the thesis for whatever reason. Information located in a thesis may be subject to specific use constraints, details of which may not be explicitly described. It is the responsibility of potential and actual users to be aware of such constraints and to abide by them. By making use of material from a digitised thesis, you accept these copyright and disclaimer provisions. Where it is brought to the attention of Trinity College Library that there may be a breach of copyright or other restraint, it is the policy to withdraw or take down access to a thesis while the issue is being resolved.

Access Agreement

By using a Digitised Thesis from Trinity College Library you are bound by the following Terms & Conditions. Please read them carefully.

I have read and I understand the following statement: All material supplied via a Digitised Thesis from Trinity College Library is protected by copyright and other intellectual property rights, and duplication or sale of all or part of any of a thesis is not permitted, except that material may be duplicated by you for your research use or for educational purposes in electronic or print form providing the copyright owners are acknowledged using the normal conventions. You must obtain permission for any other use. Electronic or print copies may not be offered, whether for sale or otherwise to anyone. This copy has been supplied on the understanding that it is copyright material and that no quotation from the thesis may be published without proper acknowledgement.

Selective Gene Fishing in Complex Genomic Environments Using Micro-Cantilevers: Applications in RNAi Therapy

Rohit Mishra, M.Sc.

A thesis submitted to the University of Dublin in partial fulfilment of the requirements for the degree of

Doctor of Philosophy

Centre for Research on Adaptive Nanostructures and Nanodevices
School of Physics

Trinity College, Dublin

Supervisor
Prof. Martin Hegner

August 2012

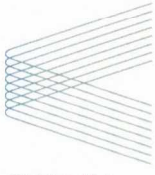

Declaration

This thesis is submitted by the undersigned for the degree of Doctor of Philosophy at the University of Dublin, Trinity College and had not been submitted to any other university as an exercise for a degree. I declare that this thesis is entirely my own work and I give my permission to the library to lend or copy this thesis upon request.

_____

Acknowledgement

I would like to take this opportunity to thank my supervisor Prof. Martin Hegner for his guidance, support and enthusiasm throughout the period of this thesis. Many thanks to Wilfried Grange for his support and genius with LabView programming; Jason Jensen for his kind help with reprogramming the instrument interface, the superfast proof reading and his enthusiastic support especially during writing of this thesis; Peter Noy for his recommendations and sharing problems & solutions regards the device; Niall Kinahan for his help with the setting up of the Temescal recipes and more importantly being a good friend; Ronan Daly for his help with the SEM; James Keaney, Matthew Campbell and Prof. Peter Humphries from the Ocular genetics unit for providing the RNAi samples; Mme. Gyöngyi for her kind support and assistance whenever needed; Eoin McCarthy and Giovanni Fois for their help with the Asylum AFM; the NanoBio group members Dorothea, Dunja, Florian, Michael, Niall, Ravi, Sinead, Vivek and Helene for being the best lab mates one could wish for; David from the physics workshop for his kind assistance; Thomas Braun for providing the processing software; Jean Pierre Ramseyer and Andreas Tonin for their advice with the device; Science Foundation Ireland and Hoffman La Roche Ltd. for their financial support.

A very special thanks to Elisa and Natali for being my best friends and making my stay in Dublin exciting; Lisa for her unconditional support; special thanks to my friends from "The dining hall chronicles" Sandeep, Mauro, Sankar, Aaron, Awadesh, Andrea, Kapi for the "craic"; thanks to the Italian connection Dania, Daniela and the McGovern for their support. Thanks a lot to my family for believing in me and being there despite the distance!

Thanks to all the members of the postgraduate room 3.20 for making it easy on a tough day. Go raibh milé maith agaibh!

Summary

Genes and their role in disease origins and proliferation have been of great interest for molecular medicine. Their functions and roles have been recently shown to be moderated by RNA interference (RNAi), a natural phenomenon occurring in living cells where short sequences of oligonucleotides (on an average ~22 base pairs) are known to control gene expression via gene silencing. The application of this technology enables us not only to understand the relationship between gene expression and diseases but also helps elucidate the governing processes of cells day to day function. Bioassays for the detection of these oligonucleotide sequences are crucial in the path for drug discovery leading to effective use of RNAi for therapeutic purposes. The current work aims at the application of a new class of nanomechanical biosensors for the detection of these oligonucleotide sequences. Microcantilever based sensors can detect such sequences based on the stress induced in a bio-functionalized microcantilever beam, causing bending when a target sequence hybridizes to a surface immobilized complementary probe sequence. They demonstrate major advantages over the conventional sensors due to their high sensitivity, low cost, low analyte requirement and fast response.

Instrumentation for microcantilever sensor device

This section describes the design, testing and implementation of the microcantilever sensor instrument for detection of oligonucleotide sequences. A new instrument using a microtranslation stage based laser scanning was developed for detecting the cantilever stress formation on a sensor array with eight microcantilevers (each 500 μm x 100 μm x 0.5 μm) spaced at a pitch of 250 μm. The laser stability, temperature control, fluidics and scanning preferences were optimized. The implementation of this new device offers finer control and higher stability of signals when compared to previous devices with a better signal-to-noise ration of ~1.5 nm with a faster and more reliable focusing ability.

Calibration of Laser deflection setup

A novel method for the calibration of the laser deflection optical setup used for detecting cantilever deflection was developed. Utilizing commercially available Atomic Force Microscope cantilevers and the equipartition theorem, a simple method for

relating the deflection of the cantilever to the final measured movement of the spot on the position sensitive detector was achieved.

Detection specificity and sensitivity of oligonucleotides

After a rigorous process optimization for sensor preparation and functionalization, we have investigated the detection specificity and the lower limits of detection for oligonucleotides using microcantilevers. The microcantilevers were able to clearly distinguish between two oligonucleotide species with the same length and sequence except for two base pairs in the centre thus establishing their specificity. Also, a new lower limit of detection of 1 femtomolar of a 12 base pair oligonucleotide in non-competitive environment was achieved.

Oligonucleotide detection in total cellular RNA extracts

The detection capability of microcantilever sensors for specific oligonucleotides in the presence of other similar competing molecules was studied. In order to apply the sensors in understanding the processes in RNAi, it is crucial to charter the sensor response with variation in target availability and presence of other competing molecules (from the total cellular RNA). We have observed that the sensor response is highly dependent on not only the target availability but also decreases with increasing background competition at a given target concentration. It is possible that the sensors can be used for qualitative detection of oligonucleotides in as high as 5 μM total RNA for a 10 pM target concentration (predicted sensor response of ~13 nm).

Insights into siRNA strand lifetimes in RNAi studies

In collaboration with the Ocular Genetics Unit (TCD), we applied the microcantilever sensors to the detection of individual strands of a short interfering RNA (siRNA, 21 base pairs) in total RNA extracts from mouse brain endothelial cells exposed for different time periods for the silencing of a tight junction protein (Claudin-5). The results show that the individual strands of the siRNA follow disparate life times within the cells thus indicating that different cellular mechanisms govern the fate of individual strands. This offers a first insight and paves way for a better understanding of siRNA pharmacokinetics in cells targeted for RNAi.

INDEX

RISC	.....	RNA induced silencing complex
RNA	.....	Ribonucleic acid
RNAi	.....	RNA interference
RT-PCR	.....	Reverse transcriptase polymerase chain reaction
SAM	.....	Self-assembled monolayer
SDS	.....	Sodium dodecyl sulphate
SEM	.....	Scanning electron microscope
siRNA	.....	short interfering RNA
SNP	.....	single nucleotide polymorphism
SSC	.....	Saline-sodium citrate buffer
ssDNA	.....	single stranded DNA
TBS	.....	Tris-buffered saline
TCD	.....	Trinity College, Dublin
TEAA	.....	Triethylammonium acetate buffer
TEMED	.....	Tetramethylethylenediamine
TJ	.....	Tight junction
UHRR	.....	Universal Human Reference RNA
UV	.....	Ultraviolet
VIS	.....	Visible range of frequencies
XPS	.....	X-ray photoelectron spectroscopy

Chapter I

Introduction

A gene is the basic unit of function and heredity in a living organism. It consists of a code in the form of DNA (deoxyribonucleic acid) which is made up of four base pairs Adenine, Thymine, Guanine and Cytosine that form the signature double helix structure[1]. The fundamental processes that control the functioning of the cell are transcription and translation of these genes, collectively known as gene expression (Fig.1.1). The "transcription" of DNA involves the creation of an equivalent copy of the genetic sequence while keeping the original intact. This copy known as messenger Ribonucleic acid (m-RNA) is then "translated" into proteins in a complex pathway that occurs in the cellular cytoplasm (in eukaryotic cells). The process of gene expression is used by all organisms to generate the macromolecular machinery for life which gives the cell control over structure and function, and is the basis for cellular differentiation, morphogenesis and the versatility and adaptability of any organism. Any changes made to this pathway because of change in the original DNA sequence (genetic mutation), disruption of the components that operate these processes (proteins etc) or foreign interference (bacterial or viral infections) leads to malfunctioning of the cell and the organs which then manifests as what one commonly calls being sick.

In its perennial search for the causes of disease, medicine has now advanced to the molecular level. Genetics, the study of the heredity and variation in living organisms, has helped the understanding of how genes pass on traits from one generation to the next including inherited diseases. Genomics, the study of the entire set of genes in a particular organism, has helped deeply in the understanding of cellular processes. The study of these areas together with nanotechnology provides the tools for more precisely targeted treatments.

The recently discovered phenomenon of gene silencing better known as RNA (ribonucleic acid) interference or simply RNAi has revealed the pathway for selective silencing of gene expression which is a natural process used by the cell to keep gene expression under control[2]. This has attracted a lot of interest since the pathway can be utilised to rapidly develop a highly promising approach for specifically down/up regulating genes to alleviate disease pathology[3] originating from genetic mutations or pathogens. This therapy, broadly known as RNAi therapy is rapidly gaining importance since it has the potential to unlock a new method of personalised treatments for individuals targeting the very root of the ailment[4,5]. A simple example would be the treatment of Huntington's disease (HD)[6]. HD is a neurodegenerative genetic disorder caused by change in the original DNA sequence (genetic mutation) for the coding of a specific protein leading to production of a mutant protein. This mutant protein directly affects muscle coordination and leads to cognitive decline in the patient. Using RNAi therapy, medical practitioners would be able to selectively shutdown the mutant Huntington's gene from producing the protein which causes the disease.

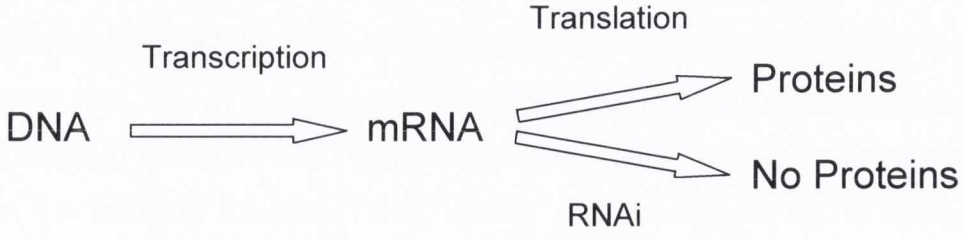

Fig.1.1: Central Dogma of molecular biology: Genetic expression and information flow from DNA to proteins. RNAi introduces post-transcription gene expression control.

Since the process of RNAi take place at a cellular level, great care and precision will be required in bringing the technology from the laboratory trials to real patients. The process of finding a suitable treatment involves many steps through which the medication has to go, one of them being drug testing and assays to determine the efficiency of delivery and effectiveness on target[7]. This is where nanomechanical sensors can play a crucial role as tools for quick, efficient and reliable sources of bio-assays for the rapid screening of the genetic material to identify the most effective agents for the RNAi therapy[8].

1.1 RNAi Therapy

1.1.1 Mechanism of RNA interference

The phenomenon of RNAi was first observed in plants and described as Post Transcriptional Gene Silencing (PTGS)[9]. The discovery in animals and the breakthrough in its understanding came from studies with the worm *Caenorhabditis elegans* in 1998 by Andrew Fire and Craig Mello who were awarded the Nobel Prize for their discovery in 2006. RNAi is a natural process that occurs in the majority of organisms ranging from fungi and plants to mammals[10]. The mechanism is guided by the RNA induced silencing complex (RISC; multi-domain protein complex) and involves short double stranded RNA molecules that, when activated by the RISC, trigger the cleavage and degradation of mRNA, hence silencing the gene and preventing the production of the encoded protein[11,12] (Fig.1.2). The two types of short double stranded RNA central to RNAi are miRNA[13] (micro RNA) and siRNA[14] (short interfering RNA). The miRNA is inherent to eukaryotic cells and is formed from its hairpin precursor pre-microRNA by cleavage performed by Dicer molecules that give it its final short double-stranded format. The siRNA is the final fully developed agent for RNAi before it binds to the RISC complex and performs the mRNA cleavage. siRNA can also be artificially introduced into a cell for specific targeting of mRNA for gene knockdown, making them an excellent tool for understanding gene function and for drug development and validation[15].

1.1.2 Applications of RNAi

RNAi opens up an area for extensive control on gene expression and also understanding the very basis of genetic control on the overall organism. This know- how can be utilised in various areas[16] including the determination of gene function, pathway analysis, identification and validation of drug targets, understanding gene redundancy and the functional screening of genes.

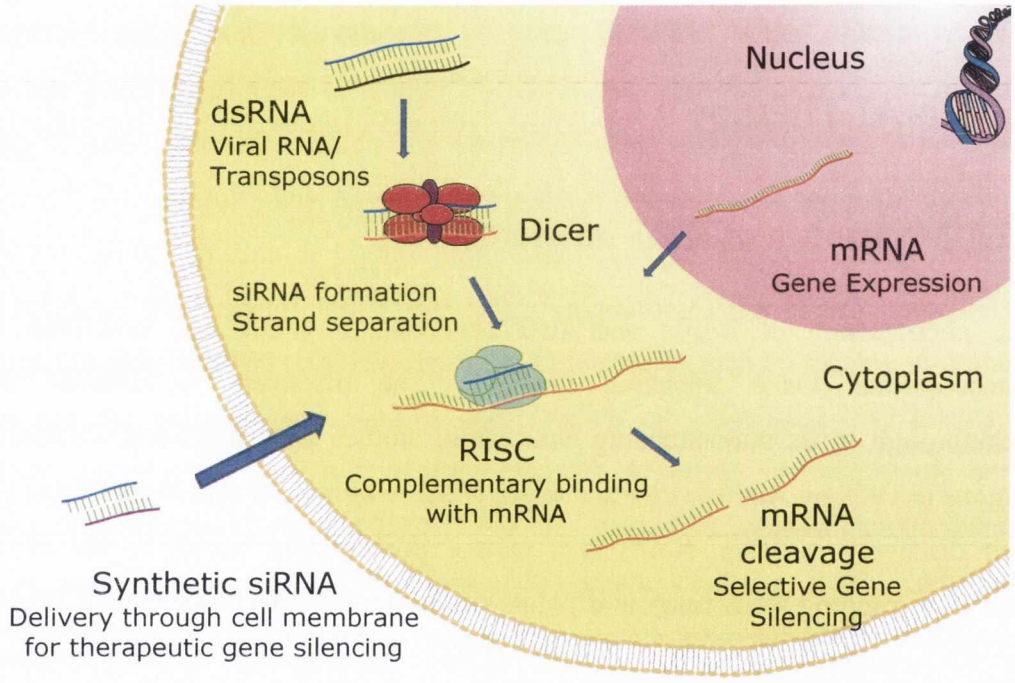

Fig.1.2: The mechanism behind gene silencing. The introduction of synthetic siRNA offers potential control over gene expression hence making it a possible application in drug screening and understanding gene expression and its effect on the organism.(dsRNA- double stranded RNA, siRNA- short interfering RNA, RISC- RNA induced silencing complex, mRNA-messenger RNA, Dicer- RNA endonuclease). The Antisense strand incorporated into the RISC complex is responsible for the cleavage of the mRNA.

The potential applications of this new discovery are vast and already various targets have been assessed viz. in drug discovery[17], macular degeneration[18], viral infections[4], hereditary disorders[19] and cancer[20]. However, the pathway to these involves tedious studies, protocols and reliable bioassays before application in vivo. The emphasis lies on applying detection strategies and techniques that provide the most speedy and reliable output.

1.2 Bioassays and detection of genetic markers

1.2.1 Why are Bioassays critical?

The typical pathway to drug discovery (Fig.1.3) involves the potential screening of hundreds of various possibilities in order to get the desired effect while having minimal disruption in the normal organism cycle[21]. This requires fast and highly reliable parallel screening and analysis of the drug candidates and their pharmacokinetics in the specified disease model. Bioassays play a crucial role here since they provide an assessment of the effectiveness of the delivery of the medicine, the following effect and the pharmacokinetics of the drug/agent.

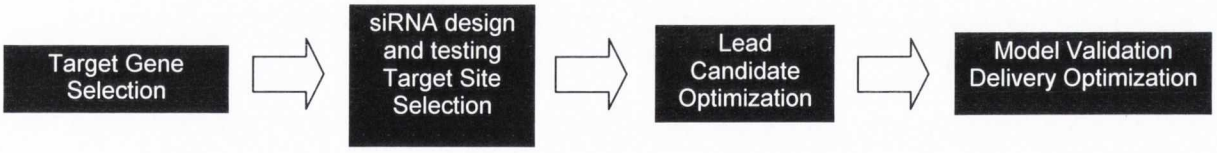

Fig. 1.3: The pathway to drug discovery. Bioassays play an important role in all the steps viz. (a) selection of the gene to be knocked down (b) designing the right siRNA sequence and its testing (c) optimize the final candidate for its effectiveness and (d) design possible methods for drug delivery.

In RNAi therapy, for understanding the biological effects of knocking down a gene, cell based assays[22], enzymatic assays[23], array analysis[24] and many tools are available. To

understand the effects and life spans of the siRNA, it is important that the bioassay is designed to work in complex genomic environments where competition from other molecules from the cellular environment is a serious challenge.

1.2.2 Methods of detection

Various methods are available presently for the screening and analysis of genetic material in both quantitative and qualitative aspects. Microarray technology and PCR (polymerase chain reaction)[25] based methods are in the forefront. Other techniques using different principles of detection such as the use of surface plasmon resonance[26] and quartz crystal microbalance[27] incorporated in various forms from normal multi-well assays to lab-on chip devices[28] have also been used. Several commercial devices and kits using microarray technology are available for the validation of genomic materials for example the Gene expression arrays from Applied Biosystems[29] and TRAC (transcription analysis with affinity capture) from Plexpress[30] and many more. The accurate detection of differences down to single nucleotide polymorphisms (SNPs) is essential and can be achieved by such methods.

On the forefront of such technologies are the DNA ELISA or the branched DNA signal amplification assay[31] and the Real Time Quantitative Polymerase Chain Reaction (qPCR)[32]. As the name suggests, qPCR is a quantitative technique that is based on amplification of the target molecule. The technology utilises sequence specific short DNA probes that are labelled with a reporter fluorophore such that they are only detected optically after the hybridization has successfully occurred. The fluorescence is plotted against the number of cycles of the PCR to relate the final amount of amplified DNA to the former number at the beginning of the PCR. This method can theoretically detect a single molecule after a large number of cycles to suitably amplify the signal. However practically there are various limitations due to the unspecific binding of the labelled oligonucleotides causing a false signal due to amplification of the wrong sequences. The DNA ELISA technology however uses amplification of the signal rather than the target amplification as in qPCR. The capture probe on a surface is hybridized

with an extender molecule that has one end free for capturing the target molecules. After an assay has been performed with a sample, the label extender is introduced that has one end hybridized to the target molecule and the other to a pre-amplifier. The binding of the final amplification molecules to the pre-amplifier provides the increase in signal for indirect detection of the target molecules. This assay is advantageous since it can be performed in cell lysates and does not require target amplification or reverse transcription.

Although a dynamic measurement over time is possible with highly complex microarrays for many techniques with high accuracy and throughput, the sensitivity of the measurements and sample preparation are serious limitations. This is where nanomechanical biosensors are suitable for application since they are[8,33]:

a. a label free technique with very low analyte requirement
b. less intensive on sample preparation
c. compact, have a fast response and are highly sensitive
d. simultaneous measurement of eight parameters (for the current sensor chip)

These sensors, measuring forces on a piconewton scale use small cantilever-form springs with a width and length in the hundreds of micrometer range but a thickness of 300 nm up to few micrometers[34]. They have already shown promising potential in various fields ranging from thermal sensing[35], pH sensing[36], gas sensing[37] and a host of other applications especially in the biotechnology sector[38]. The scope of this work will add and extend the application of these nanomechanical sensors into the field of RNAi and siRNA sensing in complex backgrounds for direct application in RNAi and other gene based therapies.

1.3 Nanomechanical sensors

In just a little over a decade, thanks to the rapid progress made in the field of micro-fabrication and availability of advanced characterization techniques, Micro

electromechanical devices (MEMS) have made unprecedented growth from the research lab to a real world application. Cantilever sensors have emerged as a new class of nanosensors utilising primarily their change in mechanical properties, for example bending under surface stress. Since their first application to observe a chemical reaction using a heat signature[35], they have been applied in many other domains such as force, heat, surface stress, magnetism, charge, radiation or chemical reactions which can be readily transduced into a mechanical motion of the cantilever by an appropriate coating[39-42]. Hence in a sensor apparatus, the cantilevers form the transduction part providing the signal as a mechanical signature[43].

Most cantilever arrays used for such purposes are fabricated from silicon since the fabrication technology is already in place and it provides silicon cantilevers with excellent reproducible mechanical properties across one chip array even in the nano dimensions which are crucial for reproducible results. Shown in Fig.1.4 is a typical cantilever array used in our group for experiments. They are microfabricated by the Micro and Nanomechanics group, IBM Zurich research laboratory in Ruschlikon, Switzerland. Each chip consists of eight cantilevers at a pitch of 250 μm. The dimensions of the cantilevers are 500 μm in length and 100 μm in width. Different thicknesses of 7 μm, 4 μm, 3 μm, 2 μm, 1 μm and 500 nm have been fabricated.

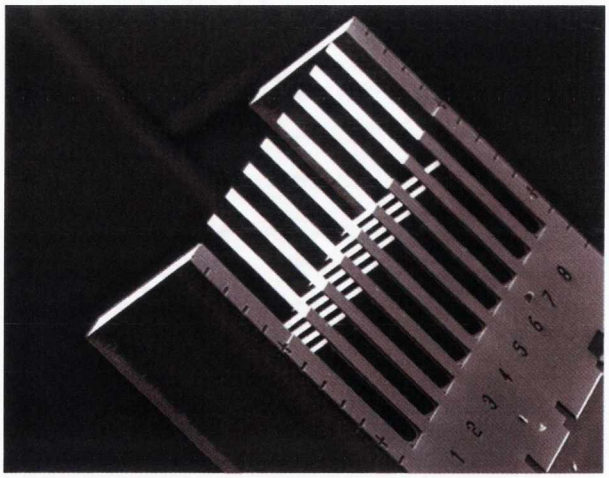

Fig.1.4: Scanning electron microscope image of a typical cantilever array. Each cantilever is 1 μm thick, 500 μm long and 100 μm wide and there are 8 cantilevers in this array with a pitch of 250 μm. Sensors were microfabricated at the IBM Zurich research laboratory, Switzerland.

Depending on the mode they are operated in, static or dynamic, they are monitored by various methods to record a signal viz. piezoresistivity[44], optical deflection[45], capacitive deflection[46], interferometry[47], optical diffraction grating[48] or a charge coupled device[49]. There are two basic modes of operation of a cantilever, static and dynamic.

a. Static mode

In this mode the cantilever bending, induced by surface processes which causes compressive or tensile surface stress is monitored[50]. This requires that the cantilevers be functionalized at least on one side. The origins of this stress can be steric hindrance, charge effects, swelling, mechanical expansion, structural changes or a combination of these[50-52]. It is important to have a proper scheme of functionalization of the cantilevers surfaces and applying differential readout since if both the cantilever surfaces react similarly to the stimulus one risks the cancellation of the signals entirely. Micromechanical cantilevers are designed to have very low spring constants, e.g. 0.02 $N.m^{-1}$ and hence they are sensitive to forces in the range of a few piconewtons. Such cantilevers are bent by forces generated by reactions or addition of even a fraction of a monolayer of atoms or molecules on the active surface. The cantilever deflection resulting due to surface stress is measured and can be quantified using the Stoneys formula[53].

$$Surface\ stress, \sigma = \frac{\Delta x E t^2}{4(1-v)L^2} \tag{1}$$

where Δx, E and v are cantilever deflection, elastic modulus and Poisson's ratio of cantilever material respectively, t is thickness and L is the length of the cantilever. The equation is only applicable for thin films where the thickness t is very small compared to the substrate thickness and the cantilever length L. When a stress inducing event occurs on the surface of the cantilever, compressive or tensile surface stress is induced in the bi-layer cantilever system. This can be understood by firstly imagining that the thin film is free from the substrate so it expands or contracts under external stimulus. Then in order to keep the film together with the substrate as a bi-layer system, an

additional force per unit length will be required to be applied along the edge of the film with an equal and opposite force being applied to the edge of the substrate (silicon microcantilever). The bending moment hence applied to the system manifests as microcantilever curvature[54,55]. Surface stress hence can be defined as the force per unit length of bare edge that must be applied to a terminating surface in order to keep it in equilibrium[56].

Mechanical transduction of biochemical reactions on the cantilevers are rooted in the chemo-mechanics of this surface stress. Molecular adsorption on a solid surface is driven by surface Gibbs free energy reduction, and such reduction leads to a change in surface stress. If the solid is of defined material and shape[57] it responds to this stress by a detectable mechanical response that can be exploited to transduce the chemical interaction occurring at the interface. This chemo-mechanical transduction has been explained from the standpoint of Gibbs interfacial thermodynamics[58,59].

To explain this system from the interfacial thermodynamics point of view, we begin with the classical fundamental equation of the internal energy of a system that involves only PV work and changes in the amount of species[60].

$$dU = TdS - PdV + \sum_{i=1}^{N} \mu_i d\, n_i \qquad (2)$$

where N is the number of species, μ_i is the chemical potential of species *i*, and n_i is the amount of species *i*. From the standard definition of Gibbs free energy

$$G = H - TS$$
$$\therefore G = U + PV - TS$$

Differentiating the above equation for G and then substituting for *dU* from Equation 2 we get

$$dG = -SdT + VdP + \sum_{i=1}^{N} \mu_i d\, n_i \tag{3}$$

Equation 3 considers the bulk scenario and hence needs to be modified to take into account an interfacial phase which will bring in an additional term for interfacial work[61].

$$dG = -SdT + VdP + \sum_{i=1}^{N} \mu_i d\, n_i + \gamma dA \tag{4}$$

where, γ is the interfacial tension and A is the interfacial area. Consider a system as shown in Fig.1.5 where a receptor R bound to a surface binds to a single ligand molecule L in a closed system in a non-ideal (water) solution under isothermal and isobaric conditions. The interfacial phase of the receptor R with a given interfacial tension is slowly replaced with a novel phase LR. Hence considering this change in interfacial tension and a corresponding change in coverage area A of the receptor (R) with the new receptor ligand complex (LR), we can relate the overall Gibbs free energy by taking into account the chemical and the surface work.

$$dG = -SdT + VdP + \Delta\gamma dA + (\mu_{LR} - \mu_R - \mu_L)\xi \tag{5}$$

where $\Delta\gamma$ is the difference between the interfacial tension of the Receptor layer and the novel Ligand+Receptor layer and ξ is the progress of the reaction (for a unitary system of R+L↔LR). At constant temperature and pressure, the Gibbs free energy of the reaction is obtained by taking a partial derivative with respect to ξ[61].

$$\Delta G = \Delta G^0 + \frac{\Delta\gamma}{\Gamma_{LR}} + RT\, ln \frac{a_{LR}}{a_R a_L} \tag{6}$$

where Γ_{LR}=dξ/dA and the chemical potentials of the individual species are expressed as $\mu_i = \mu_i^0 + RT\ lna_i$. At equilibrium, the Equation 6 rearranges into the van't Hoff isotherm for the system as

$$\Delta G^0 = -\frac{\Delta\gamma}{\Gamma_{LR}} + RT\ ln\ k \tag{7}$$

This result clearly indicates that the Gibbs energy for the reaction is split into chemical and surface work. The surface pressure π is the physical manifestation of the work involved in the creation of the novel interfacial phase driven by the receptor/ligand binding reaction i.e. π = - $\Delta\gamma$[62].

In our current scenario of the hybridization event of a target oligonucleotide (L) to a surface bound probe (R), the surface work involved in the hybridization event causes a change in surface pressure that manifests itself as bending of the microcantilever beam. This means that the bending of the microcantilever is due to variation of the applied stress and also its response to the formation of a novel interface (surface pressure)[61]. Hence, for the chemical equilibrium of the binding of a single ligand molecule, L, to a single receptor molecule, R, immobilized on a cantilever surface, occurring in a closed system in a non-ideal (water) solution at isothermal and isobaric conditions, the Gibbs free energy can be given as follows[61].

$$\Delta_r G^0 = \frac{\pi}{\alpha(\Gamma_R)_i} + RTln[C_L(1/\alpha - 1)] \tag{8}$$

where $[C_L]$ is the equilibrium bulk concentration of the target L, $(\Gamma_R)_i$ is the interfacial excess density (moles) of the receptor molecules on the surface and α is the hybridization efficiency defined as $\alpha = [\Gamma_{LR}]/(\Gamma_R)_i$ (Here $[\Gamma_{LR}]$ is the interfacial excess density of the hybridized LR molecules). The relation again clearly indicates that the whole standard work of the reaction, $\Delta_r G^0$, splits into the chemical and surface work.

The heat of reaction for the hybridization of the target on the surface might cause thermodynamic variations at the interface and this effect has been used to measure such quantities before using bi-metallic microcantilevers[39,63,64]. However we do not believe that such variations will affect the results of cantilever deflection for our purposes since most of these events occur at a very short time scale (a few seconds to couple of minutes) as compared to our studies. The system is thermally equilibrated in the buffer solution in a much larger enclosure (as compared to the sensor surface) and the final defections are all taken against an in-situ reference.

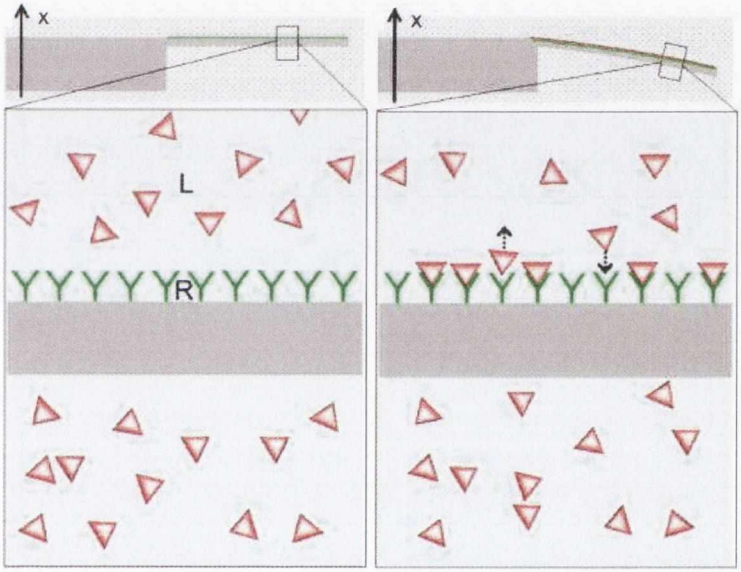

Fig. 1.5: Binding of ligand (L) molecules to receptor (R) molecules confined onto the microcantilever top surface changes the surface stress i.e. the surface pressure, on that face and the cantilever responds by a downward bending (the reaction exerts a compressive surface stress, viz. a downward surface pressure, on the cantilever). Depending on the interaction, the stress might be tensile in nature hence moving the cantilevers upwards[61].

b. Dynamic mode

In this mode, the cantilevers act as a microbalance as they are driven by external energy at their resonance frequency and a binding event on the cantilever's functionalized side induces a drop in the resonance frequency of the cantilever which is directly related to the mass of the adsorbed/bound material[65]. The quality factor of the vibration is very low in liquids at the fundamental frequencies. The higher resonance harmonics are therefore tracked to get proportionally larger frequency shift since they provide better sensitivity. Measurements have been shown to be possible as low as 1 zg (10^{-21}g)[66] in

vacuum. Recently a carbon nanotube based nanomechanical resonator has shown a resolution of 1.7 yoctogram (1 yg = 10^{-24} g), which corresponds to the mass of one proton[67].

Despite high sensitivity, microcantilever sensing setups are prone to noise sources such as temperature drifts, changes in refractive index, flow rate changes, ionic interactions, electronic noise and mechanical sources of noise. However, most non-intrinsic noise sources can be eliminated by differential read-out using an in-situ reference cantilever. The dynamic range of the sensors depends on the application. They have been shown to detect from millimolar to picomolar concentration of nucleotides[33] in the static mode and detection of prostate-specific antigen (MW 33kDa) over a dynamic range of concentrations from 60 mg/mL to 0.2 ng/mL (1.8 mM to 6.06 pM) in a background of human serum albumin (MW 67kDa) and human plasminogen (MW 87kDa) at 1 mg/ml[39] (i.e. 14.9 μM and 11.5 μM respectively) in the dynamic mode.

1.4 Bio-Nanomechanical sensors

Single nucleotide polymorphisms (SNPs) within a gene sequence or the genome are the main concern of the genomics research and its application. Point mutations cause several diseases[68] such as Thalassemia, Tay Sachs, Alzheimer's disease etc. Therefore efforts to detect the single nucleotide polymorphisms will aid in the early diagnosis of these diseases and eventually aid in their treatment. An effective and reliable way of detecting such single base mismatches is by using microcantilevers, which are extremely sensitive to specific biomolecular recognition. The static mode especially has been used to measure the hybridization of DNA/RNA, binding of transcription factor to DNA[45] and various protein interactions[69]. Thiolated DNA/RNA probes specific for the particular target sequence are immobilized on the gold-coated microcantilever. Hybridization with the fully complimentary target sequence causes a net positive deflection of the cantilever because of a reduction in the configurational entropy.

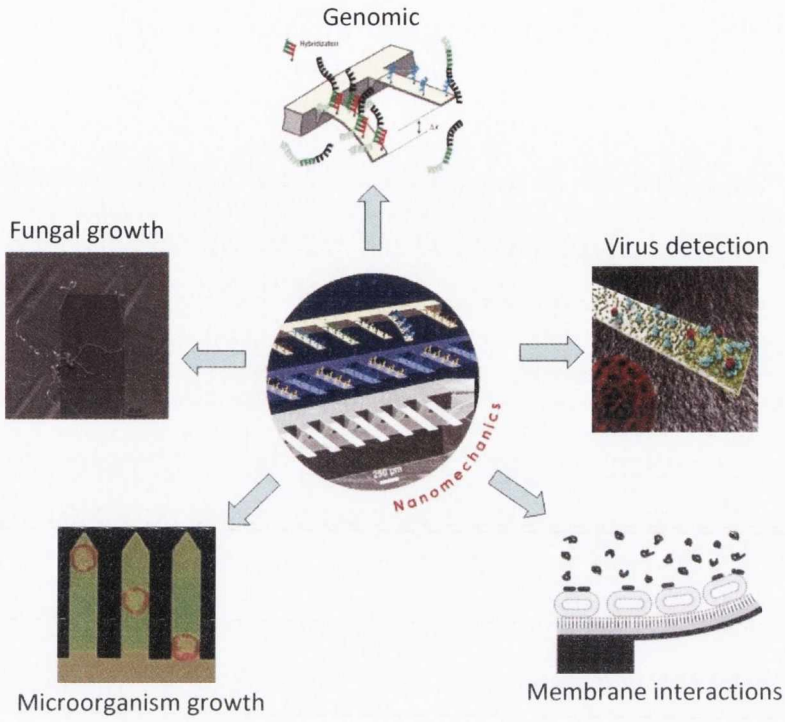

Fig.1.6: Cantilevers in Bio-nanotechnology offer a diverse scope of application. A range of applications are depicted here from detection of oligonucleotides for genomics, study of fungal & micro-organism growth and study of bimolecular interactions in membranes to mention a few.

Single base pair mismatches have been detected between two 12-mer oligonucleotides[69]. Lately, cantilever arrays have been used for binding assays in parallel and detect down to femtomoles of DNA on the cantilever (in an offline method) at a DNA concentration in solution of 1 fM[70]. Recently, the detection of mRNA biomarkers in total cellular RNA has also been demonstrated. Differential gene expression of the gene 1-8U, a potential marker for cancer progression or viral infections, has been measured in a complex background. The measurements provided results within minutes at the picomolar level without target amplification, and are sensitive to single base mismatches[33]. Moreover, cantilevers have found application in detection of fungal growth[71], micro-organism proliferation[72], interaction on membrane proteins[73] and detection of viral particles[74]. The possibilities are hence endless with the right functionalization of the surface (Fig.1.6).

1.5 Scope

The fishing of genes in complex environments has been a challenge with existing methods with regards to their sensitivity, extensive sample preparation and the time required. Cantilevers have already proven that it is possible for genetic screening even in total cellular extracts and hence their application in gene related therapies such as RNAi holds vast potential when explored. The major advantages of employing microcantilevers as sensors over the conventional sensors include their high sensitivity, low cost, low analyte requirement, non-hazardous procedure with fewer steps (no labels), quick response and low power requirement. A major factor for large scale applications is the fact that an array of microcantilevers can be employed for the diagnosis of a large numbers of analytes. Various disease biomarkers can be detected in a single multiplexed readout array thus having tremendous high throughput analysis capabilities. The technology holds the key to the next generation of highly sensitive sensors and hence the goal is to extend the capabilities of cantilevers and their application in RNAi therapy.

The current work presented here deals with various aspects of oligonucleotide detection using microcantilevers. It includes the development of a new enhanced instrument, establishing an enhanced sensing capability when compared to current standards, and understanding the sensor performance in a background of RNA molecules. Also presented here is the eventual application of the sensors to providing an insight into the siRNA molecules that are responsible for RNAi in the reversible opening of the blood-brain barrier. The document is structured into goal-oriented chapters. The instrumentation Chapter II deals with the design, assembly and testing of a new device using precision stages for scanning and positioning. Chapter III details the optimization of the sensor functionalization process. Chapter IV details a new method devised for the calibration of the deflection of the cantilevers on the position sensitive detector. Chapter V describes detection limits of the sensors for oligonucleotides in buffer solution where a new lower detection limit was established. Chapter VI illustrates the sensor behaviour in background total cellular RNA for varying target concentrations. Chapter VII

describes the first insights provided by microcantilever bioassay into the field of RNA interference and detection of siRNA. Chapter VIII provides a short summary and outlook for future work.

References

1 Watson, J. D. & Crick, F. H. C. Molecular Structure of Nucleic Acids - a Structure for Deoxyribose Nucleic Acid. *Nature* **171**, 737-738 (1953).

2 Fire, A. *et al.* Potent and specific genetic interference by double-stranded RNA in Caenorhabditis elegans. *Nature* **391**, 806-811 (1998).

3 Check, E. A crucial test. *Nat Med* **11**, 243-244, doi:Doi 10.1038/Nm0305-243 (2005).

4 Bitko, V., Musiyenko, A., Shulyayeva, O. & Barik, S. Inhibition of respiratory viruses by nasally administered siRNA. *Nat Med* **11**, 50-55, doi:Doi 10.1038/Nm1164 (2005).

5 Soutschek, J. *et al.* Therapeutic silencing of an endogenous gene by systemic administration of modified siRNAs. *Nature* **432**, 173-178, doi:Doi 10.1038/Nature03121 (2004).

6 Walker, F. O. Huntington's disease. *Lancet* **369**, 218-228 (2007).

7 Chanda, S. K. & Caldwell, J. S. Fulfilling the promise: drug discovery in the post-genomic era. *Drug Discov Today* **8**, 168-174 (2003).

8 Hoheisel, J. D. Microarray technology: beyond transcript profiling and genotype analysis. *Nat Rev Genet* **7**, 200-210, doi:Doi 10.1038/Nrg1809 (2006).

9 Waterhouse, P. M., Graham, H. W. & Wang, M. B. Virus resistance and gene silencing in plants can be induced by simultaneous expression of sense and antisense RNA. *P Natl Acad Sci USA* **95**, 13959-13964 (1998).

10 Montgomery, M. K., Xu, S. Q. & Fire, A. RNA as a target of double-stranded RNA-mediated genetic interference in Caenorhabditis elegans. *P Natl Acad Sci USA* **95**, 15502-15507 (1998).

11 Bagasra, O. & Prilliman, K. R. RNA interference: The molecular immune system. *J Mol Histol* **35**, 545-553 (2004).

12 Agrawal, N. *et al.* RNA interference: Biology, mechanism, and applications. *Microbiol Mol Biol R* **67**, 657-+, doi:Doi 10.1128/Mmbr.67.4.657-685.2003 (2003).

13 Bartel, D. P. MicroRNAs: Target Recognition and Regulatory Functions. *Cell* **136**, 215-233, doi:DOI 10.1016/j.cell.2009.01.002 (2009).

14 Dorsett, Y. & Tuschl, T. siRNAs: Applications in functional genomics and potential as therapeutics. *Nat Rev Drug Discov* **3**, 318-329, doi:Doi 10.1038/Nrd1345 (2004).

15 Lu, P. Y., Xie, F. Y. & Woodle, M. C. SiRNA-mediated antitumorigenesis for drug target validation and therapeutics. *Curr Opin Mol Ther* **5**, 225-234 (2003).

16 Martin, S. E. & Caplen, N. J. Applications of RNA interference in mammalian systems. *Annu Rev Genom Hum G* **8**, 81-108, doi:DOI 10.1146/annurev.genom.8.080706.092424 (2007).

17 Liszewski, K. RNAi in drug discovery & therapeutics - Combining tools and technologies to improve delivery and efficicacy of key compounds. *Genetic Engineering News* **26**, 28-+ (2006).

18 Melnikova, I. Wet age-related macular degeneration. *Nat Rev Drug Discov* **4**, 711-712, doi:Doi 10.1038/Nrd1827 (2005).

19 O'Connor, T. P. & Crystal, R. G. Genetic medicines: treatment strategies for hereditary disorders. *Nat Rev Genet* **7**, 261-276, doi:Doi 10.1038/Nrg1829 (2006).

20 Bernards, R. RnAi Delivers Insights into Liver Cancer. *Cell* **135**, 793-795, doi:DOI 10.1016/j.cell.2008.11.001 (2008).

21 Rademann, J. & Jung, G. Drug discovery - Integrating combinatorial synthesis and bioassays. *Science* **287**, 1947-1948 (2000).

22 Denison, M. S. *et al.* Recombinant cell bioassay systems for the detection and relative quantitation of halogenated dioxins and related chemicals. *Talanta* **63**, 1123-1133, doi:DOI 10.1016/j.talanta.2004.05.032 (2004).

23 Belzacq-Casagrande, A. S. *et al.* Pharmacological screening and enzymatic assays for apoptosis. *Front Biosci* **14**, 3550-3562, doi:Doi 10.2741/4070 (2009).

24 Spisak, S. & Guttman, A. Biomedical Applications of Protein Microarrays. *Curr Med Chem* **16**, 2806-2815 (2009).

25 Raymond, C. K., Roberts, B. S., Garrett-Engele, P., Lim, L. P. & Johnson, J. M. Simple, quantitative primer-extension PCR assay for direct monitoring of microRNAs and short-interfering RNAs. *Rna* **11**, 1737-1744, doi:Doi 10.1261/Rna.2148705 (2005).

26 Nelson, B. P., Grimsrud, T. E., Liles, M. R., Goodman, R. M. & Corn, R. M. Surface plasmon resonance imaging measurements of DNA and RNA hybridization adsorption onto DNA microarrays. *Anal Chem* **73**, 1-7 (2001).

27 Bizet, K., Gabrielli, C., Perrot, H. & Therasse, J. Validation of antibody-based recognition by piezoelectric transducers through electroacoustic admittance analysis. *Biosens Bioelectron* **13**, 259-269 (1998).

28 Weigl, B. H., Bardell, R. L. & Cabrera, C. R. Lab-on-a-chip for drug development. *Adv Drug Deliver Rev* **55**, 349-377, doi:Doi 10.1016/S0169-409x(02)00223-5 (2003).

29 Nuwaysir, E. F. *et al.* Gene expression analysis using oligonucleotide arrays produced by maskless photolithography. *Genome Res* **12**, 1749-1755, doi:Doi 10.1101/Gr362402 (2002).

30 Kataja, K., Satokari, R. M., Arvas, M., Takkinen, K. & Soderlund, H. A highly sensitive and multiplexed method for focused transcript analysis. *J Microbiol Meth* **67**, 102-113, doi:DOI 10.1016/j.mimet.2006.03.013 (2006).

31 Collins, M. L. *et al.* A branched DNA signal amplification assay for quantification of nucleic acid targets below 100 molecules/ml. *Nucleic Acids Res* **25**, 2979-2984 (1997).

32 Ro, S., Park, C., Jin, J. L., Sanders, K. M. & Yan, W. A PCR-based method for detection and quantification of small RNAs. *Biochem Bioph Res Co* **351**, 756-763, doi:DOI 10.1016/j.bbrc.2006.10.105 (2006).

33 Zhang, J. *et al.* Rapid and label-free nanomechanical detection of biomarker transcripts in human RNA. *Nat Nanotechnol* **1**, 214-220, doi:DOI 10.1038/nnano.2006.134 (2006).

34 Waggoner, P. S. & Craighead, H. G. Micro- and nanomechanical sensors for environmental, chemical, and biological detection. *Lab Chip* **7**, 1238-1255, doi:Doi 10.1039/B707401h (2007).

35 Gimzewski, J. K., Gerber, C., Meyer, E. & Schlittler, R. R. Observation of a Chemical-Reaction Using a Micromechanical Sensor. *Chem Phys Lett* **217**, 589-594 (1994).

36 Watari, M. *et al.* Investigating the molecular mechanisms of in-plane mechanochemistry on cantilever arrays. *J Am Chem Soc* **129**, 601-609, doi:Doi 10.1021/Ja065222x (2007).

37 Kooser, A., Gunter, R. L., Delinger, W. D., Porter, T. L. & Eastman, M. P. Gas sensing using embedded piezoresistive microcantilever sensors. *Sensor Actuat B-Chem* **99**, 474-479, doi:DOI 10.1016/j.snb.2003.12.057 (2004).

38 Raiteri, R., Grattarola, M., Butt, H. J. & Skladal, P. Micromechanical cantilever-based biosensors. *Sensor Actuat B-Chem* **79**, 115-126 (2001).

39 Goeders, K. M., Colton, J. S. & Bottomley, L. A. Microcantilevers: Sensing chemical interactions via mechanical motion. *Chem Rev* **108**, 522-542, doi:Doi 10.1021/Cr0681041 (2008).

40 Carrascosa, L. G., Moreno, M., Alvarez, M. & Lechuga, L. M. Nanomechanical biosensors: a new sensing tool. *Trac-Trend Anal Chem* **25**, 196-206, doi:DOI 10.1016/j.trac.2005.09.006 (2006).

41 Lavrik, N. V., Sepaniak, M. J. & Datskos, P. G. Cantilever transducers as a platform for chemical and biological sensors. *Rev Sci Instrum* **75**, 2229-2253, doi:Doi 10.1063/1.1763252 (2004).

42 Lang, H. P., Hegner, M. & Gerber, C. Cantilever array sensors. *Materials Today* **8**, 30-36, doi:10.1016/s1369-7021(05)00792-3 (2005).

43 Lang, H. P., Hegner, M., Meyer, E. & Gerber, C. Nanomechanics from atomic resolution to molecular recognition based on atomic force microscopy technology. *Nanotechnology* **13**, R29-R36 (2002).

44 Mukhopadhyay, R. *et al.* Cantilever sensor for nanomechanical detection of specific protein conformations. *Nano Lett* **5**, 2385-2388, doi:Doi 10.1021/Nl051449z (2005).

45 Huber, F., Hegner, M., Gerber, C., Guntherodt, H. J. & Lang, H. P. Label free analysis of transcription factors using microcantilever arrays. *Biosens Bioelectron* **21**, 1599-1605, doi:DOI 10.1016/j.bios.2005.07.018 (2006).

46 Blanc, N., Brugger, J., deRooij, N. F. & Durig, U. Scanning force microscopy in the dynamic mode using microfabricated capacitive sensors. *J Vac Sci Technol B* **14**, 901-905 (1996).

47 Reinstaedtler, M., Rabe, U., Scherer, V., Turner, J. A. & Arnold, W. Imaging of flexural and torsional resonance modes of atomic force microscopy cantilevers using optical interferometry. *Surf Sci* **532**, 1152-1158, doi:Doi 10.1016/S0039-6028(03)00183-3 (2003).

48 Olcum, S. *et al.* in *Lasers and Electro-Optics 2009 and the European Quantum Electronics Conference. CLEO Europe - EQEC 2009. European Conference on.* 1-1.

49 Yue, M. *et al.* A 2-D microcantilever array for multiplexed biomolecular analysis. *J Microelectromech S* **13**, 290-299, doi:Doi 10.1109/Jmems.2003.823216 (2004).

50 Wu, G. H. *et al.* Origin of nanomechanical cantilever motion generated from biomolecular interactions. *P Natl Acad Sci USA* **98**, 1560-1564 (2001).

51 Godin, M. *et al.* Cantilever-based sensing: the origin of surface stress and optimization strategies. *Nanotechnology* **21**, doi:Artn 075501
Doi 10.1088/0957-4484/21/7/075501 (2010).
52 Mathad, A. G. & Patrikar, R. M. in *Students' Technology Symposium (TechSym), 2010 IEEE.* 12-16.
53 Stoney, G. G. The Tension of Metallic Films Deposited by Electrolysis. *Proceedings of the Royal Society of London. Series A, Containing Papers of a Mathematical and Physical Character* **82**, 172-175 (1909).
54 Flinn, P. A., Gardner, D. S. & Nix, W. D. Measurement and Interpretation of Stress in Aluminum-Based Metallization as a Function of Thermal History. *Ieee T Electron Dev* **34**, 689-699 (1987).
55 Hoffman, R. W. Stress Distributions and Thin-Film Mechanical-Properties. *Surf Interface Anal* **3**, 62-66 (1981).
56 Vermaak, J. S., Mays, C. W. & Kuhlmann.D. On Surface Stress and Surface Tension .I. Theoretical Considerations. *Surf Sci* **12**, 128-& (1968).
57 Finot, E., Passian, A. & Thundat, T. Measurement of mechanical properties of cantilever shaped materials. *Sensors-Basel* **8**, 3497-3541, doi:Doi 10.3390/S8053497 (2008).
58 Butt, H. J. A sensitive method to measure changes in the surface stress of solids. *J Colloid Interf Sci* **180**, 251-260 (1996).
59 Cherian, S. & Thundat, T. Determination of adsorption-induced variation in the spring constant of a microcantilever. *Appl Phys Lett* **80**, 2219-2221, doi:Doi 10.1063/1.1463720 (2002).
60 Gibbs, J. W. *The scientific papers of J. Willard Gibbs. Vol. I, Thermodynamics.* (Longmans, Green and Co., 1906).
61 Bergese, P., Oliviero, G., Alessandri, I. & Depero, L. E. Thermodynamics of mechanical transduction of surface confined receptor/ligand reactions. *J Colloid Interf Sci* **316**, 1017-1022, doi:DOI 10.1016/j.jcis.2007.08.048 (2007).
62 Adamson, A. W. & Gast, A. P. *Physical chemistry of surfaces.* (J. Wiley, 1997).
63 Berger, R., Gerber, C., Gimzewski, J. K., Meyer, E. & Guntherodt, H. J. Thermal analysis using a micromechanical calorimeter. *Appl Phys Lett* **69**, 40-42 (1996).
64 Barnes, J. R. *et al.* A Femtojoule Calorimeter Using Micromechanical Sensors. *Rev Sci Instrum* **65**, 3793-3798 (1994).
65 Dorignac, J., Kalinowski, A., Erramilli, S. & Mohanty, P. Dynamical response of nanomechanical oscillators in immiscible viscous fluid for in vitro biomolecular recognition. *Phys Rev Lett* **96**, doi:Artn 186105
Doi 10.1103/Physrevlett.96.186105 (2006).
66 Ilic, B., Yang, Y. & Craighead, H. G. Virus detection using nanoelectromechanical devices. *Appl Phys Lett* **85**, 2604-2606, doi:Doi 10.1063/1.1794378 (2004).
67 ChasteJ *et al.* A nanomechanical mass sensor with yoctogram resolution. *Nat Nano* **7**, 301-304, doi:http://www.nature.com/nnano/journal/v7/n5/abs/nnano.2012.42.html#supplementary-information (2012).

68 Wallace, D. C., Lott, M. T., Shoffner, J. M. & Brown, M. D. Diseases Resulting from Mitochondrial-DNA Point Mutations. *J Inherit Metab Dis* **15**, 472-479 (1992).

69 Fritz, J. *et al.* Translating biomolecular recognition into nanomechanics. *Science* **288**, 316-318 (2000).

70 Mertens, J. *et al.* Label-free detection of DNA hybridization based on hydration-induced tension in nucleic acid films. *Nat Nanotechnol* **3**, 301-307, doi:DOI 10.1038/nnano.2008.91 (2008).

71 Nugaeva, N. *et al.* Micromechanical cantilever array sensors for selective fungal immobilization and fast growth detection. *Biosens Bioelectron* **21**, 849-856, doi:DOI 10.1016/j.bios.2005.02.004 (2005).

72 Gfeller, K. Y., Nugaeva, N. & Hegner, M. Micromechanical oscillators as rapid biosensor for the detection of active growth of Escherichia coli. *Biosens Bioelectron* **21**, 528-533, doi:DOI 10.1016/j.bios.2004.11.018 (2005).

73 Ghatkesar, M. K., Lang, H. P., Gerber, C., Hegner, M. & Braun, T. Comprehensive Characterization of Molecular Interactions Based on Nanomechanics. *Plos One* **3**, doi:Artn E3610 Doi 10.1371/Journal.Pone.0003610 (2008).

74 Braun, T. *et al.* Quantitative time-resolved measurement of membrane protein-ligand interactions using microcantilever array sensors. *Nat Nanotechnol* **4**, 179-185, doi:Doi 10.1038/Nnano.2008.398 (2009).

Chapter II

Instrumentation

2.1 Introduction

The instrument is based primarily on the laser deflection system for detection of the bending of the cantilever array sensor for static mode and can be defined as a combination of five distinct units as defined in Fig. 2.1.

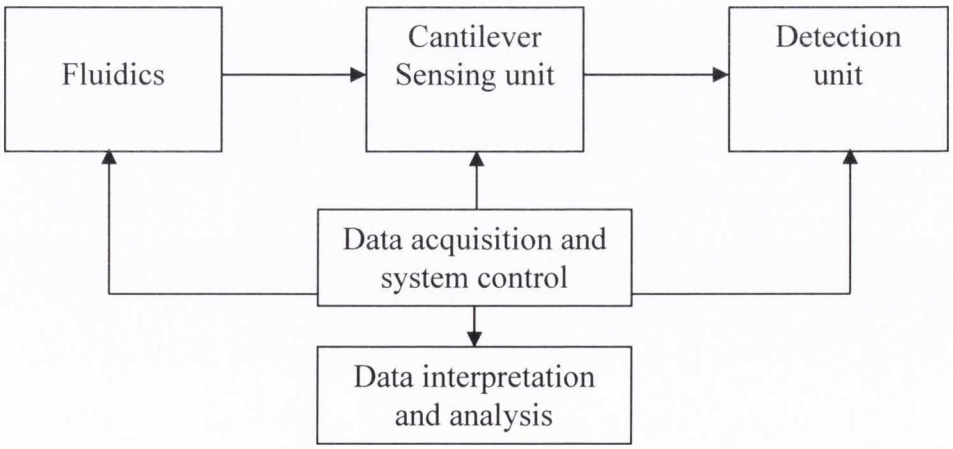

Fig 2.1: Schematic of the instrumental setup with five well defined units including both the analogue and the digital control units.

The sensing cantilever array is the principal unit placed in the fluidic system and the detection unit records the response. The laser scanning and optical deflection setups are completely new units designed, tested and implemented in the scope of this thesis which include the laser cage setup, micro-translation stage, XYZ translation stage, chamber holder, detector holder and the prism mirror arrangement. Additionally new sample loop-injection valve and modified fluidics were also implemented. All of the major units are controlled using a data acquisition and management device from a computer run using previously custom-made LabVIEW® DAQ software. The software unit was modified with new additions to accommodate micro-translation stage based laser scanning. The final interpretation and data analysis is done using a custom made program NOSEtools[1] written in Igor Pro. Individual units are described in detail in the following chapters.

2.2 Sensing Unit

The cantilever sensor is part of an array on a single silicon chip (chip body dimensions are 3.85 x 2.45 x 0.51 mm) with eight individual sensors each positioned at a pitch of 250 μm provided by IBM Zurich Laboratories (Fig. 2.2). Side bars are introduced in some designs for ease of handling and protection of fragile sensors. However we prefer to use cantilever sensor chips without side bars since they might interfere with the flow of solutions in the chamber and prevent proper exposure of the cantilevers to the samples. Each individual cantilever is 500 μm x 100 μm x 0.5 μm. The array design has a major advantage over single cantilever systems in that they provide multiple internal references and test sensors. The chips were obtained by reactive ion etching of Silicon on Insulator (SOI) wafer at the IBM Research Labs designed according to specifications of the Nanobio group at University of Basel (2003 and 2005).

2.3 Fluidics

Since all the biological experiments were performed in solution and require fluid flow,

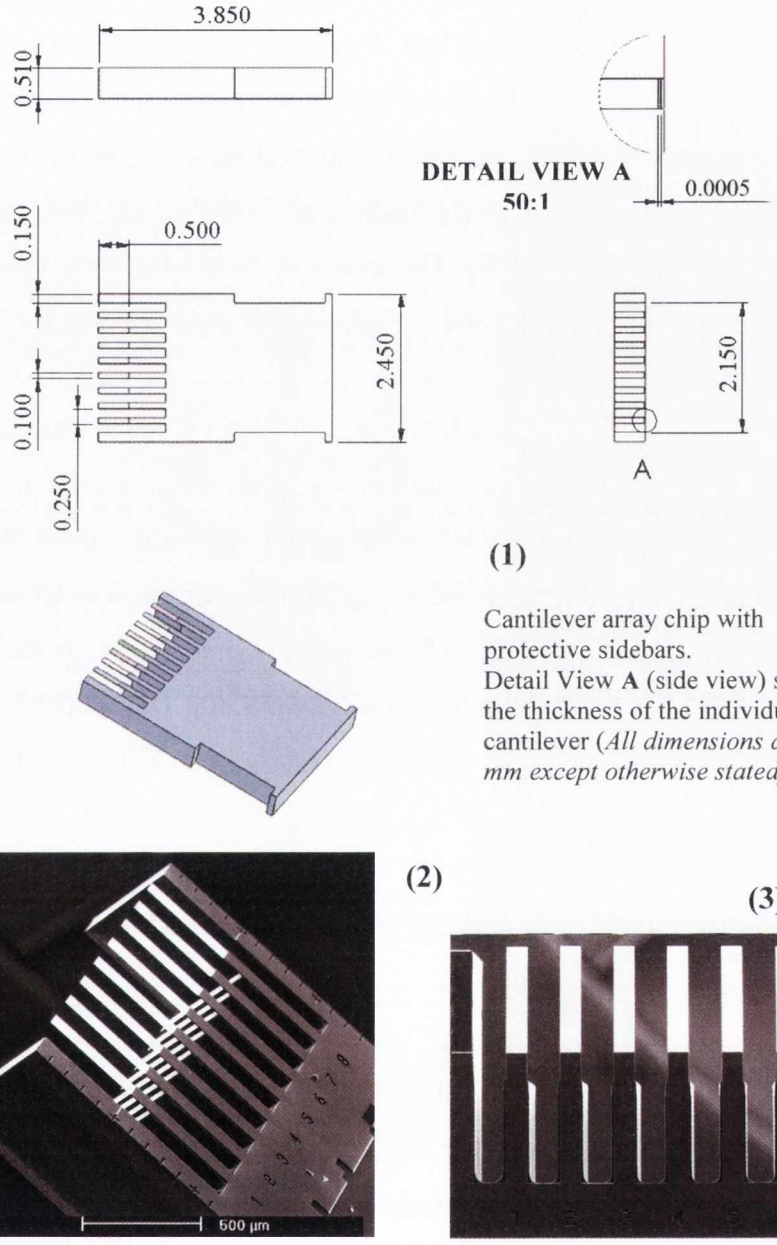

Fig 2.2: Details of the Cantilever sensor array. (1) Schematic drawing for sensor array and microcantilever with dimensions (2) SEM image of a sensor array showing eight distinct microcantilevers (3) SEM image of individual cantilevers spaced at a pitch of 250 µm on a sensor array. The chips were obtained by reactive ion etching of Silicon on Insulator (SOI) wafer at the IBM Research Labs, Switzerland. The current study employs microcantilevers that are 500 nm thin (detail view A).

the sensor array was placed inside a fluidic chamber providing an inert environment and ease of operation for flow of liquids. The flow chamber is a combination of a main body (flow cell) where the sensor is placed, a cantilever holding clamp, elastomer ring seals, covering glass, top metallic cover and side tube clamps (Fig. 2.3). The flow cell and the cantilever array holding clamp are made from grey, opaque and biologically inert polymer poly-ether-ether-ketone (PEEK). The assembly shows the array holder used to pin down the cantilever in the chamber and the subsequent glass window for the laser.

The glass window (2 mm thick; Mirogard, Schott, Germany) is made from special high transparency glass with anti-reflective coatings on both sides leading to near 99% transmission of incident light in our application range. The laser enters the chamber orthogonal to the glass before it deflects off the cantilever surface in order to avoid any reflection/refraction artifacts. The fluid cell has an inlet and outlet for the fluid flow using flexible translucent Teflon tubing (0.3 mm ID, 1.58 mm OD; Supelco). The flow is maintained using a programmable syringe pump (Genie Plus, Kent Scientific) and a 6 port valve (Vici AG, DE) allows to switch between alternate fluids (buffers, target solutions etc.) through the flow cell when the syringe is used in the withdraw mode. A constant flow rate of 150 µl/min was maintained in the flow cell for all injections except otherwise stated.

A Peltier element (Fig. 2.4) is placed in the fluid chamber right below the fluid cell. This allows mechanical calibration of the cantilever sensors and normalization of the mechanical response by performing a temperature pulse experiment before and after injection of biological samples. The normalization keeps the nanomechanical response comparable and accounts for the small differences in the characteristics the cantilevers might have.

2.4 Optical setup

The laser beam based deflection system has been used most widely to measure the cantilever bending in the static mode because of the ease of use, robustness of the

readout technique and availability of high sensitivity position sensitive detectors (PSD) which allow sub angstrom resolution[2,3]. Adapted from standard AFM systems, a low power laser is reflected off the surface of the cantilever onto a position sensitive detector. The actual displacement of the cantilever is obtained from calibrating the change in position of the laser spot on the PSD which we discuss later in detail.

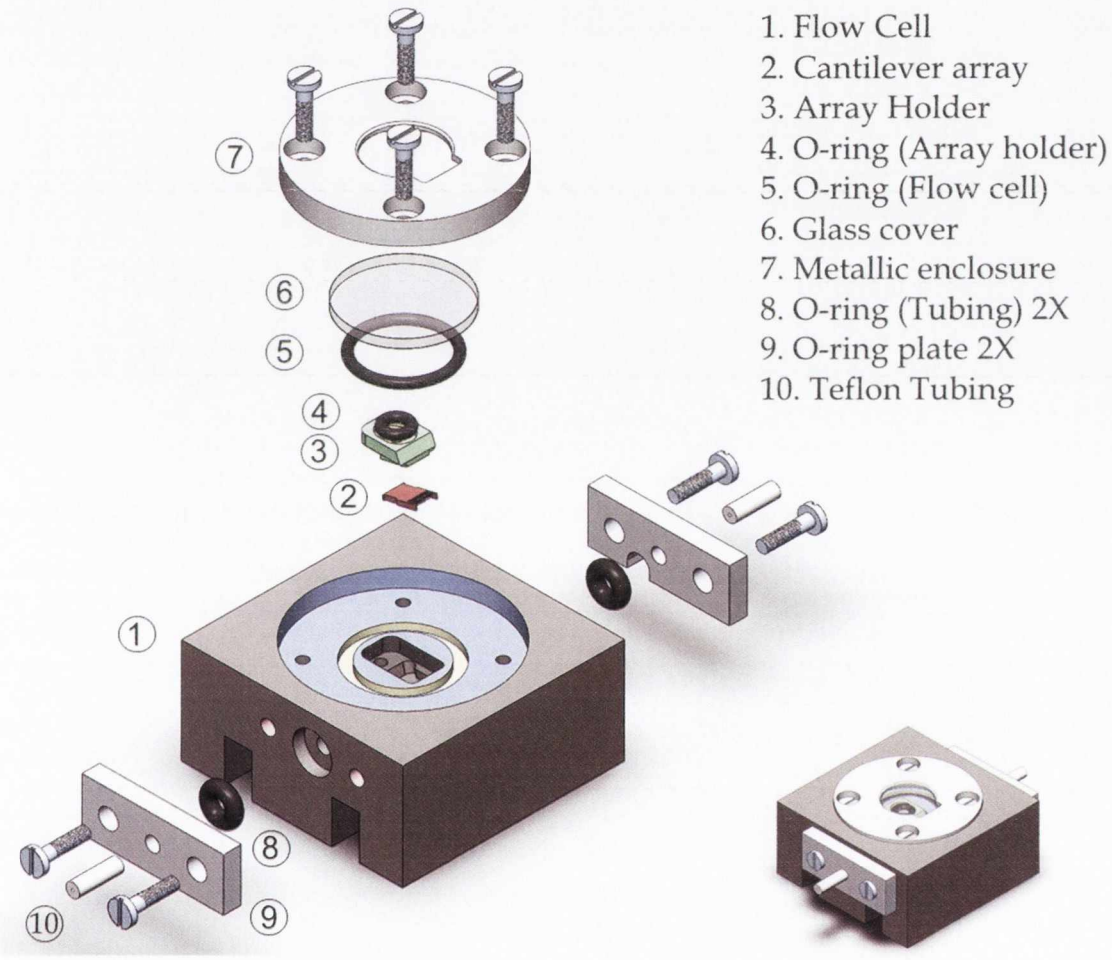

Fig. 2.3: Graphical assembly of the flow cell. The cantilever is placed in the flow chamber, clamped and the chamber is sealed allowing fluid flow through the cell by the Teflon tubing inlet and outlet. The final volume of the chamber with the array inserted is ~ 14 µl. The chamber base where the cantilever is mounted is at an angle of 12° to the laser beam.

The laser used in the present setup is a 633 nm Fiber Coupled Single-Wavelength Diode Laser (Newfocus) with a SWL-7500 controller (Fig. 2.5). The laser is collimated using a F240-APC-B fiber collimation package (Thorlabs) which is pre-aligned to collimate

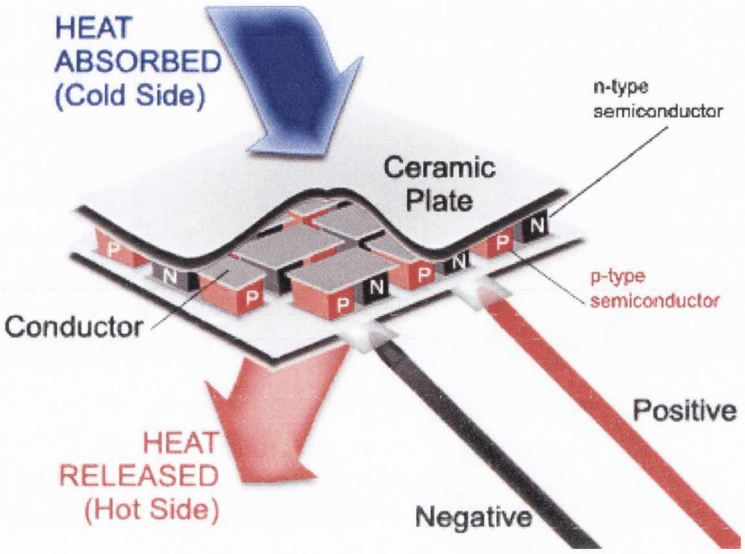

Fig. 2.4: Peltier element[4] used for the nanomechanical calibration and normalization of the sensor response. The "hot" side is placed right below the flow cell in the chamber setup to impart a quick heat pulse. In the static mode, the heat pulse also helps ascertain the nature of stress perceived by the cantilever (compressive or tensile).

laser beam propagating from the tip of a fiber with diffraction-limited performance at the design wavelength. The receptacle of the housing is angled and the beam is aligned with the mechanical axis of the collimation package. With a collimated beam diameter D_{COLL} of 1.4 mm, the laser is focussed using an achromatic doublet (Thorlabs, AC254-040-A1-ML – Mounted Ø1") with a focal length f of 40 mm which results in a spot size D_{CL} of 23.03 µm on the cantilever surface when in focus (solid angle of convergence θ is ~ 0.035). The spot size on the cantilever D_{CL} was calculated using the given equation below[5].

$$D_{CL} = \frac{4\lambda}{2\pi \arctan(D_{COLL}/2f)} \quad (1)$$

The laser has to be operated at the factory default settings for best optimal performance so as to avoid any artefacts in the measurements due to fluctuating sum signal that might arise from unstable laser power. The current laser is operated at factory parameters of 87 mA and 21.6 °C for optimal performance which gives a laser power of ~ 2.4 mW. At this power, the laser when reflected off the surface of the gold coated cantilever saturates the current in the PSD (above 10V) and hence has to be lowered. As a result an absorptive neutral density filter was introduced between the focussing element and the collimator (ND 1.3, Thorlabs) which allows a theoretical transmission of 5%. The collimation, focussing and the laser head are all composed into one unit using a cage assembly consisting of two cage plates, two cage plate adaptors, removable filter holder and four cage assembly rods (Thorlabs).

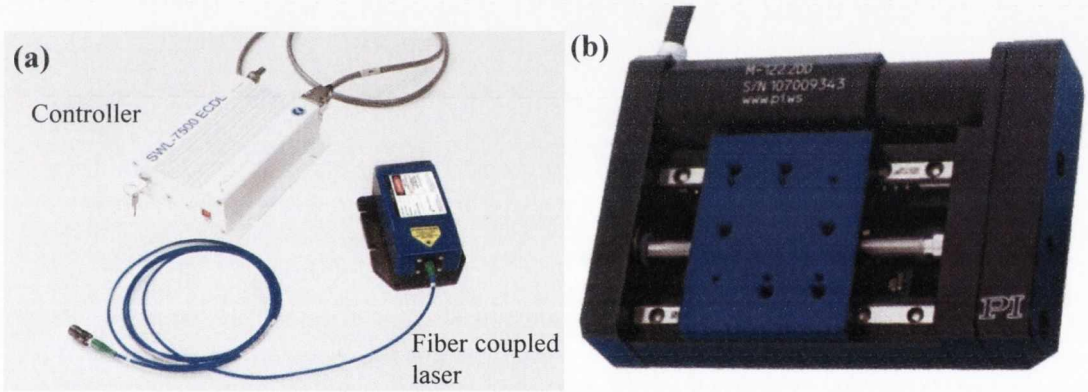

Fig. 2.5: Laser and positioning stage. (a) 633 nm Laser with optic fibre coupling and controller. The laser is always operated at factory optimal settings. (b) The high precision translation stage on which the laser assembly is mounted. It allows fast (max. 20 mm/s) and precise movement of the laser spot (with 200 nm reproducibility) for multiplexed scanning of the cantilever array.

The focussed laser spot on a single cantilever in the array reflects off the surface to reach the PSD. For a multiplexed reading of the cantilever array, the laser spot has to scan across the cantilever array (where cantilevers are at a pitch of 250 μm) with high speed, high precision and reproducibility. This is achieved using a precision micro-translation stage (M-122.2DD, Physik Instrument) onto which the entire laser cage assembly is mounted. The stage consists of a folded drive train with the DC servo motor

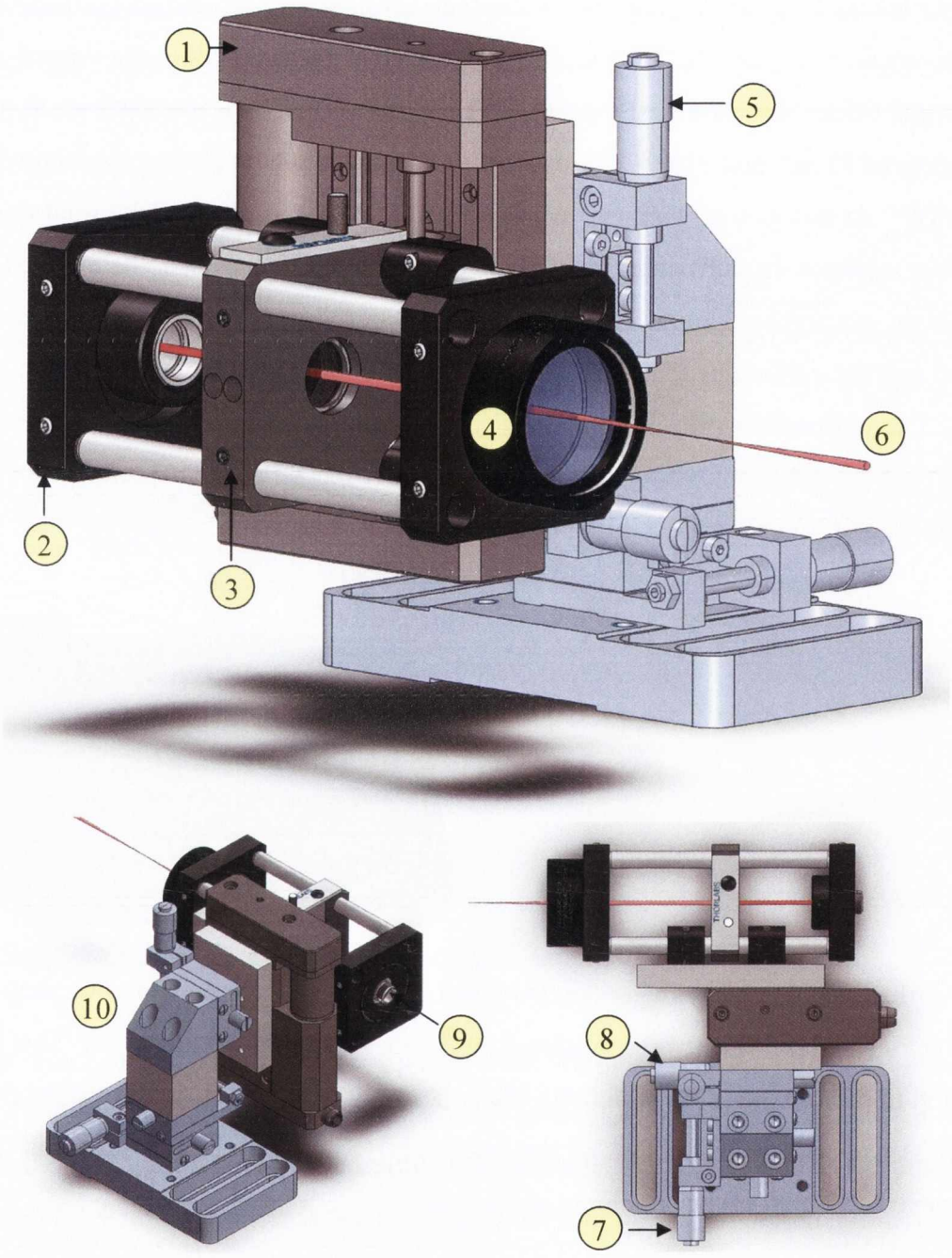

Fig. 2.6: Full assembly of the laser positioning and focussing assembly. 1: Micro-translation stage. 2: Cage Plate (2X). 3: Cage Removable Filter plate with ND1.3 filter. 4: Achromatic doublet focussing unit (f = 40 mm). 5: Micrometer (positioning spot along cantilever width). 6: Laser beam. 7: Micrometer (positioning spot along cantilever length). 8: Micrometer (laser spot focussing on cantilever). 9: Laser fiber coupling to collimation package. 10: XYZ translation stage body

and drive screw side-by-side. Equipped with a non-contacting optical linear encoder and a preloaded, precision-ground, ball-screw, this stage provides high accuracy and excellent repeatability (Specifications: Travel Range: 25 mm, 0.1 μm Optical Linear Encoder, Min. Incremental Motion 0.2 μm, Max. Velocity: 20 mm/s). In the present device, the stage is operated at 10 mm/s at a pitch matching the cantilevers (i.e. 250 μm) with a stop time of 500 ms on each cantilever.

The micro-translation stage is coupled onto a breadboard (M6 Thorlabs) using a XYZ Gothic-Arch stainless steel linear translation stage (9061-XYZ-M, platform size 25 mm, 6.5 mm travel with 10 μm resolution, Newfocus) with thumbscrew locks. This allows one to control the laser head and scanning assembly in XYZ directions with high precision using micrometers. This is crucial in order to obtain a proper positioning and focus of the laser onto the cantilever surface as regards the origin of a scan. Fig.2.6 details all the assembly of the laser unit along with the translational stage and the XYZ positioning stage (overall setup shown in Fig.2.8)

The PSD is essentially a PIN (layered semiconductor device with a wide, lightly doped 'near' intrinsic semiconductor region between a p-type semiconductor and an n-type semiconductor region) diode device that converts the position of a light or radiation spot into signal currents with high position resolution and linearity. The current device is a custom made one dimensional PSD (1L10-10-A_SU15, Sitek, Sweden) based on the lateral effect photodiode principle with an effective sensor area of 10 mm x 10 mm. There are mainly three terminals on the PSD (Fig.2.7), one on the back side providing a bias voltage (5-15 V) and two electrodes on the front side measuring the current with a maximum rise time of 110 ns. The rise time is the reaction time required for the PSD to provide a full signal and has to be considerably lower than the laser spot stop time when scanning cantilevers arrays in a time multiplexed manner. A photoelectric current is generated by the incident light which flows through the device and can be seen as an input bias current divided into two output currents, I_1 and I_2 (Fig.2.7).

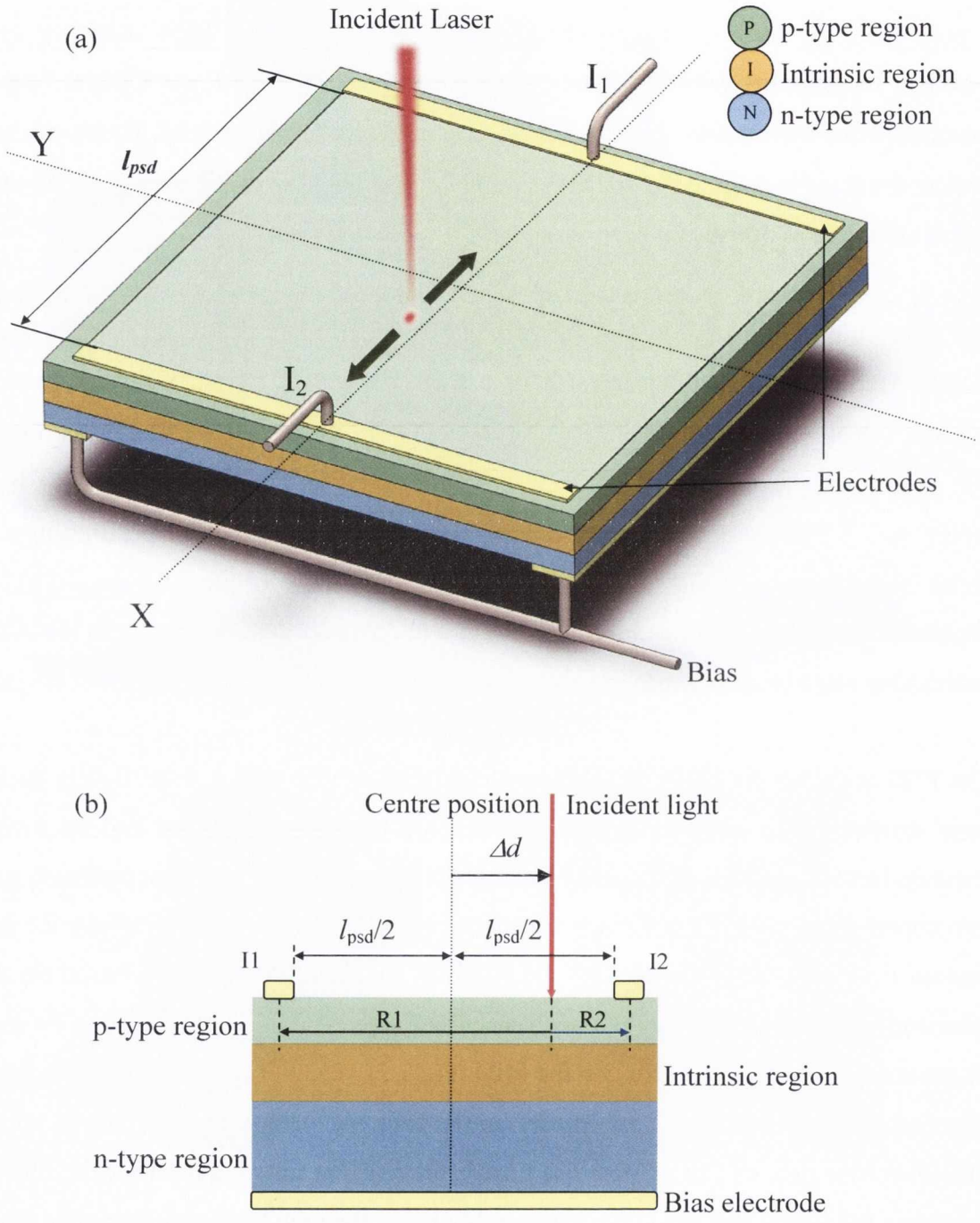

Fig. 2.7: Schematic of a one dimensional position sensitive detector. l_{psd} denotes the active PSD length whereas I_1 and I_2 are the electrode currents (a) depicts a 3D representation of the PSD (b) cross section of the PSD showing the incident light and the division of the currents as I1 and I2 in proportion to the resistance R1 and R2.

Assuming that the p-type region has perfectly homogenous resistivity, the resistances R1 and R2 are proportional to the distances from the electrodes (Fig. 2.7 b). Hence the ratio of the currents I1 and I2 will give the exact position of the center of gravity of the incident light spot Δd from the origin [6,7] (the notation Δd denotes a "change in position" and is always in respect to the origin and can hence be also referred to as the "current position" but in always referenced to the centre position).

$$\frac{I_1}{I_2} = \frac{R_2}{R_1} = \frac{0.5l_{psd} - \Delta d}{0.5l_{psd} + \Delta d} \tag{2}$$

Rearranging Equation 2 we get eventually,

$$\Delta d = \frac{I_1 - I_2}{I_1 + I_2} \frac{l_{psd}}{2} \tag{3}$$

Hence, for the active length of the PSD designated as $l_{psd,}$ (defined in mm) the change in position of the spot on the surface of the PSD, Δd (defined in nm) is then given by the following equation:

$$\Delta d = \frac{I_1 - I_2}{I_1 + I_2} \frac{l_{psd}}{2} 10^6 \tag{4}$$

The terms I_1-I_2 and I_1+I_2 are the differential signal and sum signal respectively and are the actual quantities obtained from the PSD post amplification. The origin for such a PSD system is the centre position when $I_1 = I_2$ and hence position is point zero. The change in position Δd is always calculated from this central axis and is given by Equation 4. It is important to note that only absolute values are obtained for the position for each cantilever and the results are later reinitialized to zero deflection start point during baseline correction using the NOSEtools software.

As evident from the Equation 3, the intensity of the incident light spot does not affect the calculation of the change in light spot position. In order to eliminate noise from higher frequency sources, the signal is low pass filtered at 5Hz for the static mode of detection providing an averaged signal for the spot position.

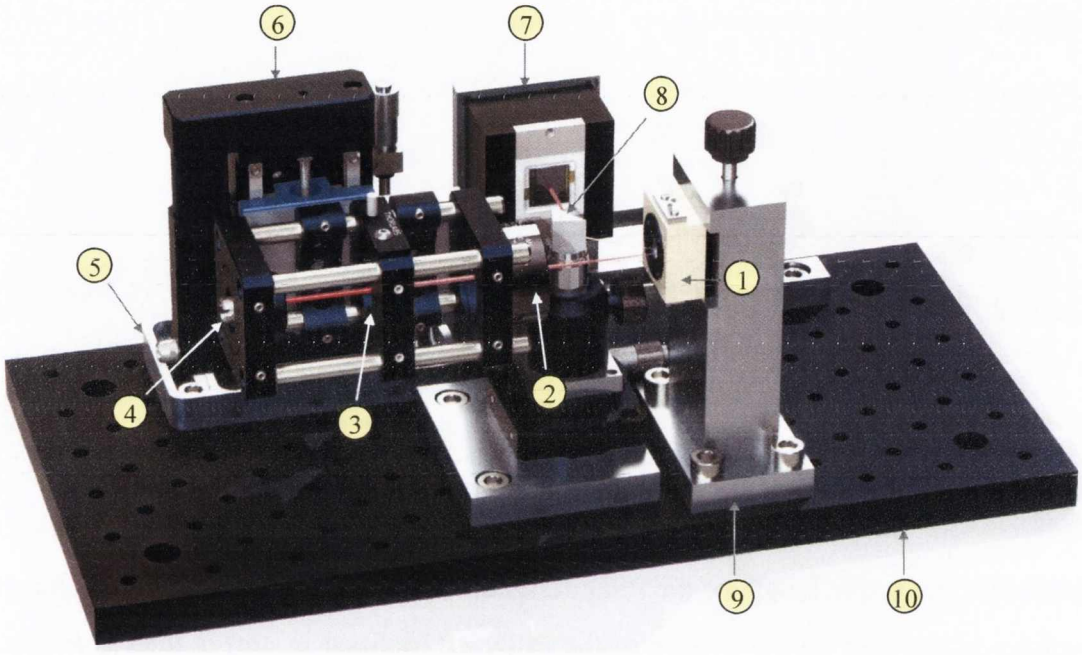

Fig. 2.8: Solidworks® rendered visual of the instrument. (1) Flow cell holder (2) Focusing lens (3) ND filter holder (4) Laser fiber optics and collimator (5) XYZ positioning stage (6) High precision positioning stage (7) PSD unit (8) Prism mirror (9) Flow cell holder (10) Mounting breadboard. The individual components are pieced together using custom-made parts designed in Solidworks® and tested using Eden 250® 3D prototyper. The entire setup is mounted on a M6 Thorlabs breadboard.

2.5 Data acquisition and system control

The instrument is controlled via a user interface created in LabVIEW® (National Instruments) which conveys information to and fro between the controlling desktop computing unit, the acquisition & control hardware and the individual device components. The control interface records the experimental parameters for further data

analysis which is performed using custom made software NoseTools in Igor PRO® (Wavemetrics). The software is designed to analyze the data (baseline corrections, normalization etc.) and finally obtain differential signals between the probes and the references in order to establish the specificity of the probe sensor (Fig.2.9).

2.5.1 Hardware units

Several hardware units are pieced together for system control and data acquisition. The heart of the system lies in the data acquisition hardware from National Instruments (DAQ) which controls all major information exchange. The PCI 6014 is a multifunctional 16 bit data acquisition card with 8 differential analog input channels that receive signals from the PSD, temperature from the thermocouples and controls the temperature regulation of the thermal enclosure. The thermocouples (SEMI 833, Hygrosens, DE) are based on the negative thermal coefficient (NTC) principle and provide a high accuracy of ± 0.7 K at room temperature. The readout from the thermocouples enables control of the Peltier based thermal enclosure (Intertronic, CH) which is powered/controlled using software controlled DC power supply (E3614A, Agilent systems).

Other hardware components are controlled with their own controller units that are interfaced with the computing unit using supplier software or the main custom made software in LabVIEW®. The laser is controlled using the SWL-7500 controller unit which is run from the PC by USB 2.0 port using supplier software where one can change the current settings of the laser or choose to run it on factory defaults. The 6-port valve from the fluidics in controlled using VICI multi-position actuator control module connected to the PC by a USB 2.0 port. The precision translation stage M122.2DD is controlled using a PCI C-843 DC-Servo-Motor controller. The programmable injection pump is run from an RS232 port using the LabVIEW® software.

2.5.2 Data analysis and interpretation

The raw data obtained from the instrument includes information on various control parameters and mainly the deflection of each cantilever as a function of time. The three temperature nodes (thermal enclosure, flow cell and ambient), the calculated cantilever deflection signal, the PSD sum & differential signals, the injection cycle number, the valve number, the flow rate & volume per injection, individual injection times and the temperature set point are all obtained by the LabVIEW® program NOSE and saved in ASCII file format as a function of time. This dataset is then interpreted in detail using the NOSETools[8] software programmed in Igor Pro.

Data processing for signals from microarray systems is of prime importance in the interpretation of the biological assays performed on the arrays. Since cantilevers are highly sensitive to most environmental stimuli it is imperative that the signal interpretation includes multiple probe cantilevers in the same environment to provide comparable results and more importantly include in-situ reference cantilevers that can provide an unbiased result. The final sensor response is hence a differential analysis of the averaged response of the probes and references cantilever sensors. However, prior to the averaging and differential analysis, it is vital that the dataset be corrected for offsets and drifts in the signals which are inherent in these systems and may lead to misleading results when ignored. More importantly all the cantilevers in an array need to be calibrated for their mechanical response so as to establish a normalized mechanical signal which takes into account the small variations within the individual cantilevers. This "Normalization" is achieved by performing a Peltier test prior to and after the experimental procedure using the Peltier heating element in the flow cell as previously explained in Fig. 2.4.

An experiment usually consists of three datasets viz. the initial Peltier test, main experiment and the final Peltier test. A raw dataset is first baseline corrected to remove the drift for all the datasets. This is done by fitting a linear model for the baseline time in the experiment (the injections in an experiment are performed only after obtaining a

stable base line for this purpose) which is extrapolated to the duration of the entire experiment and subtracted from the raw data for each sensor.

The dataset from the Peltier test is analyzed using the Static Peltier Peak module in NOSETools. The test causes a downward bending of the cantilever due to compressive stress (as respect the gold surface on the top) due to the bi-metallic effect since gold expands faster than the underlying silicon layer. From the baseline corrected dataset of the test a lowest point search is performed. The dataset is then divided by the individual low point and then multiplied by the average bending for all the cantilevers. This normalization factor is then used in the subsequent main experiment to account for the individual nanomechanical behavior of the cantilevers. Once the main experiment has been normalized, the references and probe cantilever signals are averaged and a final differential response is obtained. The software allows one to time extract data from the entire set (such as an individual injection cycle) so that one can analyze individual assays. This also allows for baseline correction within the individual cycle since the progression of drift in between individual injection cycles in the experiments can be non-linear. For experimental data with high drift and high non-linear behavior of the baseline, the software offers another algorithm called alignment. Here, the data is aligned pair wise to a calculated average response (probes and references are averaged separately) and then aligned using a standard Levenburg-Marquardt algorithm before getting a normalized differential response.

The software allows data management and operation in a semi-automated mode allowing systematic final sensor data representation in a simple and effective manner. The data handling is divided into sections that represent a particular operation being performed on the dataset thus allowing multiple operations in a step-by-step manner. The dataset is opened as an *Experiment* file where one assigns the raw dataset to a *Project* which remains uninfluenced throughout the operations. Each *Project* can be made up of multiple *Instances* where each *Instance* has time-scaled data that is then baseline corrected and normalized. Fig: 2.10 summarizes the data flow and operations of the software.

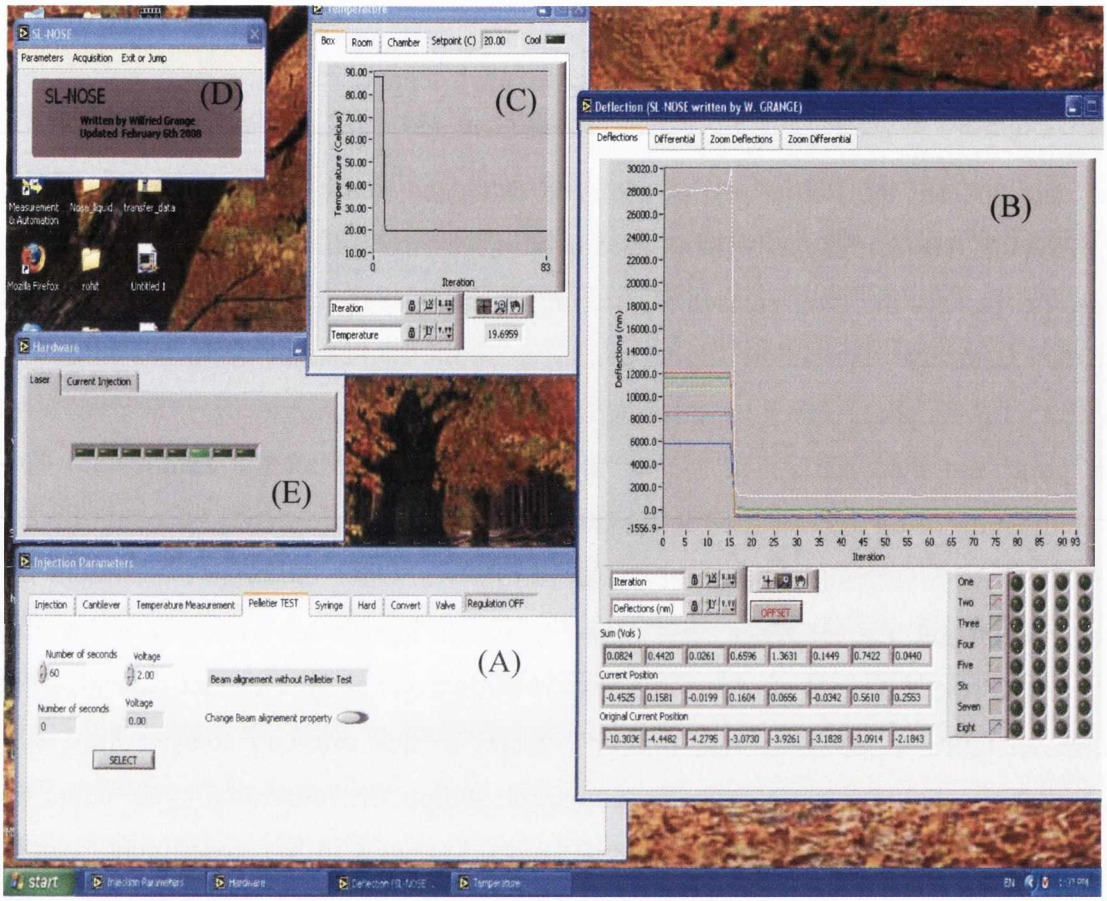

Fig. 2.9: Software interface for controlling the NOSE instrument. There are five distinct modules. Module A gives access to various control parameters on the system such as acquisition and scanning rates, peltier test parameters, syringe pump rate and volume settings, temperature set points, valve selection among others. Module B shows the real time data from the events unfolding on the cantilevers by plotting the response (deflection) as a function of time. It also contains a module to display real time differential signal between two individual cantilevers. Module C represents the temperature control module displaying the set points and the temperatures from the chamber, the enclosure and the room. Module D is the mother frame from where all other command modules are accessed. Module E shows the current position of the laser on the array, the injection cycle and the parameters for the peltier test when it is conducted. The software is designed in LabVIEW® (National Instruments. USA).

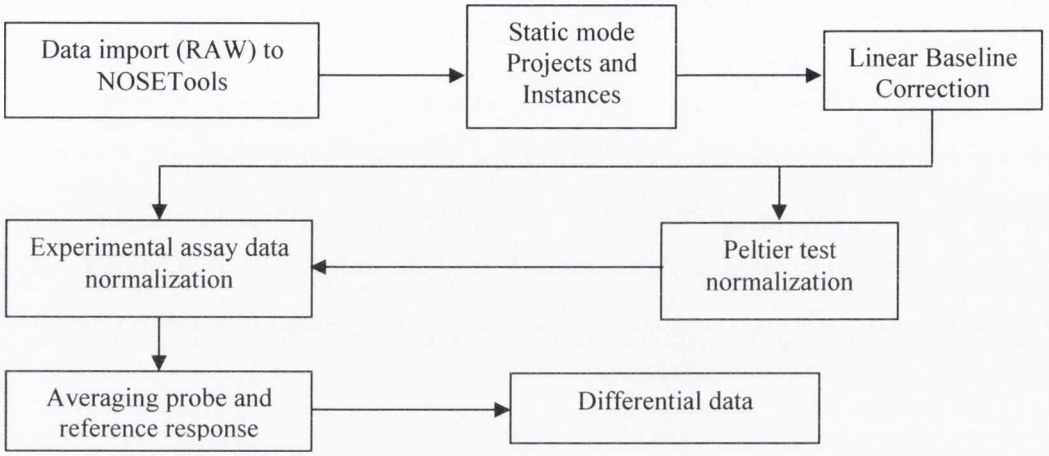

Fig. 2.10: Flow chart representing the data operation path of the NOSETools program.

An overall schematic for the instrument when fully assembled in shown below.

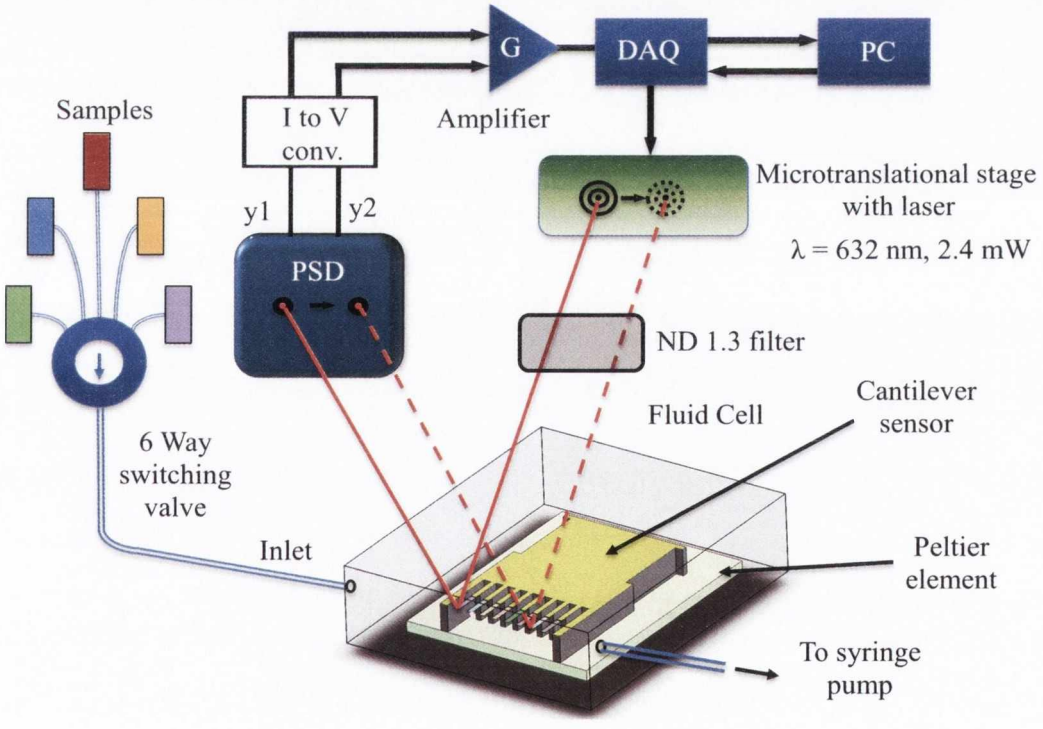

Fig. 2.11: Overall arrangement of the instrumental setup. It includes the liquid cell, laser + translational stage (for positioning and scanning), 6-port switching valve, PSD, electronic control unit and power supply, computer interface with data acquisition card (DAQ), temperature controlled enclosure and a syringe pump for the fluid flow.

2.6 Instrument optimization

The new instrumental setup required testing, calibration and protocol implementations before any experiments could be performed. The various tasks included in this process included thermocouple calibration, PSD calibration, fine tuning of the temperature control and deflection calibration. The calibration of the deflection is dealt with in detail in Chapter IV. The other process parameters that were optimised are described in the sub-sections below.

2.6.1 Characterization of the PSD

The laser used to detect the nanomechanical motion of the cantilever after reflecting from the apex of the cantilever diverges on to the position sensitive detector (PSD) which measures the change in the position. Hence it's important to have the beam impinging on the PSD within the linear area of response in order to avoid artefacts. A linearity test was performed in order to ascertain this range.

A laser beam of 0.5 mm diameter was fashioned using a pinhole from a red laser pointer (which was run on stable DC power supply). The laser beam is placed in the centre of one of the ends (electrode E2 in this case) of the 10 cm x 10 cm PSD and moved straight across from electrode E2 to E1 (Fig. 2.12). As the spot moves from E2 to E1, the magnitude of bias at electrode E2 (I2) decreases and the one at E1 (I1) increases. The corresponding sum and difference signal (I_1+I_2 and I_1-I_2) when plotted as a function of the travelled distance, indicate that an effective area of 9 mm on the PSD has a linear response for the position of the laser beam for beam diameter of around 0.5 mm.

When performing experiments, it is essential to place the reflected laser spot as close as possible to the centre of the PSD sensing range (difference signal of zero). The position may not be the same for all the eight cantilevers within a single chip since they show different mechanical behaviour depending on the handling and type of surface functionalization. In a real experiment, the eight cantilever spots are then aligned with

respect to the centre line at the average mean position of the eight sensors. Hence it is essential that the PSD has a broad linear range in order to avoid any false signals before and during the experiment.

2.6.2 Calibration of the thermocouples

The thermocouples (Hygrosens SEMI833ET) used for the temperature controlled enclosure were calibrated against standard refrigeration unit and an incubator also using a mercury thermometer as an analogue reference.

The thermocouples follow a linear response to temperature (within the expected range of operation) which can be expressed as:

$$T = AV + B \tag{5}$$

where, T = temperature, V= thermocouple voltage and A & B are constants. Calibrations were performed for three sensors viz. room, chamber and box on each instrument (Fig.2.13). The results are summarized in Table 2.1.

Table 2.1: Thermocouple calibration values for two different setups

Instrument	**Calibration values**	
	A	**B**
NOSE 1		
Box	-21.7249	87.5955
Room	-21.7223	87.7387
Chamber	-21.6648	87.3983
NOSE 2		
Box	-22.6958	88.27274
Room	-23.9532	91.63786
Chamber	-23.6293	90.86761

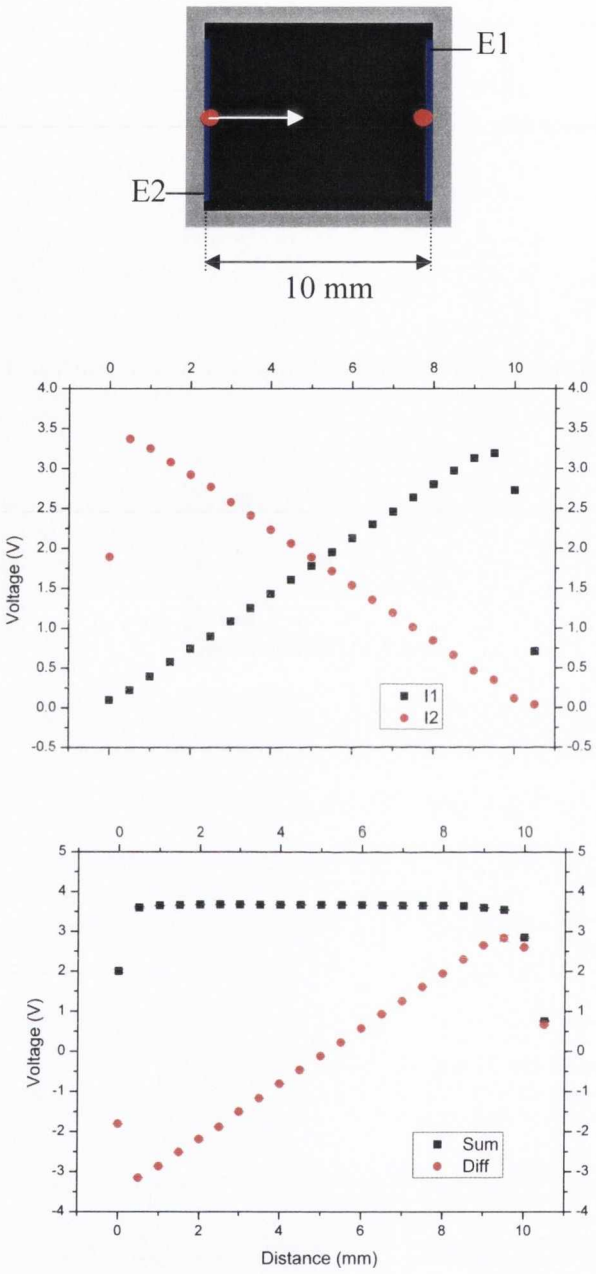

Fig. 2.12: Response characteristics of the SiTek PSD 10 mm length. Laser spot was moved across the PSD as shown above from one electrode to the other in order to determine the active linear length of the PSD. The active length of the PSD is ~ 9 mm with only the edges being non-linear. The laser spot for a measurement is placed as close as possible to the center of this linear range.

As can be seen in Fig 2.12, the PSD shows good linearity within the active length (nearly 9 mm). However, for an experiment, the PSD position is adjusted such that the laser spot is always placed in the middle of the PSD (Diff = 0), to ensure proper tracking of the change in position.

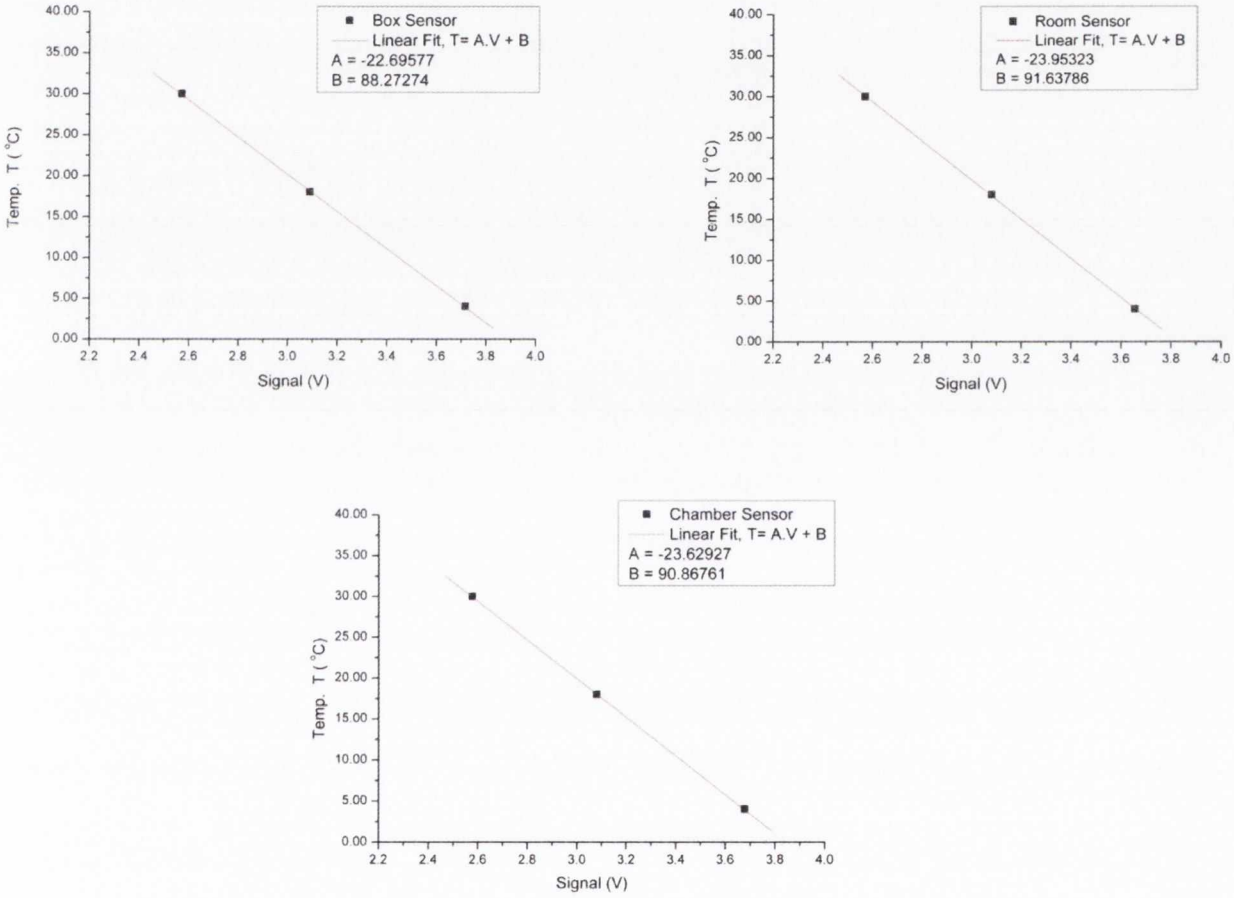

Fig. 2.13: Calibration of thermocouples for NOSE instrument 2. The calibration was performed using a standard refrigeration unit, an incubator and a mercury thermometer as analogue references. The values obtained from the linear fitting as per Equation 5 are then inserted into the LabVIEW® program hardware access file in order to convert the thermocouple signals to a temperature value.

References

1 Braun, T. *et al.* Digital processing of multi-mode nano-mechanical cantilever data. *Journal of Physics: Conference Series* **61**, 341 (2007).

2 Meyer, G. & Amer, N. M. Simultaneous Measurement of Lateral and Normal Forces with an Optical-Beam-Deflection Atomic Force Microscope. *Appl Phys Lett* **57**, 2089-2091 (1990).

3 Meyer, G. & Amer, N. M. Novel Optical Approach to Atomic Force Microscopy. *Appl Phys Lett* **53**, 1045-1047 (1988).

4 Wavelength Electronics, I. http://www.teamwavelength.com/info/temperaturecontrollers.php. (2008).

5 Newport-Corporation. Gaussian Beam Optics Tutorial. *http://www.newport.com/servicesupport/tutorials/default.aspx?id=112* (2012).

6 Andersson, H. Position Sensitive Detectors - Device Technology and Applications in Spectroscopy. *Mid Sweden University Doctoral Thesis 48* (2008).

7 Bakker, M. d. The PSD Chip – High Speed Acquisition of Range Images. *Ph.D. dissertation, Delft Univ. of Technol., Netherlands* (2000).

8 Braun, T. *et al.* Processing of kinetic microarray signals. *Sensor Actuat B-Chem* **128**, 75-82, doi:DOI 10.1016/j.snb.2007.05.031 (2007).

Chapter III

Sensor Functionalization and Process Optimization

3.1 Introduction

Biosensors can be broadly defined as the combination of a sensing layer, the transducer element and the recording unit. The sensing layer consists of the receptor molecule (DNA, protein etc.) while the transducer element is optical, electrical, magnetic, thermal, chemical or mechanical element that converts the interaction to a comprehensible signal. The interface between the sensor layer and the transducer is very crucial to the workings of the biosensor and an optimized surface chemistry and functionalization procedure are vital to its success. The key to a good interface lies in choosing the right surface chemistry, immobilization technique and surface activation methods and then optimising the conditions for high performance.

Nanomechanical cantilever biosensors used in this study detect RNA/DNA material using the principle of hybridization which eventually produces stress in the cantilever causing it to bend. The cantilever is functionalized with thiolated probe ssDNA

molecules that are anchored to the sensor surface. This is achieved using an intermediate gold layer between the underlying silicon sensor and the thiolated probe molecule. The thiol functional group from the probe molecule deprotonates upon adsorption to the gold surface to create a strong gold thiol bond[1].

$$ssDNA - SH + Au \rightarrow ssDNA - S - Au + e^- + H^+$$

Hence for optimal cantilever sensor performance, the following procedures had to be tested and optimized.

1. Cantilever silicon surface preparations
2. Interfacial gold layer
3. Pre-biofunctionalization surface activation

3.2 Cantilever surface preparation

Cantilever arrays that are obtained from the manufacturer (IBM Research Lab, Zürich) have particulate and organic contamination left over from the microfabrication process on the surface (as visualised using dark field microscopy). The cantilevers hence have to be pre-cleaned in order to get rid of these contaminants since their presence interferes with the proper optimal gold layer deposition on the cantilevers. The conventional protocol for this procedure uses cleaning with a 12% chlorinated trisodium phosphate and alkali phosphate surfactant (RBS™ 83463, Sigma Aldrich,DE) followed by piranha cleaning (detailed protocol in Appendix A1). This method had some shortcomings that had to be eliminated and the process optimised in order to obtain clean silicon surface before coating.

The first step involved using cleaning in RBS followed by a rinse in NaCl solution to get rid of the surfactant followed by rinse in Nanopure water for the salt removal. This posed a problem with the total removal of the salt deposits on the cantilevers using the rinse with Nanopure water. It was observed that the salt deposits take a very long time

to be removed from the cantilever surface following the RBS cleaning and can be difficult to get rid of completely in certain cases. Hence this step was abandoned in favour of using an initial exposure to UV-ozone cleaning for 2 mins (Boekel UV Clean Model 135500, low energy 0.5 Amp; UVC excitation at 184.9 nm in combination with 253.7 nm) followed by a long rinse in Acetone bath to get rid of surface organic contaminants and particulate matter. The method is adapted from standard protocols for silicon surface preparation from the semi-conductor industry and provided better results compared to the previous RBS steps[2].

The steps following after the initial RBS clean in the protocol use 50-50 mixture of hydrogen peroxide and 99.99% sulphuric acid (Piranha solution). This agent is a very effective oxidiser, removing most organics and hydroxylates from the surface rendering it hydrophilic. However, the solution is extremely hazardous because of its strong oxidising and acidic nature. Piranha solutions get very hot when freshly prepared and cannot be disposed of with any other organic laboratory waste since it can cause a substantial explosion and hence injury and burns to the user. In addition when used for cantilever cleaning, especially with the 500 nm thin cantilever sensors, the rapid gas bubble formation due to oxidation on the surface and the multiple number of subsequent cleaning steps with nanopure water and ethanol can cause permanent bending of the cantilevers. This poses a major problem with proper implementation of the sensor chip later on in the fluidics since the laser path after deflection from the cantilever can become out of bounds of the prism mirror/PSD arrangement due to geometry constraints.

In order to eliminate these shortcomings, an alternative protocol was introduced that uses plasma cleaning and a quick clean in a solvent thereafter. In order to oxidise the surface and remove organic contamination, a three minute oxygen plasma step was introduced[3]. The plasma cleaner essentially generates plasma which contains positive ions, electrons, neutral gas atoms or molecules, UV light and also excited gas atoms and molecules. Ultra-violet light generated in the plasma is very effective in the breaking most organic bonds of surface contaminants. A second action is the cleaning carried out by the energetic oxygen species created in the plasma. These species react with organic

surface contaminants to form mainly water and carbon dioxide which are continuously pumped away from the chamber during the process[4,5]. The plasma process is seen as a good alternative to wet chemical cleaning as discussed in the Table 3.1.

Table 3.1: Advantages of the plasma cleaning over piranha cleaning

Plasma Cleaning	**Wet chemical cleaning (Piranha protocol)**
Better process control in terms of power, gas pressure, processing time etc.	Process dependant on chemical preparation and user capability
Complete removal of organic residues	Reliability of the final surface quality depends on the proper neutralization and hence require post cleaning steps
Waste disposal is not a problem	Large volumes of mixed waste are produced which require proper disposal
Does not involves use of highly corrosive solutions	Involves use of highly explosive and corrosive solutions

The plasma cleaning was performed in the Diener PICO Barrel Asher using oxygen gas for the plasma operating at 0.3 mbar for 3 minutes at 160 W, 40 kHz power setting for the device. A new holder was designed for this purpose so as to avoid any physical damage to the cantilevers when placed in the Asher.

A new protocol was finally established that encompasses the aforementioned changes for cleaning of the silicon cantilever sensor chip (Details in Appendix A2). The protocol was used for all sensor chips prior to the deposition of the interfacial gold layer.

3.3 Functional gold layer deposition

The immobilization of probe molecules on the cantilever surface is done using thiol chemistry which requires a functional gold layer. The gold layer was deposited onto the

cantilever using two different methods viz. thermal deposition and e-beam deposition to find the most optimum method. In both methods a thin adhesion layer of titanium was used to avoid flaking of the gold surface from the silicon.

The thermal method was performed in the BOC Edwards Auto 500 deposition tool. A tungsten boat was used to melt gold which was then deposited onto the cantilever surface. The tool was pumped down initially to ~ $4.3x10^{-7}$ Torr and then operated at the following average parameters for the whole procedure: E-beam Titanium Coating of 2 nm: 47 mA, 0.02 nm/s, deposition pressure $1.4x10^{-6}$ Torr. Thermal Au coating of 20 nm: 10 mA, 0.02 nm/s, deposition pressure $5.0x10^{-5}$.

This method however posed some problems. The thermal gold deposition in the tool caused the target for the deposition to overheat hence causing permanent bending of the cantilevers (radiation heating from the tungsten boat at a distance of ~ 20 cm). Also since the device was not fully automated, precision control on the rate of deposition could not be obtained. In light of these shortcomings, the deposition of the metal layers was then switched to another device that offered far better control on the deposition parameters and caused no significant mechanical damage to the cantilevers.

The device finally used to deposit the functional gold layer on the cantilevers was the Temescal FC-2000 Evaporation System. The system posed several advantages over the previous method of thermal gold deposition in the Auto 500. The system allows fine power control hence providing better deposition rate control, better scanning control for uniform heat dissipation in the metal, interlocks for ease of operation etc. The cantilevers were deposited with gold/titanium in this system using the optimised parameters in Table 3.2 after several trials.

To determine the quality of the gold deposition, an AFM (Asylum MFP 3D) analysis was carried out to determine the roughness and the grain size of the gold surface in the tapping mode (Fig. 3.1). The scan was performed on the body of the chip from a regular deposition to provide a closest possible representation of the gold surface on a cantilever. The roughness analysis on the representative area gives an RMS Roughness

of ~ 0.8 nm (500 nm x 500 nm scan area) with a maxima and minima at 3.15 nm and 3.52 nm respectively. A sectional analysis for the grain size reveals a distribution of the sizes ranging from 20 nm to 50 nm averaging at 35 nm.

Table 3.2: Optimized system parameters for the Temescal Evaporation system for metal functionalization of the microcantilevers.

Parameter	**Ti Deposition**	**Au deposition**
Base Pressure (Torr)	$2x10^{-6}$	$2x10^{-6}$
Final thickness (nm)	2	21
Deposition rate (Å/s)	0.02	0.05
Deposition pressure (Torr)	$2x10^{-5}$	$2x10^{-5}$

After the functionalization, the cantilevers are finally stored in vacuum or argon in a sealed chamber (AS-One, Japan) to prevent any contamination and used within a week for further bio-functionalization.

3.4 Pre-bio functionalization surface activation

Freshly prepared gold surfaces are known to foul quickly under normal laboratory conditions due to the initial high surface energy that causes the adsorption of organic molecules from the environment[6,7]. When comparing the energy associated with the gold- thiol chemisorption (~40 kcal/mol)[8] to the heat of adsorption of an organic contaminant from air such as methane (~20 kcal/mol)[9], one concludes that such contaminants when pre-adsorbed on the gold surface will influence the self assembly process of the thiolated probe molecules[7].

To ensure proper surface functionalization, various methods have been used for cleaning of gold substrates that mostly involve strong oxidising agents: using chemical oxidizing solutions[10], electrochemistry[11], combinations of the two[12] and UV/ozone plasma treatment[13]. The UV Ozone cleaning[14] method is a photo-sensitized damage free

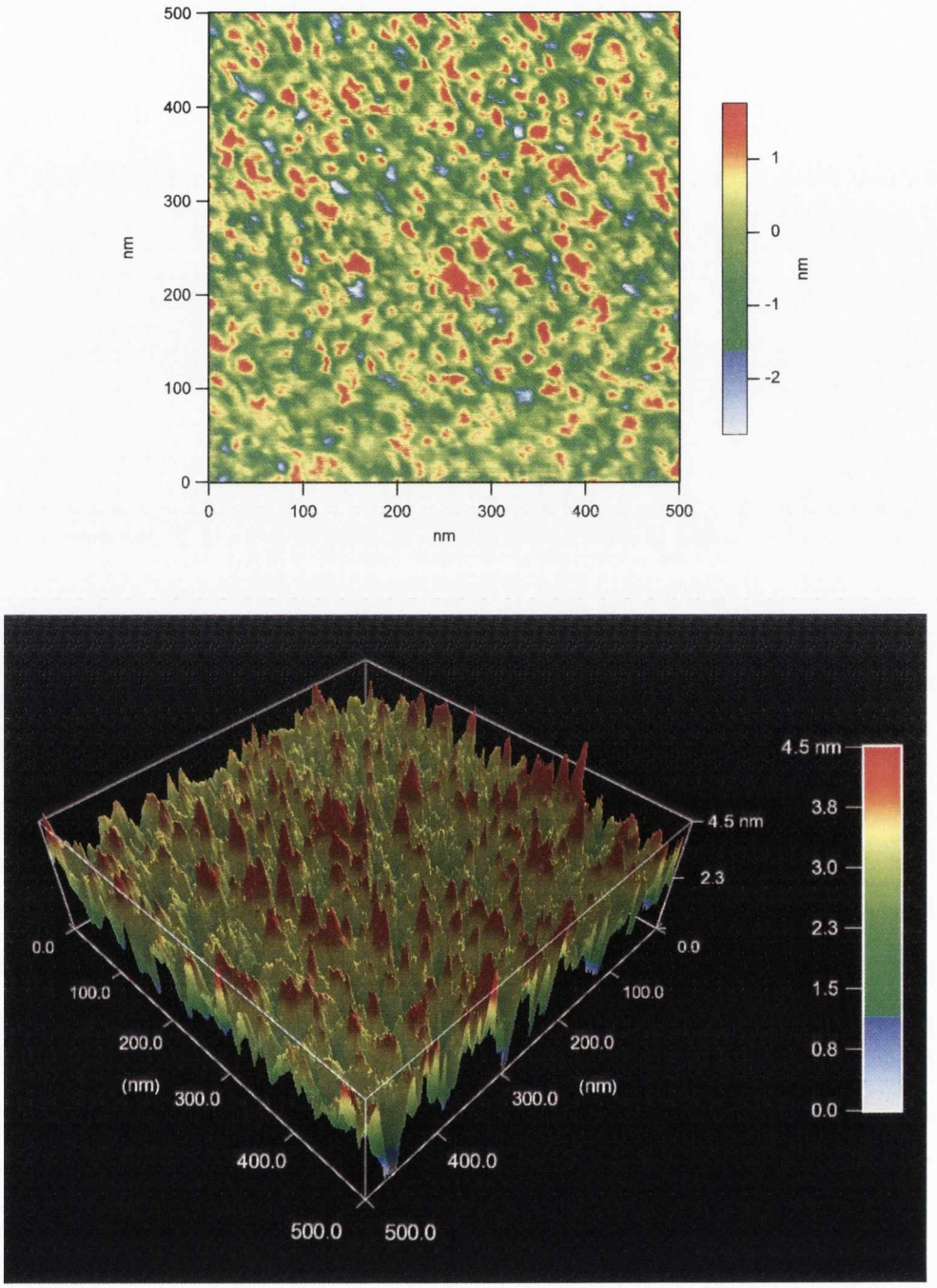

Fig. 3.1: AFM (Asylum MFP 3D) analysis of the Gold deposition on the cantilevers in tapping mode (500 nm x 500 nm scan area). RMS roughness analysis: 0.8 nm (maxima: 3.15 nm and minima 3.52 nm). Sectional grain size analysis reveals sizes varying from 20 to 50 nm (Average: 35 nm).

oxidation process in which substrate organic surface contaminant molecules are excited and/or dissociated by the absorption of short wavelength UV radiation. The surface organics react with oxygen radicals simultaneously generated in the system by the dissociation of molecular oxygen and ozone leading to products that desorb from the surface. For the purposes of activating the gold surface on the cantilevers, we choose the UV cleaning method for its ease of operation, lack of hazardous chemicals and no water-air interfacial crossing for the cantilevers which can cause cantilever bending as per previous experiences.

To test the efficiency of the UV/Ozone cleaning process, flat silicon substrates (1 cm x 1 cm) were Au/Ti coated using the Temescal tool as described in the previous pages. Three different configurations were tested. One coated substrate was exposed to a solution of 1-Octadecanethiol (Sigma Aldrich) in ethanol for 2 hrs, then blow dried with nitrogen and stored under argon for 24 hours; second was exposed to laboratory air for 24 hours and the third was stored under Argon immediately after the deposition process also for 24 hours. All the samples where then tested for water surface wettability visually, pre and post UV/Ozone treatment for 2 minutes each in a Boekel UV Clean system followed by rinse in 1:1: nanopure water : ethanol solution and blow dried under nitrogen.

The substrate treated with 1-Octadecanethiol in ethanol lead to a formation of the thiol self-assembled monolayer (SAM) on the surface. This rendered the surface hydrophobic which was evident from the very low surface wettability and high contact angle. Post UV/ozone cleaning showed very high hydrophilic nature and hence high wettability thus establishing that the cleaning was effective for removal of organic SAM layers from the gold. The second substrate that was exposed to laboratory conditions showed also a marked increase in wettability after the cleaning indicating the contamination on the gold layer when exposed to laboratory conditions. The third substrate that was stored immediately under argon after deposition did show slightly higher wettability after the treatment but the change was not as pronounced when compared to the previous samples indicating that storage under the inert gas did decelerate the rate of surface contamination. Previous studies[13-15] using this method to activate gold surface

report similar conclusions which have been verified using surface analytical techniques such as XPS etc.

3.5 Bio-functionalization

The cantilevers from the sensor array are tuned as transducers for biosensing by immobilization of specific probe molecules on the gold coated surface rendering them sensitive to binding/interaction events on the surface. The bio-functionalization is performed usually using two techniques for cantilevers viz. capillary functionalization and the ink jet method. We extensively utilise the capillary immersion method for our sensors.

3.5.1 Capillary method

The capillary method involves an instrumental setup that uses precisely arranged glass capillary tubes (ID 0.180 mm, OD 0.25 mm, length 75 mm, King Precision, USA) with a pitch matching that of the cantilever sensors on the array. Before setting up the arrangement for the capillaries, they are cleaned with 50:50 ethanol (HPLC grade): Nanopure Water in a Petri dish and then dried on a hot plate. This is followed by oxygen plasma cleaning of the capillaries (Asher, USA) for 5 mins at 0.3 mbar chamber pressure. This ensures clean and debris-free capillaries which are also rendered highly hydrophilic and hence facilitate easier liquid siphoning from the reservoir. The cantilevers are then functionalised by insertion into the capillaries which are filled with thiolated probe molecules that are suspended in an appropriate buffer solution to facilitate the immobilization of the probes on to the gold surface (Fig. 3.2). Different probes can be used at the same time to functionalize the chip making it possible to have varied probes and references on the same sensor chip. One of the downsides of this method is that the complete insertion of the asymmetrically gold functionalized cantilever into the probe solutions leads to interaction of the probes with the bare silicon side.

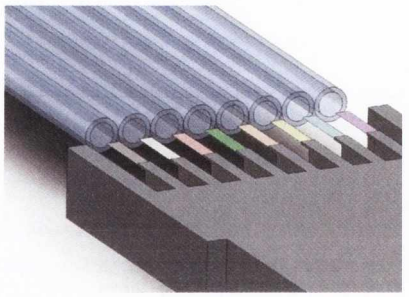

(a)

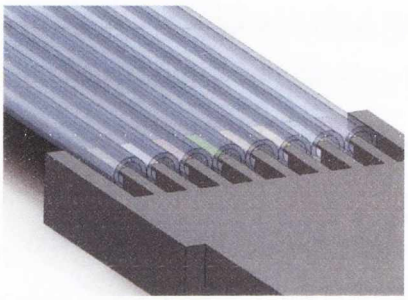

(b)

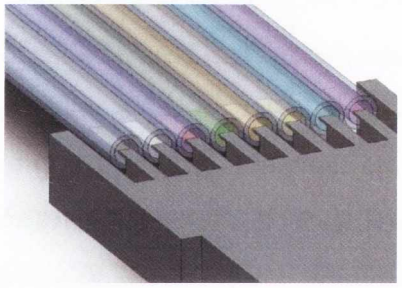

(c)

Fig 3.2: Capillary functionalization of microcantilever array. Parts a) and b) represent the setting up of the cantilevers in line with the capillaries in a custom made instrument while c) represents the cantilever functionalization using different probe solutions allowing multiple probe and control assays.

The capillaries are filled in from reservoirs of the functionalising solution comprising 50 mM Triethylammonium acetate buffer (TEAA) + Probe oligonucleotides at one end while having the cantilever sensors immersed at the other. The array is functionalized

for 30 mins followed by washing step in 50 mM TEAA for 5 mins to remove unbound molecules and then stored in the hybridization buffer for further use. In certain cases, after the surface activation with the UV Ozone cleaning, the cantilevers exhibited some bending that was found to be related to charge accumulation on the surface. This was dealt with by grounding the sensor chip once it was mounted on the capillary functionalization setup prior to capillary insertion.

3. 6 Conclusions

A visual summary of the process for the functionalization is seen in Fig 3.3. This is one of the most crucial steps in the cantilever diagnostic device development. The formation of the self-assembled monolayer of the probes on the cantilever surface is essential for obtaining a clear and reproducible hybridization signal. To ensure this every step was optimised right from the pre-cleaning to the final cantilever bio-functionalization. This included improvement on the cleaning steps (introduction of plasma cleaning), highly controlled deposition of the metal functional layer, pre-cleaning prior to bio-functionalization and optimised capillary method.

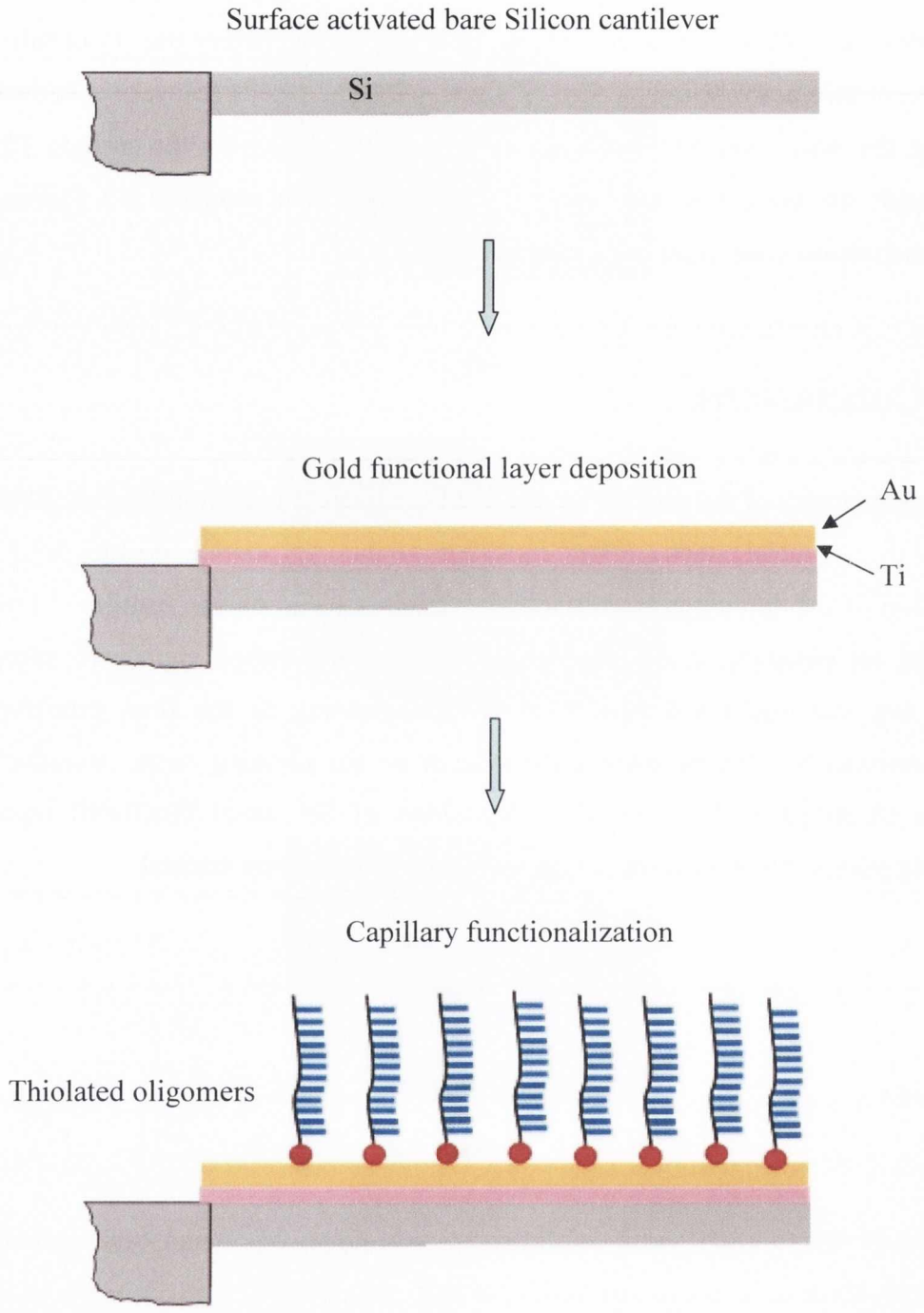

Fig 3.3: Schematic summary of the Cantilever sensor functionalization process depicting (not to scale) the surface activation and surface functionalization. Functionalized cantilevers with probes were stored in the hybridization buffer (SSC 1X 1M NaCl or Gibco PBS 1X) prior to the experiments to equilibrate.

References

1 Luderer, F. & Walschus, U. Vol. 260 *Topics in Current Chemistry* (ed Christine Wittmann) 37-56 (Springer Berlin / Heidelberg, 2005).

2 Reinhardt, K. A., Reidy, R. F. & Wiley, I. *Handbook of cleaning in semiconductor manufacturing fundamentals and applications*, <http://dx.doi.org/10.1002/9781118071748> (2011).

3 Reinhardt, K. A. & Kern, W. *Handbook of silicon wafer cleaning technology*, <http://www.knovel.com/knovel2/Toc.jsp?BookID=2225> (2008).

4 Hook, D. A., Ohlhausen, J. A., Krim, J. & Dugger, M. T. Evaluation of Oxygen Plasma and UV Ozone Methods for Cleaning of Occluded Areas in MEMS Devices. *J Microelectromech S* **19**, 1292-1298, doi:Doi 10.1109/Jmems.2010.2067193 (2010).

5 Lin, Y.-S. A surface analysis on oxygen plasma-cleaned gold pattern-plated substrates for wire bondability. *Surface and Coatings Technology* **173**, 47-57, doi:10.1016/s0257-8972(03)00508-5 (2003).

6 Smith, T. The Hydrophilic Nature of a Clean Gold Surface. *J Colloid Interf Sci* **75**, 51-55 (1980).

7 Bain, C. D. *et al.* Formation of Monolayer Films by the Spontaneous Assembly of Organic Thiols from Solution onto Gold. *J Am Chem Soc* **111**, 321-335 (1989).

8 Dubois, L. H. & Nuzzo, R. G. Synthesis, Structure, and Properties of Model Organic-Surfaces. *Annu Rev Phys Chem* **43**, 437-463 (1992).

9 Trapnell, B. M. W. The Activities of Evaporated Metal Films in Gas Chemisorption. *Proc R Soc Lon Ser-A* **218**, 566-576 (1953).

10 Evans, S. D., Sharma, R. & Ulman, A. Contact-Angle Stability - Reorganization of Monolayer Surfaces. *Langmuir* **7**, 156-161 (1991).

11 Strong, L. & Whitesides, G. M. Structures of Self-Assembled Monolayer Films of Organosulfur Compounds Adsorbed on Gold Single-Crystals - Electron-Diffraction Studies. *Langmuir* **4**, 546-558 (1988).

12 Finklea, H. O., Snider, D. A. & Fedyk, J. Passivation of Pinholes in Octadecanethiol Monolayers on Gold Electrodes by Electrochemical Polymerization of Phenol. *Langmuir* **6**, 371-376 (1990).

13 Samant, M. G., Brown, C. A. & Gordon, J. G. Structure of an Ordered Self-Assembled Monolayer of Docosyl Mercaptan on Gold(111) by Surface X-Ray-Diffraction. *Langmuir* **7**, 437-439 (1991).

14 Ron, H., Matlis, S. & Rubinstein, I. Self-Assembled Monolayers on Oxidized Metals. 2. Gold Surface Oxidative Pretreatment, Monolayer Properties, and Depression Formation. *Langmuir* **14**, 1116-1121, doi:10.1021/la970785v (1998).

15 Ron, H. & Rubinstein, I. Alkanethiol Monolayers on Preoxidized Gold. Encapsulation of Gold Oxide under an Organic Monolayer. *Langmuir* **10**, 4566-4573, doi:10.1021/la00024a030 (1994).

Chapter IV

Calibration Factor, G

Cantilever array based sensor devices widely utilise the laser based optical deflection method for measuring static cantilever deflections mostly with home built devices with individual geometries. In contrast to scanning probe microscopes[1,2], cantilever array devices have no additional positioning device such as a piezo-stage. As the cantilevers are used in more and more sensitive measurements, it is important to have a simple, rapid and reliable calibration relating the deflection of the cantilever to the change in position measured by the position sensitive detector. We developed a simple method for calibrating such systems utilising commercially available AFM cantilevers and the equipartition theorem.

4.1 Introduction

Cantilever based sensor devices have extensively developed from the atomic force microscope (AFM) operating in the static mode[3-5] (surface stress based; qualitative method) and the dynamic mode[6-8] (frequency based; quantitative method) depending on the application. The most frequently used method of signal transduction where cantilevers are employed is change in surface stress being converted into a mechanical

signal through cantilever bending[9]. This deflection is an indication of the chemical[10], physical[11] or biophysical[12] process that occurs on the cantilever interface.

The laser beam based deflection system[13] has been used most widely to measure the cantilever bending in the static mode because of the ease of use, robustness of the readout technique and availability of high sensitivity position sensitive detectors (PSD) which allow sub angstrom resolution[14,15]. Subsequently several studies have been made to determine the limitations of this technique along with its resolution and sensitivity[16-19]. One also comes across various techniques for determining the relation between the cantilever bending and the change in spot position observed by the PSD[20-23]. The simple geometric calculation of this factor safely presumes that the bending of the cantilever is very small such that it can be assumed to be half that of the deflection angle of the laser beam[22]. Most other methods are tedious and require specialised methods[20] for determining this factor and may additionally require precise measurement of the angles[24] (azimuthal and incidence), distance between the cantilever surface and the PSD etc. which gets more complicated for beam directing methods with complex geometries using mirrors. Discussed here is a simple plug & measure system for determining this deflection factor (G) using commercially available AFM cantilevers and applying the equipartition theorem for small cantilever deflections.

The displacement of the laser spot on the PSD (Δd) can be related to the cantilever bending (Δx) using geometrical methods[22]. Fig 4.1 is a schematic representation (not to scale) of the laser path. As all the angles are very small, it can be assumed that the bending angle of the cantilever is equal to half the deviation of the deflected beam, Θ. Hence the slope of the lever can be calculated as,

$$\frac{\Theta}{2} = \frac{\Delta d}{2s} \tag{1}$$

where s is the distance from cantilever to the PSD.

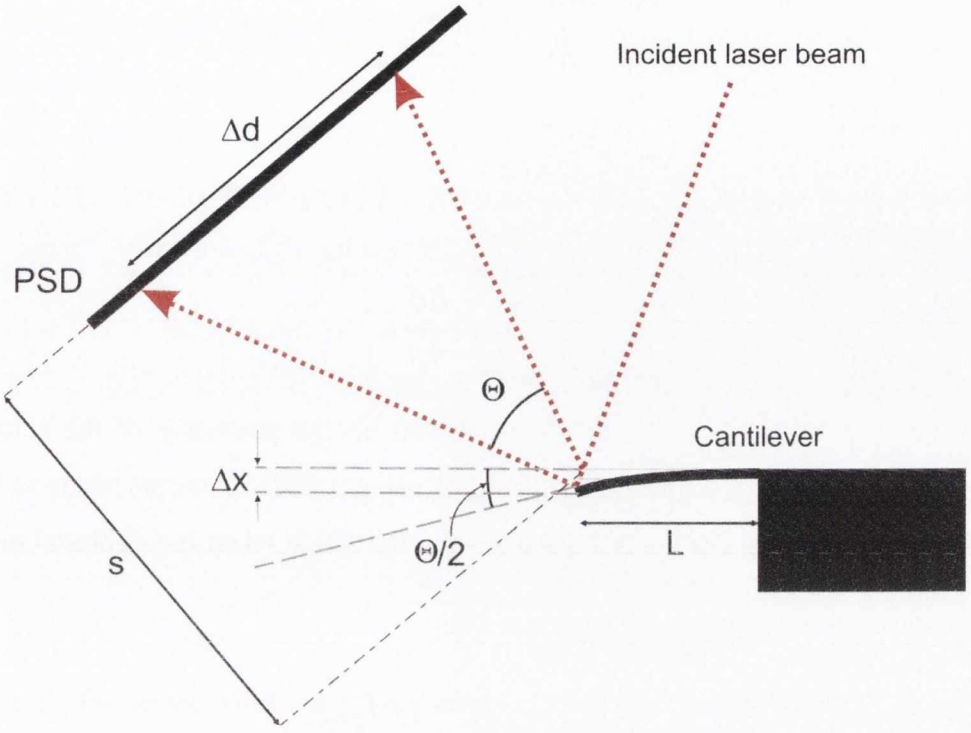

Fig. 4.1: Schematic representation of the geometry of the laser deflection setup. The bending of the cantilever represented by Δx is measured by the PSD as Δd. The active length of the PSD is l_{psd}.

When a bending moment M applied to the free end of the rectangular cantilever causes a deflection angle of $\Theta/2$ and a deflection of Δx, they can be defined as[25,26]

$$\left(\frac{\theta}{2}\right) = \frac{ML}{EI}$$

$$\Delta x = \frac{ML^2}{2EI}$$

where E is the elastic modulus, I is the moment of inertia and L is the length of the cantilever. Combining above equations, the small deflection Δx can be defined then as,

$$\Delta x = \frac{\theta/2}{2} L \tag{2}$$

By combining the equations 1 and 2,

$$\Delta x = \frac{\Delta d}{4s} L \tag{3}$$

Hence, the value of Δx can be calculated based on the geometry of the setup. The absolute relationship used for relating Δx (nm) using a PSD, however needs to include the geometrical factor needed for a particular setup which when incorporated gives the relationship as below.

$$\Delta x = G \frac{I_1 - I_2}{I_1 + I_2} \frac{l_{psd}}{2} \tag{4}$$

where I_1-I_2 is the difference signal and I_1+I_2 is the sum signal obtained from the PSD and l_{psd} is the active PSD length in mm. It is important to note that Δd (nm) for a PSD is generally defined as (when l_{psd} is defined in mm)

$$\Delta d = \frac{I_1 - I_2}{I_1 + I_2} \frac{l_{psd}}{2} 10^6 \tag{5}$$

Equation 3 gives purely a geometrically calculated value with the aforesaid assumption that if the deflection angle of the laser is Θ, the cantilever bending angle is $\Theta/2$; it includes errors arising from differences in design and actual geometry such as the position and angle of the laser, the angle of the cantilever holder and the reflecting mirror and the placement of the PSD. A more rigorous approach is needed to take into account not just the theoretical factors but also practical constraints of the setup.

The equipartition theorem relates the thermal energy of a system to its temperature in classical thermodynamics. Thermal noise of a cantilever can be quantified using this

theorem[27,28]. The equipartition theorem states that if a system is in thermal equilibrium every independent quadratic term in its total energy has a mean value equal to $1/2k_BT$ where k_B is the Boltzmann constant, T is the absolute temperature. The equipartition theorem relates this total energy to the potential energy of a rectangular cantilever with a mean square deflection of the cantilever caused by thermal vibrations as follows[29]

$$\frac{1}{2}\kappa\langle x^2\rangle = \frac{1}{2}k_bT$$

$$\therefore \langle x^2\rangle = {k_bT}/{\kappa} \tag{6}$$

where κ is the spring constant of a rectangular cantilever with finite thickness and length provided the bending is small. From Equation 6, one can determine the average thermal displacement of a cantilever provided the spring constant is known. The deflection factor can hence be calculated if this thermal displacement can be related to the deflection obtained on a PSD.

Combining Equations (4) and (6)

$$\left[G\,\frac{I_1 - I_2}{I_1 + I_2}\,\frac{l_{psd}}{2}\right]^2 = {k_bT}/{\kappa}$$

Hence deflection factor,

$$G = \frac{2}{l_{psd}}\sqrt{\frac{k_bT}{\kappa\left(\frac{I_1 - I_2}{I_1 + I_2}\right)^2}} \tag{7}$$

The term $\left(\frac{I_1-I_2}{I_1+I_2}\right)^2$ in the above equation is obtained from the PSD signals, using a power spectral analysis program (Virtual instrument, Labview, National Instruments)

normalized to the sum signal of the PSD, and is the area under the first resonance peak of a cantilever beam of known spring constant. The program essentially obtains the power spectrum which is a computation of the single-sided, scaled spectrum of the time domain signal from the PSD into the frequency domain. For a signal *x(t)*, the complex spectrum is obtained by a Fast Fourier Transform (FFT) defined as (in the frequency domain):

$$X(f) \equiv \int_{-\infty}^{+\infty} x(t)e^{-2\pi ft}\,dt$$

This gives furthermore the definition of the one sided power spectrum (in Sq. Amplitude/Hz) which is defined as:

$$Powerspectrum, \phi(f) \equiv |X(f)|^2/n^2 \equiv |X(f)||X(f)|^*/n^2$$

where *n* is the number of points in the signal and * denotes the complex conjugate. The integral of the power spectrum (area under the curve) provides the final value according to the Parseval's theorem which states that the area under the energy spectral density curve is equal to the total energy[30].

It is important to note that only the area under the first resonance peak is considered in further measurements, neglecting the higher modes since their contribution was seen to be minor (modelled as a simple harmonic oscillator with one degree of freedom). The spring constant of the calibration cantilevers hence needs to be measured as well. There are several methods available to perform such calibration to obtain spring constants[31-37] including the most frequently used thermal noise method. We have chosen the thermal calibration module in the Asylum MFP-3D AFM[38,39] (Asylum research, USA) which has been shown to measure the values with relatively good accuracy and reproducibility[39]. The method records the change in PSD position as a function of cantilever angular bending when pressed against a hard surface using a closed loop piezo actuator and then converts it into values for cantilever spring constant using a pre-

determined sensitivity factor called inverse optical lever sensitivity. With the rest of the terms known in the Equation 7, the calibration factor can be calculated.

4.2 Materials and methods

Different sets of commercially available AFM cantilevers were used viz. Mikromasch CSC38/AIBS "B" (Mikromasch, Estonia) and NTMDT CSCS12 "E" (NT-MDT, Russia) cantilevers for the measurement of the thermal noise spectrum and final calibration (Fig.4.2). The cantilevers were calibrated using the Asylum MFP-3D AFM to get individual values for their spring constant, κ (Table 4.1)

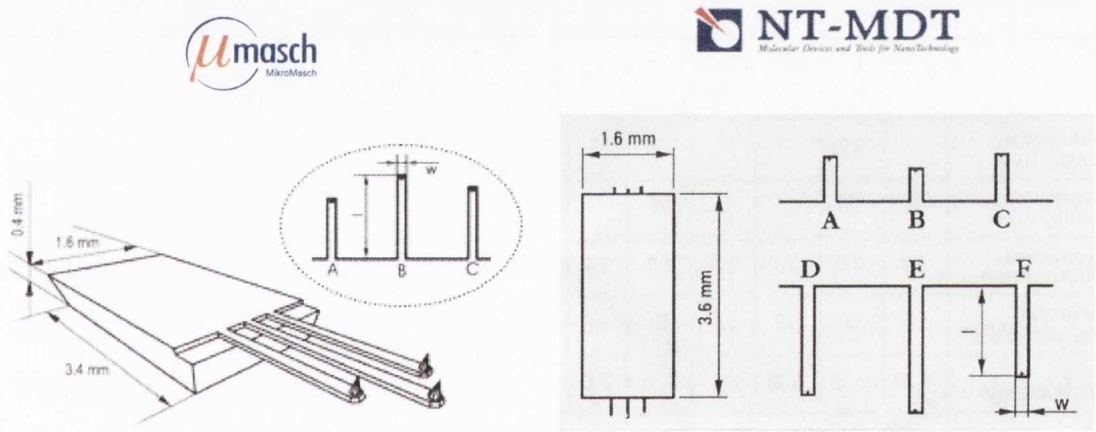

Fig. 4.2: Cantilever chips used for the calibration. The NTMDT cantilever chip is 0.45 mm thick while the Micromasch is 0.4 mm thick. Cantilever B was used from the Micromasch chip while cantilever E was used from the NTMDT chip.

The cantilevers were recalibrated using the Asylum MFP-3D to get individual values. Since the cantilevers did not fit exactly into the experimental chamber (the chamber is designed for the IBM cantilever array which are thicker and wider), separate holders were used for the cantilevers to make them fit in so as to maintain the right position of the AFM cantilevers in the cell like the cantilever array. The holders were designed

using Solidworks® software and fabricated using the EDEN 250 polymer 3D prototyper (Objet, Israel).

Table 4.1: Manufacturer specifications of the cantilevers used for calibration factor measurement.

Specifications	**Mikromasch CSC38/AIBS "B"**			**NTMDT CSCS12 "E"**		
	Min	**Typical**	**Max**	**Min**	**Typical**	**Max**
Length (*l*) μm		350			350	
Width (*w*) μm		35			35	
Thickness, μm	0.7	1.0	1.3	0.9	1.0	1.1
Resonant Freq. (kHz)	7	10	14	8	10	12
Force constant (N/m)	0.01	0.03	0.08	0.02	0.03	0.04

The power spectrum of the thermal noise was obtained using a 150kHz band pass position sensitive detector (SiTek, Sweden). This detector is a modified version of the low pass 5Hz sensor which is used for performing static mode biological experiments. The PSD amplification electronics was modified with the 150 kHz as the cut-off frequency (f_c) by changing the RC circuits so as to match the required range. Since the cantilevers chosen for calibration had an expected range of first order resonance frequencies between 7 and 14 kHz, the 150 kHz limit was large enough to encompass all the necessary modes for the peak area calculations. The cut-off frequency is given by the following equation for the RC based amplification circuit.

$$f = \frac{1}{2\pi RC}$$

where R– Resistance (in ohms), C– Capacitance (in Farads). Hence for R = 10KΩ and C = 100 pF, a cut-off of 159.13 kHz was attained (Appendix A3 shows the modified design).

A LabVIEW® program was used to obtain the averaged power spectrum from the differential and sum signals from the PSD. The parameters for obtaining the power spectrum had to be chosen so as to eliminate effects such as aliasing which leads to truncated or artificially small resonance peaks and also electronic noise. Also it was necessary to choose the number of samples and the sampling frequency such that it avoided overloading the system and the data acquisition card (DAQ, National instruments). A study of the influence of the number of samples on the area under the peak was conducted to find an optimal sample acquisition rate. Keeping in mind all these details and following the Nyquist theorem[40] (signal must be sampled at a rate at least greater than twice the highest frequency component of the signal) the parameters which were chosen for the power spectral analysis were as follows: Sampling frequency: 100 kHz, Number of samples: 10,000 and Number of averages: 5000. The area under the first resonance peak was obtained using a Lorentzian fit in Origin graphical software (OriginLab Corporation, USA). The area hence calculated along with the spring constant values was then used to determine the value of G for a particular setup. Two different cantilevers were used for the calibration of each setup with three trials on each cantilever and the values were finally averaged (Fig. 4.3). Between each trial the cantilever was taken out of the holder chamber and reinserted. The laser power and the temperature of the chamber were kept constant for all trial measurements.

Lorentzian peak fitting function:

$$y = y_0 + \frac{2A}{\pi}\left[\frac{w}{4(x - x_c)^2 + w^2}\right]$$

where, y_0 = baseline offset, A = total area under the curve from the baseline, x_c = centre of the peak, w = full width at half maximum (FWHM).

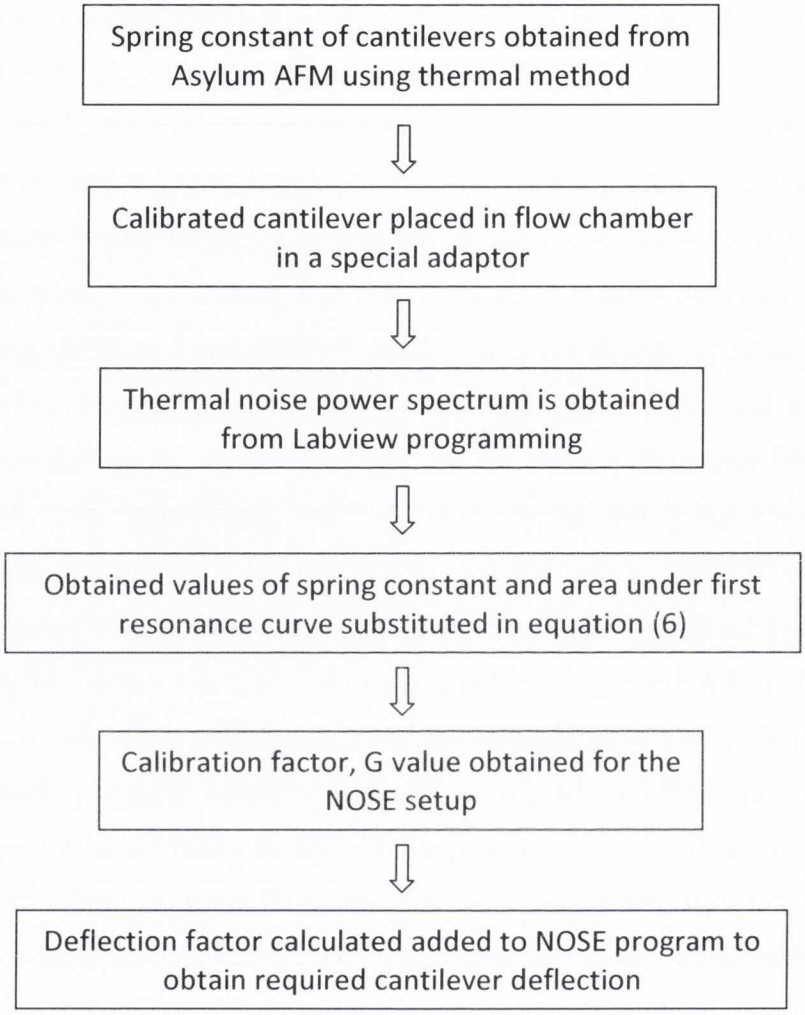

Figure 4.3: Calibration Protocol for the laser based deflection mechanism of the microcantilever based sensor setup using AFM cantilevers.

4.3 Results

4.3.1 Geometric method for calibration factor

For our present instrumental scheme, the geometrical calculation for both the setups is the same as derived below. For: s = 61 mm (for instrument 1 and 2) and L = 500 μm Equation 3 can be modified to obtain the following,

$$\Delta x = \frac{\Delta d}{488}$$

Substituting Δd from Equation (5)

$$\Delta x = 2049 \frac{I_1 - I_2}{I_1 + I_2} \frac{l_{psd}}{2} \tag{8}$$

Comparing equations (4) and (8) the deflection factor G from geometric calculations is 2049 for the particular geometry and is the same for any instrument made to this scheme. The value of L has a variation of 2% in the manufacturing and will be reflected in the geometric factor.

4.3.2 Calibration factor *G* using Equipartition theorem

4.3.2.1 Determination of spring constants for the cantilevers using Asylum AFM

The spring constants for the calibration cantilevers were determined as an average of three trials during which the cantilevers were removed and replaced in the AFM setup in order to average out errors. A typical example of the thermal calibration in the AFM is shown in Fig. 4.4. The averaged values of the cantilevers are summarised in Table 4.2.

4.3.2.2 Thermal noise data acquisition from the instrumental setups

Calibration factor, G was calculated for two different deflection setups both identical with respect to geometrical design using the previously mentioned cantilever sets. The powerspectrum was obtained when keeping the differential signal as close as possible to zero (centre of the PSD) and the sum signal as high as possible. Fig. 4.5 shows a sample powerspectrum obtained for Cantilever E1 on the second trial.

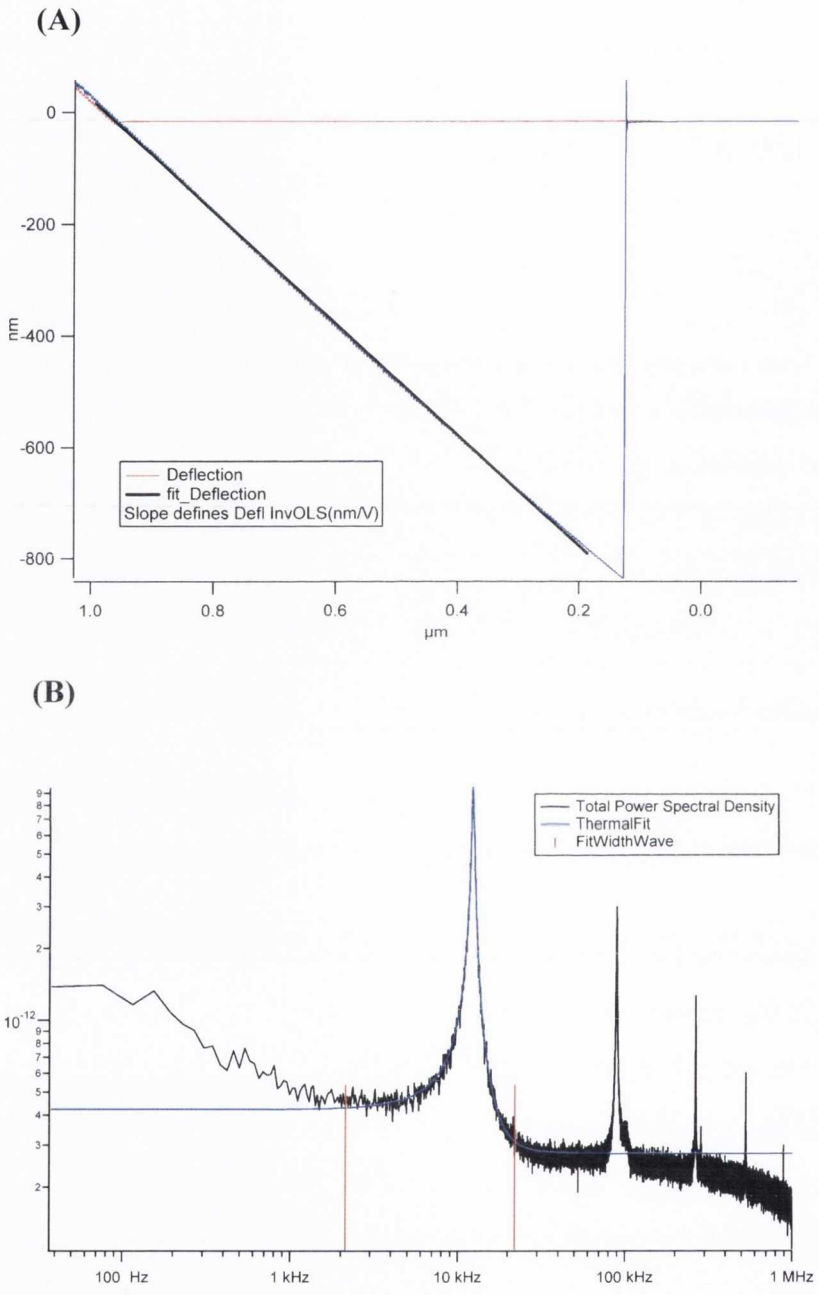

Fig. 4.4: Thermal method for spring constant calculation from the Asylum AFM for Micromasch cantilever B1. A) Force curve obtained from the AFM for calculating the calibration of the deflection on the AFM detector in nm/V. B) Thermal power spectrum of the cantilever in air showing the resonance peak and a Lorentzian fit (blue trace) on the noise data.

Table 4.2: Spring constants κ of the calibration cantilevers obtained from a thermal calibration using the Asylum AFM.

	Micromasch B cantilevers			
	Trial 1	Trial 2	Trial 3	Average
Cant B1				
Defl InvOLS (nm/V)	128.98	134.59	132.84	
f_{res} (kHz)	12.168	12.168	12.168	
κ (pN/nm)	68.77	69.08	71.12	69.66
Cant B3				
Defl InvOLS (nm/V)	141.56	150.53	146.59	
f_{res} (kHz)	16.896	16.936	16.936	
κ (pN/nm)	170.78	159.61	169.82	166.74

	NTMDT Cantilevers E				
	Trial 1	Trial 2	Trial 3	Trial 4	Average
Cant E1					
Defl InvOLS (nm/V)	291.14	271.83	308.69	208.07	
f_{res} (Hz)	11100	11060	11024	11100	
κ (pN/nm)	31.53	31.85	33.86	33.33	32.64
Cant E3					
Defl InvOLS (nm/V)	289.71	360.68	425.94	297.47	
f_{res} (Hz)	12779	12740	12779	12779	
κ (pN/nm)	53.74	53.4	50.79	54.6	53.13

According to the power spectrum analysis, we relate the vibrational amplitude in ambient air to the spring constant using Equation 6. Table 4.3 summarizes the results for the calibration of the instruments using the above set of cantilevers and substituting the values of the spring constant and the area under the power spectrum in to Eq. 7.

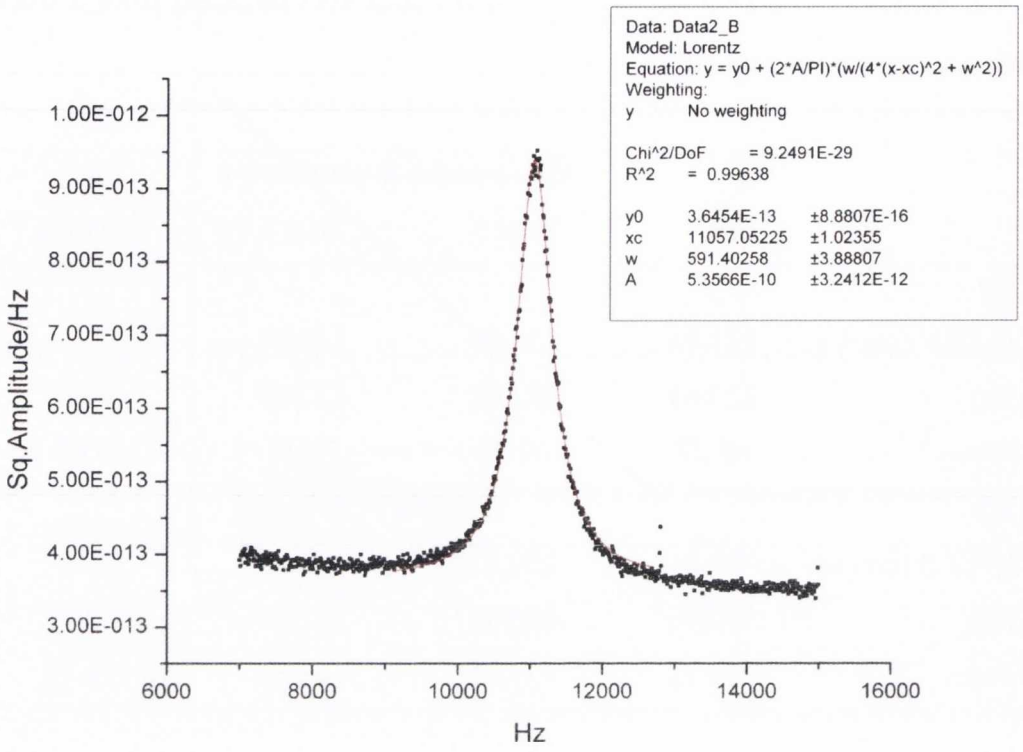

Fig 4.5: Thermal noise powerspectrum of NTMDT cantilever E1 on trial 2 for calibration of Setup 2. The area obtained under the peak after a Lorentzian fit (uniform broadening and best fitting parameters) is later used for determining the calibration factor.

From the set of values of the *G* factor (Table 4.3), it can be seen that the two setups differ from the theoretical geometric value and also from each other. The difference between the two values (the value of *s* differs by ~13.518 mm between the two when back calculated from the obtained calibration factors) indicates that the two setups despite having similar geometry have different travel lengths of the laser from the cantilever surface to the PSD. This could be attributed mainly to the change in position & tilt of the mirror, small differences in the setting up & machining of the home made systems and angles of the cantilever holders and hence the manner in which the lasers spot is reflected by the mirror onto the PSD. It is hence important to note that modifications of any kind to such laser deflection systems require a recalibration especially when the differential measurements are close ranged. When compared to results from the geometric method, it is clear that the method we propose shows the

variation between individual deflection setups despite their similar geometric design within reasonable error margins (5-10%).

Table 4.3: Calibration factors for the Cantilever deflection Setups

		Deflection factor *G* SETUP 1		
		Area under curve	***G***	**Average *G***
Cant B1				
(κ = 69.66 pN/nm)	Trial 1	5.20E-10	2128	**2077.5**
	Trial 2	4.51E-10	2284	SE 57.8
	Trial 3	4.98E-10	2175	
Cant B2				
(κ =166.74 pN/nm)	Trial 1	2.49E-10	1986	
	Trial 2	2.50E-10	1982	
	Trial 3	2.70E-10	1910	

		Deflection factor *G* SETUP 2		
		Area under curve	***G***	**Average *G***
Cant E1				
(κ = 32.64 pN/nm)	Trial 1	7.93E-10	2517	**2679.5**
	Trial 2	5.36E-10	3062	SE 114.3
	Trial 3	6.01E-10	2891	
Cant E3				
(κ = 53.13 pN/nm)	Trial 1	3.92E-10	2807	
	Trial 2	5.50E-10	2368	
	Trial 3	5.22E-10	2432	

(SE denotes standard error)

4.4 Conclusions

The importance of having sensitive measurements especially in systems involving a differential analysis is of foremost significance for ensuring the reliability of cantilever sensor systems. Establishing the occurrence of an event of interest on the cantilever surface using *in situ* reference cantilevers is absolutely essential to eliminate convoluted environmental signals. Hence a reliable method to calibrate the deflection of the cantilever is mandatory.

We demonstrate here a simple and reliable method for rapid calibration of laser based deflection systems. Using commercially available AFM cantilevers we can show that the relationship between the spot movement on the PSD and the actual cantilever deflection can be determined although within the accuracy of the assumptions and the thermal calibration method (~5-10%)[41]. The method was used to calibrate comparable cantilever array systems with a mirror used for deflecting the laser onto the PSD because of space restrictions. This indicates the application of the method to more complex geometries without the need for accurate measurement of other physical parameters of the geometry.

References

1 Binnig, G., Quate, C. F. & Gerber, C. Atomic Force Microscope. *Physical Review Letters* **56**, 930-933 (1986).

2 Binnig, G., Rohrer, H., Gerber, C. & Weibel, E. Tunneling through a controllable vacuum gap. *Applied Physics Letters* **40**, 178-180 (1982).

3 Watari, M. *et al.* Investigating the molecular mechanisms of in-plane mechanochemistry on cantilever arrays. *J Am Chem Soc* **129**, 601-609, doi:Doi 10.1021/Ja065222x (2007).

4 Huber, F., Hegner, M., Gerber, C., Guntherodt, H. J. & Lang, H. P. Label free analysis of transcription factors using microcantilever arrays. *Biosens Bioelectron* **21**, 1599-1605, doi:DOI 10.1016/j.bios.2005.07.018 (2006).

5 Mertens, J. *et al.* Label-free detection of DNA hybridization based on hydration-induced tension in nucleic acid films. *Nature Nanotechnology* **3**, 301-307 (2008).

6 Tabard-Cossa, V., Godin, M., Beaulieu, L. Y. & Grutter, P. A differential microcantilever-based system for measuring surface stress changes induced by electrochemical reactions. *Sens. Actuator B-Chem.* **107**, 233-241 (2005).

7 Braun, T. *et al.* Quantitative time-resolved measurement of membrane protein-ligand interactions using microcantilever array sensors. *Nature Nanotechnology* **4**, 179-185, doi:Doi 10.1038/Nnano.2008.398 (2009).

8 Ilic, B., Yang, Y. & Craighead, H. G. Virus detection using nanoelectromechanical devices. *Applied Physics Letters* **85**, 2604-2606, doi:Doi 10.1063/1.1794378 (2004).

9 Wu, G. H. *et al.* Origin of nanomechanical cantilever motion generated from biomolecular interactions. *P Natl Acad Sci USA* **98**, 1560-1564 (2001).

10 Gimzewski, J. K., Gerber, C., Meyer, E. & Schlittler, R. R. Observation of a Chemical-Reaction Using a Micromechanical Sensor. *Chem Phys Lett* **217**, 589-594 (1994).

11 Berger, R., Gerber, C., Gimzewski, J. K., Meyer, E. & Guntherodt, H. J. Thermal analysis using a micromechanical calorimeter. *Applied Physics Letters* **69**, 40-42 (1996).

12 Braun, T. *et al.* Conformational change of bacteriorhodopsin quantitatively monitored by microcantilever sensors. *Biophys J* **90**, 2970-2977, doi:DOI 10.1529/biophysj.105.072934 (2006).

13 Meyer, G. & Amer, N. M. Novel Optical Approach to Atomic Force Microscopy. *Applied Physics Letters* **53**, 1045-1047 (1988).

14 Alexander, S. *et al.* An Atomic-Resolution Atomic-Force Microscope Implemented Using an Optical-Lever. *J Appl Phys* **65**, 164-167 (1989).

15 Walther, K. A., Brujic, J., Li, H. B. & Fernandez, J. M. Sub-angstrom conformational changes of a single molecule captured by AFM variance analysis. *Biophys J* **90**, 3806-3812, doi:DOI 10.1529/biophysj.105.076224 (2006).

16 Putman, C. A. J., Degrooth, B. G., Vanhulst, N. F. & Greve, J. A Theoretical Comparison between Interferometric and Optical Beam Deflection Technique

for the Measurement of Cantilever Displacement in Afm. *Ultramicroscopy* **42**, 1509-1513 (1992).

17 Lee, E. J., Park, Y., Kim, C. S. & Kouh, T. Detection sensitivity of the optical beam deflection method characterized with the optical spot size on the detector. *Curr. Appl. Phys.* **10**, 834-837.

18 Garcia-Valenzuela, A. & Villatoro, J. Noise in optical measurements of cantilever deflections. *J Appl Phys* **84**, 58-63 (1998).

19 GarciaValenzuela, A. Limits of different detection schemes used in the optical beam deflection method. *J Appl Phys* **82**, 985-988 (1997).

20 Hu, Z. Y., Seeley, T., Kossek, S. & Thundat, T. Calibration of optical cantilever deflection readers. *Rev Sci Instrum* **75**, 400-404, doi:Doi 10.1063/1.1637457 (2004).

21 Godin, M., Tabard-Cossa, V., Grutter, P. & Williams, P. Quantitative surface stress measurements using a microcantilever. *Applied Physics Letters* **79**, 551-553 (2001).

22 Miyatani, T. & Fujihira, M. Calibration of surface stress measurements with atomic force microscopy. *J Appl Phys* **81**, 7099-7115 (1997).

23 Dcosta, N. P. & Hoh, J. H. Calibration of Optical-Lever Sensitivity for Atomic-Force Microscopy. *Rev Sci Instrum* **66**, 5096-5097 (1995).

24 Beaulieu, L. Y., Godin, M., Laroche, O., Tabard-Cossa, V. & Grutter, P. Calibrating laser beam deflection systems for use in atomic force microscopes and cantilever sensors. *Applied Physics Letters* **88**, doi:Artn 083108
Doi 10.1063/1.2177542 (2006).

25 Sarid, D. *Scanning force microscopy with applications to electric, magnetic, and atomic forces*. (Oxford University Press, 1991).

26 Gere, J. M. & Timoshenko, S. P. *Mechanics of materials*. (Van Nostrand Reinhold, 1972).

27 Binnig, G. Force Microscopy. *Ultramicroscopy* **42**, 7-15 (1992).

28 Martin, Y., Williams, C. C. & Wickramasinghe, H. K. Atomic Force Microscope Force Mapping and Profiling on a Sub 100-a Scale. *J Appl Phys* **61**, 4723-4729 (1987).

29 Butt, H. J. & Jaschke, M. Calculation of Thermal Noise in Atomic-Force Microscopy. *Nanotechnology* **6**, 1-7 (1995).

30 Diniz, P. S. R., Da Silva, E. A. B. & Netto, S. L. *Digital signal processing : system analysis and design*. (Cambridge University Press, 2002).

31 Levy, R. & Maaloum, M. Measuring the spring constant of atomic force microscope cantilevers: thermal fluctuations and other methods. *Nanotechnology* **13**, 33-37 (2002).

32 Jericho, S. K. & Jericho, M. H. Device for the determination of spring constants of atomic force microscope cantilevers and micromachined springs. *Rev Sci Instrum* **73**, 2483-2485, doi:Doi 10.1063/1.1471351 (2002).

33 Hutter, J. L. & Bechhoefer, J. Calibration of Atomic-Force Microscope Tips. *Rev Sci Instrum* **64**, 1868-1873 (1993).

34 Sader, J. E., Chon, J. W. M. & Mulvaney, P. Calibration of rectangular atomic force microscope cantilevers. *Rev Sci Instrum* **70**, 3967-3969 (1999).

35 Ma, H. L., Jimenez, J. & Rajagopalan, R. Brownian fluctuation spectroscopy using atomic force microscopes. *Langmuir* **16**, 2254-2261 (2000).

36 Cleveland, J. P., Manne, S., Bocek, D. & Hansma, P. K. A Nondestructive Method for Determining the Spring Constant of Cantilevers for Scanning Force Microscopy. *Rev Sci Instrum* **64**, 403-405 (1993).

37 Sader, J. E., Larson, I., Mulvaney, P. & White, L. R. Method for the Calibration of Atomic-Force Microscope Cantilevers. *Rev Sci Instrum* **66**, 3789-3798 (1995).

38 Walters, D. A. *et al.* Short cantilevers for atomic force microscopy. *Rev Sci Instrum* **67**, 3583-3590 (1996).

39 Proksch, R., Schaffer, T. E., Cleveland, J. P., Callahan, R. C. & Viani, M. B. Finite optical spot size and position corrections in thermal spring constant calibration. *Nanotechnology* **15**, 1344-1350 (2004).

40 Meddins, B. *Introduction to digital signal processing*, <http://www.engineeringvillage.com/controller/servlet/OpenURL?genre=book&isbn=9780750650489> (2000).

41 Burnham, N. A. *et al.* Comparison of calibration methods for atomic-force microscopy cantilevers. *Nanotechnology* **14**, 1-6 (2003).

Chapter V

Detection Specificity and Sensitivity of Oligonucleotides

We demonstrate here the capability of cantilever sensors in detecting very low concentration of short oligonucleotides and their capability to distinguish mismatch sequences with high sensitivity. Cantilever sensor arrays functionalized with probe molecules and control reference molecules to obtain differential signal were exposed to target molecules in buffer solution to obtain an assay.

5.1 Introduction

Bioassays obtained using various biosensors are increasingly being used not only as indicators of pathology or physiological conditions but also as tools for drug development[1]. Bioassays for drug development in any area including the RNAi sector have to demonstrate high specificity between match and mismatch, large range of detection (micromolar to picomolar) and possibility to detect targets in high noise and competitive backgrounds[2,3] like in total cellular RNA extracts from cell lines probed for

RNAi response. Establishing these criteria for the cantilever based biosensors are critical to their application as a diagnostic and drug development tool.

Three distinct gene sequences were used in this study (Table 5.1). The BioB2, which is a twelve base sequence from a gene that is involved in the expression of the CAMP factor in *Streptococcus* bacterial strains which causes cell lysis[4-6], was used for studying the lower limits of detection of the cantilevers sensors. The HS f71 probe sequence (21 base pairs matching the Sense strand) is taken from a gene that encodes coagulation factor VII[7] in human blood which is a vitamin K-dependent factor essential for haemostasis, a mutation of which causes coagulopathy[8,9]. This sequence was used to determine the sequence specific nature of the cantilever assay. A 22 base pair oligonucleotide sequence HSA let7b comp is a probe complementary to the mature sequence hsa-let-7b-5p[10] from a let7-b microRNA[11] (miRNA) and was used as a positive control in the experiments. The expression levels of this family of miRNAs is known to be used as a prognostic marker at different values in various types of cancerous cells and hence offers diagnostic insight[12-15].

5.2 Materials and methods

5.2.1 Probe and target preparation

For detecting complementary oligonucleotide sequence, thiolated probe molecules were designed with a thiol and $(CH_2)_6$ linker modifications at the 5' position of a single stranded DNA and obtained from Microsynth (Balgach, CH). The thiolated probe molecules are suspended in a protective solution containing Dithiothreitol (DTT). DTT acts as a protecting agent against oxygen mediated dimerization[16] of the thiol ends which is known to interfere with the subsequent immobilization of the probes onto Gold surfaces. Prior to using the probes for functionalization the DTT is extracted by using liquid-liquid extraction using diethyl ether (DEE) (Sigma Aldrich) as the organic phase. The DTT molecules are relatively more soluble in the organic DEE phase and hence a

multi-step extraction (5X) using fresh DEE at each step is used to remove DTT from the probe solution. Thereafter the aqueous phase was analyzed with the Nanodrop ND-1000 UV- Vis (Thermo Fischer, USA) to determine the probe concentration. The desalted target solutions are immediately blanketed with argon gas and stored at -20°C for further use. Table 5.1 enlists the probe molecules and their respective targets. The HSf71 mismatch sequence is designed with two mismatch sequences marked in red when compared to the HSf71 target molecule to determine the specificity of the sensors.

Table 5.1: Probes and target oligonucleotides

Oligos	**Sequence**	**Function**
Bio-B2 (Probe)	*SH* -$(CH_2)_6$- 5'-TGC TGT TTG AAG-3'	Match sequence BioB2-C
Unspec12 (Reference)	*SH* - $(CH_2)_6$- 5'-ACA CAC ACA CAC-3'	Unspecific sequence 12mer for reference cantilever
HSf71 (Probe)	*SH* – $(CH_2)_6$- 5' ATG TGG AAA AAT ACC TAT TCT -3'	Detect target sequence HSf71 match
HSA let7b comp (Probe)	*SH* - $(CH_2)_6$- 5'AAC CAC ACA ACC TAC TAC CTC A-3'	Positive control
BioB2- C (Target)	5'– CTT CAA ACA GCA– 3'	Complementary sequence for BioB2 probe
HSf71 match (Target)	5'– AGA ATA GGT ATT TTT CCA CAT -3'	HSf71 Antisense match
Let7b (Target)	5'- TGA GGT AGT AGG TTG TGT GGT T -3'	Target for Positive control
HSf71 Mismatch	5'-AGA ATA GGT ATA ATT CCA CAT -3'	Mismatch sequence for probe HSf71 match

Their sequence was obtained from P. Noy, our collaborator from a miRNA project at Hoffmann-la-Roche. The target oligonucleotides are also obtained from Microsynth (Balgach, CH) suspended in nuclease free water. When prepared for experimental purposes, the target molecules were re-suspended in an appropriate buffer.

5.2.2 Sensor functionalization

Cantilever arrays with eight cantilevers each 500 µm long, 100 µm width, 500 nm thick were used. They were cleaned using the optimized plasma cleaning procedure previously discussed in Chapter III (Section 3.2). Each chip was coated with 2 nm Titanium and 20 nm Gold using the Temescal Evaporator at the rate of 0.2 Å/s and 0.5 Å/s respectively. The cantilever sensor array chip was bio-functionalized with the selected thiolated oligo probes using the capillary method (Refer Chapter III, Section 3.5). Before the incubation of the cantilevers in different probe solutions is performed, the chip surface is activated using a 2 min UV Ozone cleaning (Boekel UV Clean Model 135500, 0.5 A). This treatment utilises photo-sensitized oxidation process with UV excitation (184.9 nm in combination with 253.7 nm) that leaves the gold surface organic contaminant free and ready for an effective thiolated probe immobilization. A functionalization solution was obtained from the stock probe solutions after DTT extraction at a concentration of 20 µM in 50 mM Triethylammonium acetate buffer (TEAA, Sigma Aldrich). As per experience, roughly 10 µl of the probe solution is needed per cantilever for a functionalization period of 30 mins. Thereafter the entire chip was washed in 50 mM TEAA for 5 mins to remove unbound probe molecules followed by storage in a small sterilized Petri dish containing the hybridization buffer (Sigma Aldrich SSC 1X, 1 M NaCl or Invitrogen PBS 1X buffer depending on the experiment) at 4 ^{o}C until experimental use. In some cases, after the sensor array was UV Ozone cleaned, it was found that the cantilevers were bent probably due to residual charge effects. This was eliminated by grounding the sensor array when it was mounted on the functionalization setup.

5.2.3 Experimental protocol

Pre-experimental checks were performed prior to the cantilevers being mounted into the flow cell. The checks are in place to ensure no contamination of the flow cells and a smooth operation during the experiment. The following checks were performed. Ensure the flow system (chamber and tubes) are clean and kept under 70% Ethanol (HPLC grade, Sigma Aldrich) always when the system in not in use. Flush the system with large excess of nanopure water and with excess of operating buffer before mounting the cantilever array into the chamber. The laser source is turned on and kept at the optimum operating current and temperature (87 mA, 21.6 ^{o}C for the current setup) at least 30 minutes prior to beginning an experiment. This is to ensure that the laser is fully stable before the scanning begins. The buffer solutions used in the experiment are degassed to avoid any bubble formation during the experiment. Samples are loaded into the 6-way valve system making sure no air bubbles are seen especially at the tips of the inserted tubes and within the tubing. All solutions for injection are prepared within a few hours prior to the experiment to ensure a minimal loss of sample molecules from solution due to unspecific adsorption to the Eppendorf tube walls. All important steps in injection sample preparation are described in detail in the Appendix A4. Since solutions are pulled through the system by a motorized syringe any unsealed junction or tubing could lead to formation of bubbles which interfere with proper readout of the experiments.

The following experimental protocol was used in all experiments with changes otherwise stated in particular instances:

The cantilever array was placed in the flow cell which was then sealed and mounted into the laser deflection setup. The laser spot was initially focussed on the cantilevers (this is a one off setting and does not need to be altered once fixed; the focussing was performed in the centre of the cantilever sensor 1) and is then fixed at the tip of the cantilever such that there are no aberrations in the spot shape or loss of sum signal on the PSD. This was accomplished using the XYZ translation stage. The PSD for measuring the change in deflection of the laser spot reflected from the cantilever was adjusted to have a high sum signal (between 2-3V) by moving it orthogonal to the

incoming laser and the laser spot was set as close to the centre of the PSD as possible (differential signal close to zero on an average) . This was to ensure that the laser spot does not impinge on the non-linear edges of the PSD or that it does not fall out from the PSD range during the experiment. The following parameter settings were used within the NOSE program unless otherwise stated: Peltier element: Set at 0.7 V for 10 secs, Syringe Pump: 150 µl/sec in the pulling mode, Scan rate of laser at 500 ms per cantilever, Temperature regulation setting at 21.5 ^{o}C.

The temperature controlled enclosure was thereafter closed and the regulation was turned on. The setup was allowed to attain thermal equilibrium (for at least 2 hours) before any measurements are made. After the system had attained thermal stability, a pre-measurement peltier test was performed. This test is used to ensure that the final evaluation of differential signals is in line with the mechanical characteristics of the individual cantilevers. The system was allowed time to regain thermal stability after this test. A baseline was obtained in the buffer prior to the injection of the target solution for at least 10 mins. The baseline is essential for data analysis as it is used to eliminate drifts that are inherent to cantilever array systems. The target solutions were thereafter injected in order to obtain an assay (800 µl unless otherwise stated). Every injection of the target was followed by a flush with the buffer solution (800 µl unless otherwise stated) at the same rate as the sample injection. After all assays had been obtained, the post-experimental peltier test was performed to ensure mechanical stability of the sensors throughout the assays.

It is important to note that despite various pre-experimental check and protocols to ensure smooth running of the experiment from functionalization to the final analysis, various problems can be encountered that hamper or completely annul the results from a cantilever sensor or a particular set of cantilever arrays. Most common problems include random bubble formations in the capillary tubing during functionalization causing improper functionalization, excessively upward or downward bent cantilever after gold coating rendering the laser scanning impractical, bubble formation in the fluid cell etc.

5.3 Specificity of cantilever assay

5.3.1 Introduction

The aim of this study was to establish the specificity of the cantilever assays to a particular gene sequence in a buffer solution. One of the primary goals of establishing any gene assay is to prove the specificity of the technique to small changes in the gene sequence of the target molecules also known as mutations. Since even a single mismatch (single nucleotide polymorphism) is a possible disease diagnostic, it is essential that the cantilever assays exhibit a distinct recognition between the mutated and the normal sequence.

The sequences chosen for this study were: HSf71 match as probe for HSf71 target gene, Let7b as a positive control/internal reference for detecting Let7b complementary sequence and a mutated target sequence HSf71 mismatch (details in Table 5.1). The Cantilever functionalization scheme is shown in Fig. 5.1 for this purpose. The cantilevers were functionalised in groups of two for each probe. The scheme shown below is however one of the possibilities and there are other schemes possible. An ideal completely functionalized array will hence contain four probes of each type.

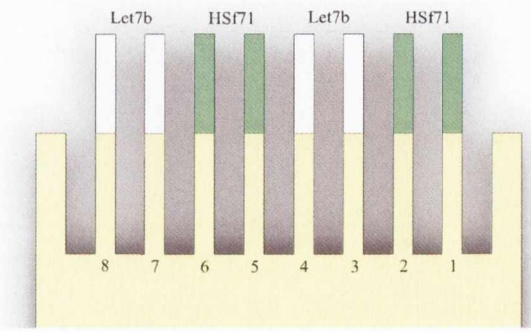

Fig. 5.1: Functionalization scheme for sensitivity to mismatch assay using thiolated HSf71 and Let7b probe molecules. For clarity with the scanning direction, the cantilevers are numbered in the sequence they are scanned with the laser deflection setup.

5.3.2 Experimental details and protocol

All the general experimental pre-checks and protocols were followed as discussed previously in this chapter. Gold coated cantilever array was functionalized using capillary solutions of the probe molecules for capturing HSf71 and Let7b gene sequences in 50 mM TEAA buffer by incubating the respective cantilevers in the solution for 20 mins. Fig 5.1 depicts the probe and reference arrangement (Let7b probe cantilever acts as a positive control and as an internal reference). Target genes HSf71, positive control Let7b and the mismatch sequence HSf71-mismatch were prepared at a concentration of 100 nM in SSC buffer 5X, 1 M NaCl for injection. After the chamber was allowed to reach the temperature set-point, the following injection cycle was executed. A pre-experiment peltier test, 0.7 V for 10 sec (~ 2 ^{o}C rise in temperature) was performed to use for data normalization. After re-attaining thermal equilibration in the sensor chamber, a stable baseline was obtained. The positive control (100 nM Let7b in SSC 5X, 1 M NaCl) was injected in the chamber at 150 µl/min (800 µl in total). After equilibration for 15 mins in the sample solution, a buffer wash of SSC 5X, 1 M NaCl was executed for 8 mins at 150 µl/min. The sensor was allowed to equilibrate for 10 mins in the buffer followed by the injection of selectivity control (100 nM HSf71-mismatch in SSC 5X, 1M NaCl) in the chamber at 150 µl/min (800 µl). After equilibration for 15 mins the chamber was flushed with buffer SSC 5X, 1 M NaCl for 8 mins at 150 µl/min. This was followed by equilibration for 10 mins in the buffer and then the injection of the final target (100 nM HSf71 in SSC 5X, 1M NaCl) at 150 µl/min (800 µl). The system was left to equilibrate for 15 mins followed by a buffer SSC 5X, 1 M NaCl injection. The final post-experiment peltier test (0.7 V for 10 sec) was performed.

5.3.3 Results

The complete raw data from the experiment with the appropriate injection tags is shown in Fig 5.2. The Peltier tests performed were used to normalize the data to remove any discrepancies arising because of variance in mechanical behaviour of the cantilevers

across the sensor chip. This main experimental data was then baseline corrected, normalized and analysed using differential calculations to obtain the final sensor response to each injection. Differential analysis was carried out by averaging the cantilevers groups Let7b and HSf71 before subtracting the Let7b response from the HSf71 to obtain a target assay.

The data analysis results of the positive control are presented in Fig. 5.3 (A and B) (Injection 1: Positive Control: 100 nM Let7b in SSC 5X, 1 M NaCl. Hatched areas in the plots indicate injections) After baseline correction and normalization of the data using the Peltier test, the average responses of the probe cantilevers (Let7b in this case) and the reference cantilevers (HSf71) were calculated to give a differential response at ~ 15 mins from the injection point. A clear differential signal of 40 nm is observed at this time point indicating a successful sensor functionalization with probe molecules. A positive control is hence established paving way for the analysis of proceeding injections.

Specificity of the sensors to the mismatch sequence was established in the second injection after regeneration of the chip with a buffer wash and incubation. The sensor response was recorded for an injection of 100 nM HSf71 mismatch sequence. The detailed analysis of the data and the results are shown in Fig 5.4. The probe cantilevers HSf71 when compared to the reference do not show any major response (~ 14 nm) to the mismatch sequence when compared to the match sequence in the next injection (refer to table 5.1 for the difference in the sequence between HS71 match and mismatch). The mismatch sequence, which differs from the match by two bases in the centre of the sequence, still has some hybridization capability along a stretch of ten bases. A robust assay for the HSf71 gene detection requires that the response to the mismatch sequence be insignificant compared to the response of the sensors to the match sequence which was demonstrated by the next injection after a buffer wash.

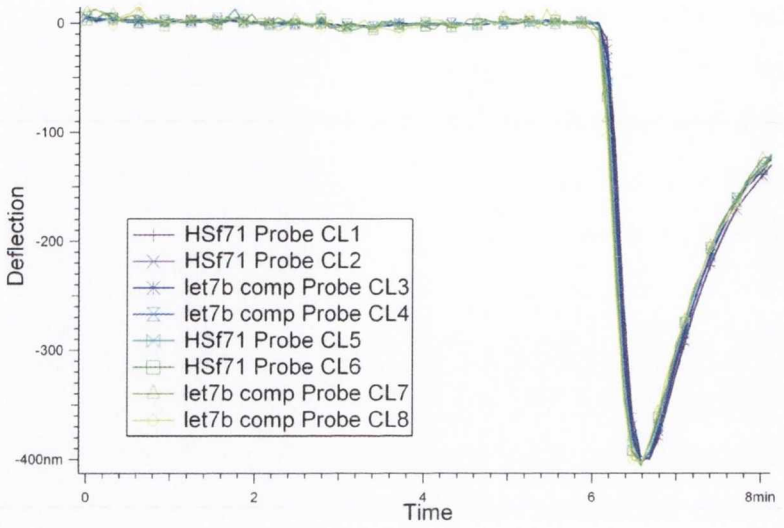

(a)

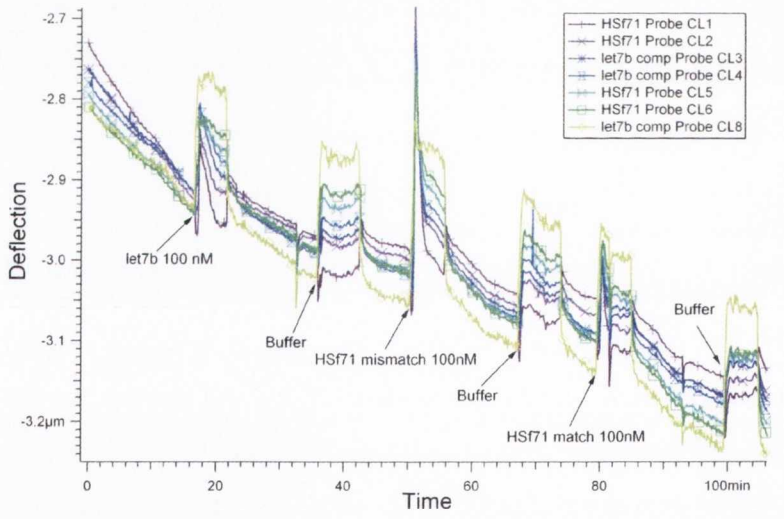

(b)

Fig 5.2: (a) Peltier Heat Test (0.7 V for 10 seconds leading to a rise of ~ 2 ^{o}C in the peltier chamber) for mechanical response normalization of the cantilever signal. After an initial baseline till ~6 mins, the peltier element is turned on to give the required heat pulse causing the bending of the cantilevers due to the bi-metallic effect. (b) Raw data from experiment before normalization of baseline correction. Individual injection points are shown in the figure including sample injection and buffer wash. The spikes at the injection points are caused because of the flow.

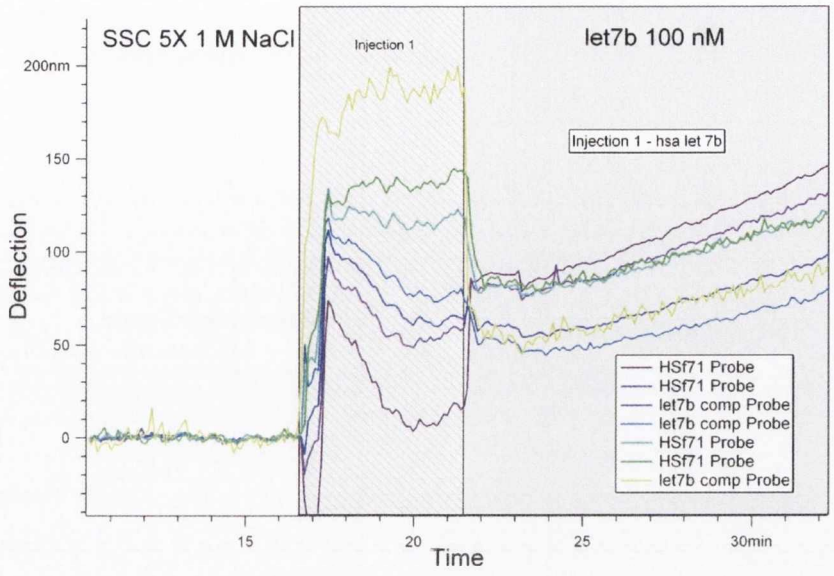

(i)

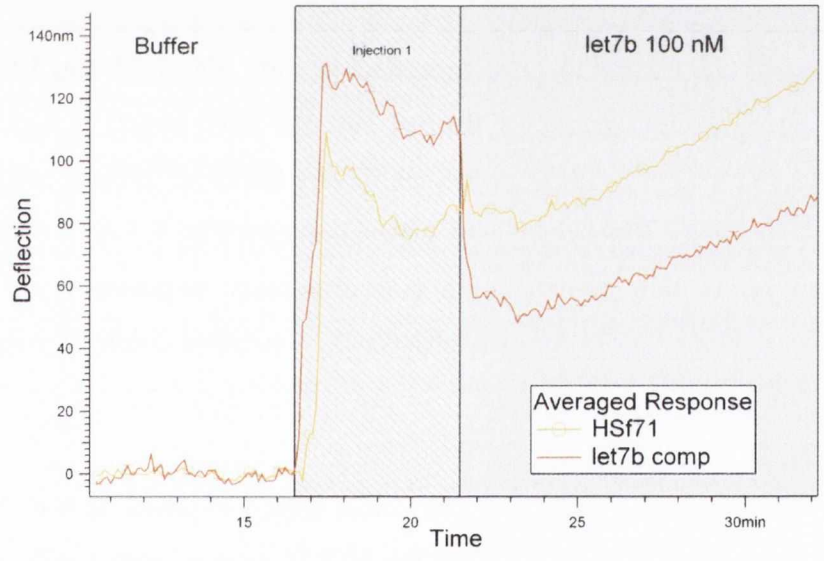

(ii)

Fig.5.3 (A): Bioassay for Let7b gene (at 100 nM concentration) detection in SSC 5X, 1 M NaCl buffer (hatched areas indicate flow). After equilibration in buffer, the sample 800 µl of 100 nM let7b target is injected (i) Baseline corrected and normalized data indicating two clear grouped bands of sensor response for the probes (Let7b) and the references (HSF71). (ii) Averaged cantilever response for probe Let7b and the HSF71 as reference (see Table 5.1).

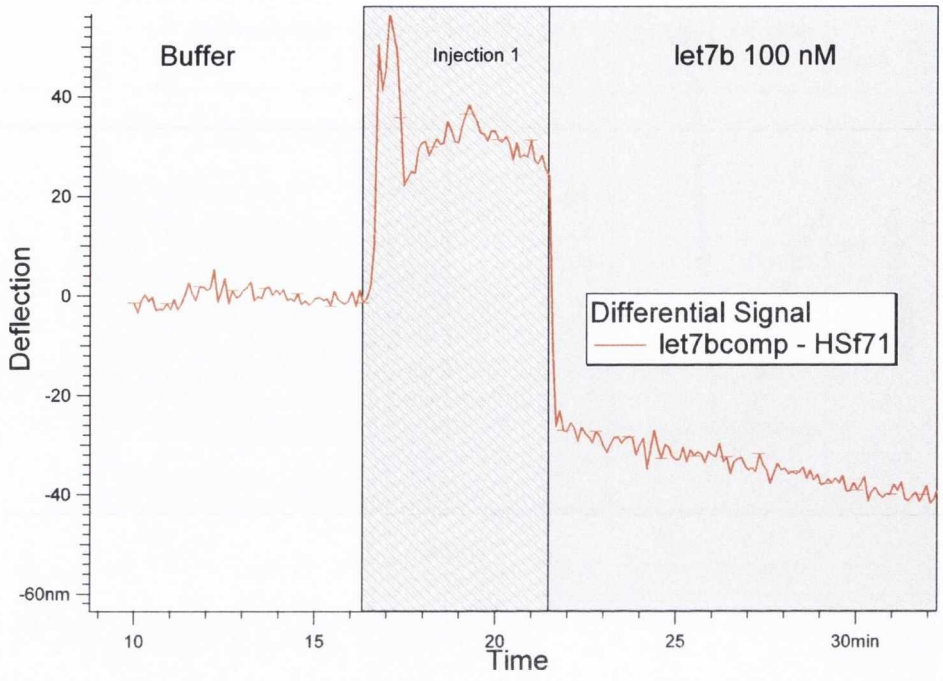

Fig.5.3 (B): Bioassay for Let7b gene detection in SSC 5X, 1 M NaCl buffer. After equilibration in buffer, the sample (800 µl of 100 nM let7b target) is injected into the chamber (hatched area) The HSf71 probe cantilevers act as an internal reference. After data normalization and differential signal subtraction (see Fig. 5.3 A) it is clear that the let7b comp probe is able to detect the complementary sequence from the sample solution (differential signal of 40 nm is observed). A positive control for the following injections is established here.

The last injection in the series was 100 nM HSf71 match sequence in SSC buffer 5X, 1 M NaCl and was assessed for response of the HSF71 sensors with Let7b acting as the internal reference. Fig 5.5 (A and B) shows the step by step analysis and results for this assay. After an averaged response is calculated, the differential signal obtained after 15 mins of injection of the target molecules is seen to be around 40 nm thus indicating a successful assay for the HSf71 gene sequence.

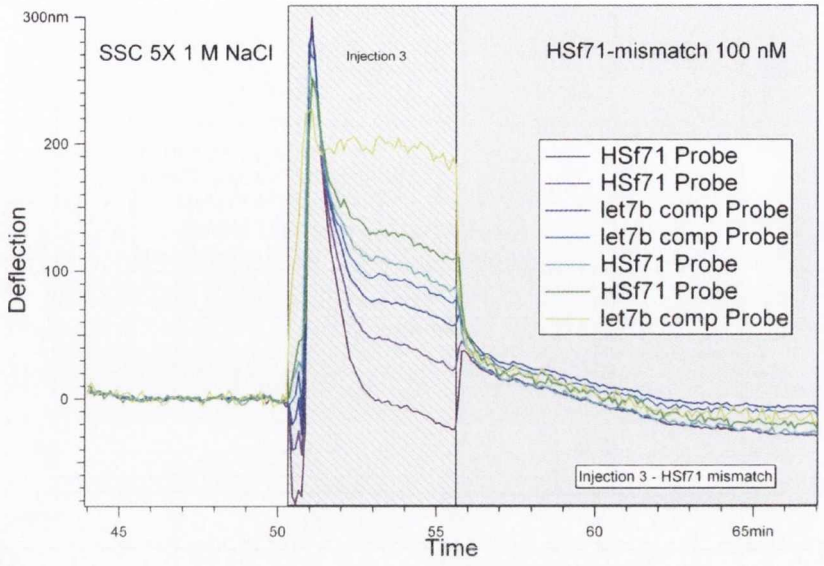

(a)

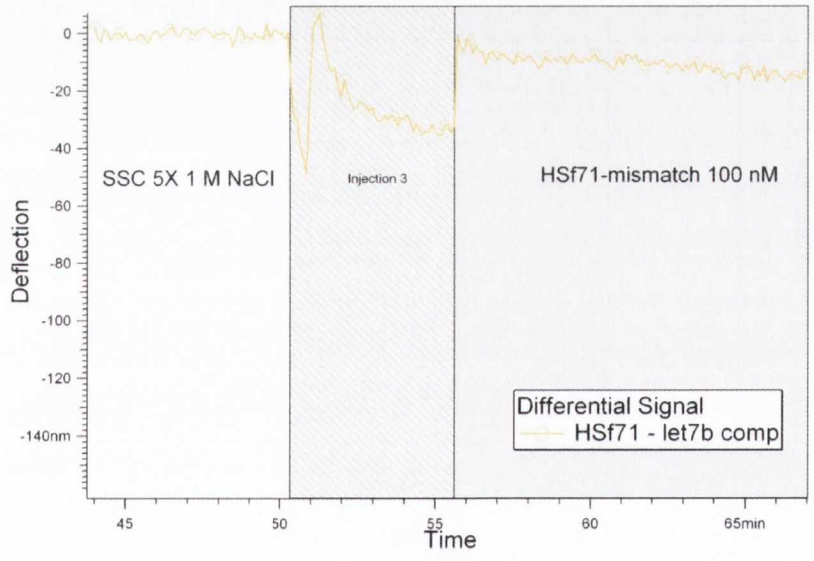

(b)

Fig 5.4: Specificity of cantilever based assay to mutations in gene sequence of HSf71 sequence (hatched areas indicate flow). The injection is for the selectivity control (800 µl of 100 nM HSf71-mismatch in SSC 5X, 1M NaCl, see Table 5.1). After differential analysis shows an averaged defection of ~14 nm compared to the averaged reference (Let7b). This value is much lower in comparison to the signal from the differential analysis from the "match" sequence in the following series of data in Fig: 5.5 (A and B).

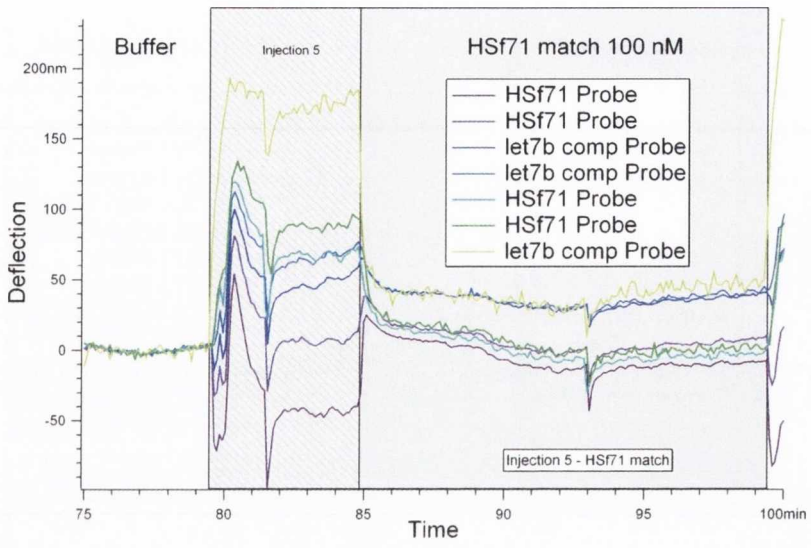

(i)

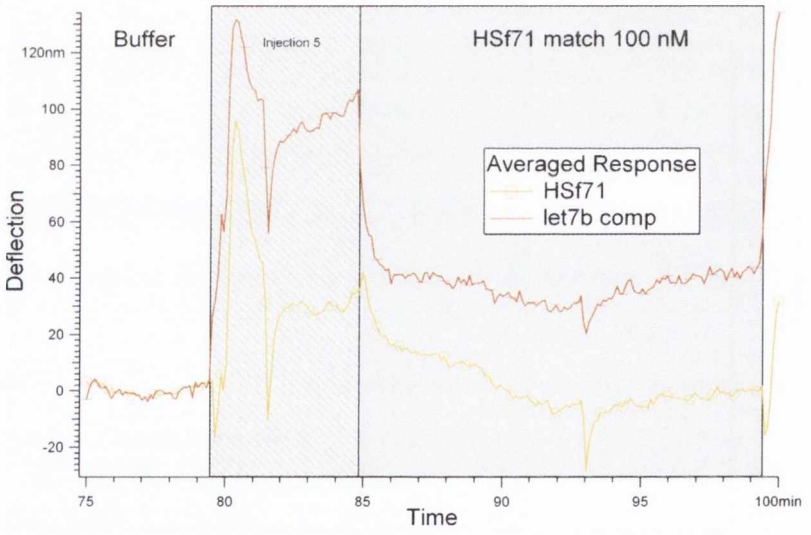

(ii)

Fig. 5.5 (A): Bioassay for HSf71-match detection in SSC 5X, 1 M NaCl buffer (hatched areas indicate flow). Following equilibration in buffer, an injection of 800 µl of 100 nM HSf71-match is shown (see Table 5.1) (i) Normalized (using peltier test) and Baseline corrected raw data. Two distinct grouped bands of response are visible for reference (let7b) and probes (HSf71) (ii) Averaged cantilever response for the probe HSf71 and reference let7b comp. The results indicate two clear sets of cantilever response before the differential analysis. The anomaly at 93 minutes in the plot is possibly because of some physical disturbance to the system and it does not affect the assay.

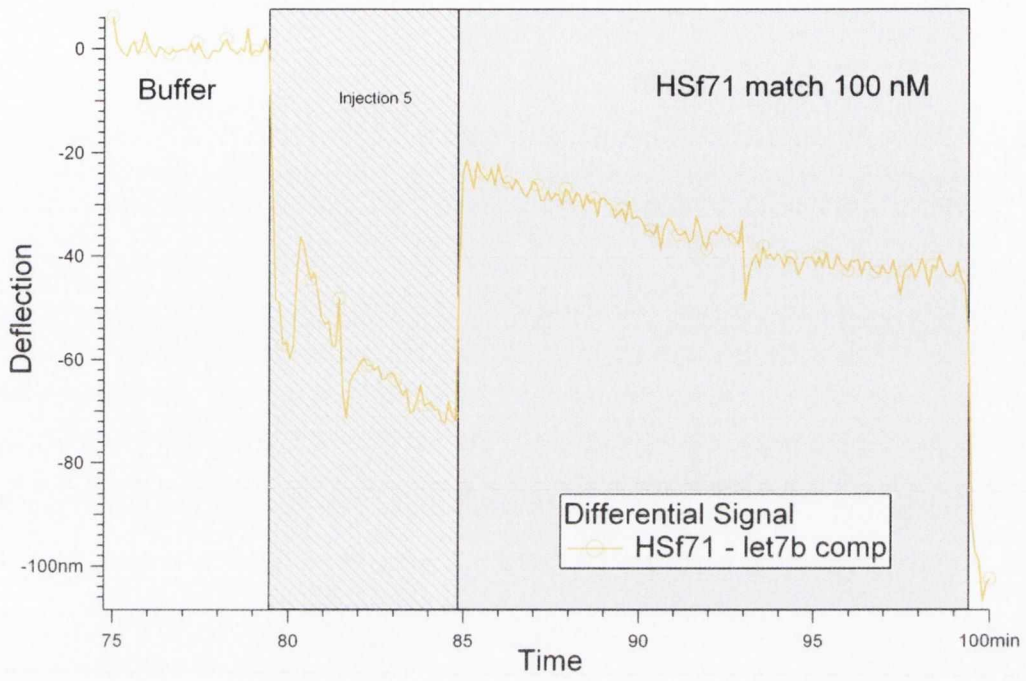

Fig. 5.5 (B): Final differential analysis of the HSf71 match assay (followed after the analysis in Fig 5.5A). Differential signal of the HSf71 probes when compared to Let7b reference. The "match" sequence (see table 5.1) clearly causes a significant deflection (~40 nm at 15 mins after injection of 100 nm HSf71 match sequence) of the HSf71 probe cantilevers when compared to the previous mismatch sequence injection (Fig 5.4). This establishes the higher specificity of the sensors to the proper sequence match by its ability to distinguish the two sequences.

5.3.4 Conclusions

From the above study, the cantilever array sensors exhibit great potential as a bioassay for gene detection as demonstrated by their capability to distinguish between a gene and its mutant species while also being capable of retaining viability after regenerated in cycles using the buffer solution.

5.4 Detection of BioB2 gene sequence at low concentrations

5.4.1 Introduction

The aim of this study was to establish the ability of cantilever sensors as a reliable tool to detect short gene sequences at very low concentrations in solution. In order to demonstrate the lower detection limits, the BioB2 Probe sequence was immobilized on some cantilevers in the array while the rest are functionalized with the Unspec12 sequence which is used as a reference. In addition to determining the lower sensitivity limits, the detection was performed in two different hybridization buffers in order to find an optimal environment for the cantilever assays with a very low signal to noise. The first buffer used was the SSC 1X, 1M NaCl which has been previously used to exhibit the lower sensitivity of cantilever array sensors to the BioB2 gene sequence. The second buffer used was Gibco PBS (Life Technologies, USA) with the detailed media formulation in Appendix A5.

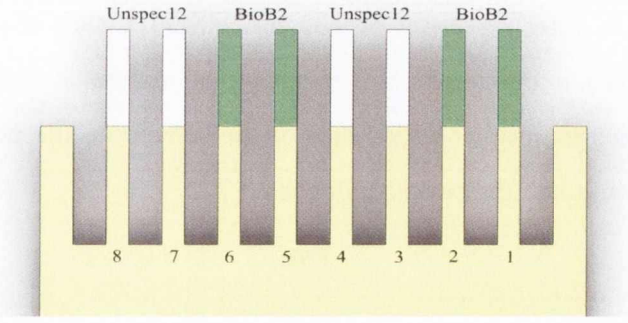

Fig. 5.6: Typical functionalization scheme of a cantilever array with 8 cantilever sensors for the BioB2 gene detection. For clarity with the scanning direction, the cantilevers are numbered in the sequence they are scanned with the laser deflection setup. The functionalization scheme varies across different cantilever arrays used in this investigation.

The functionalization scheme involves using two cantilevers as either probes or references in random order. A typical scheme for a cantilever array with eight individual arrays is shown in Fig. 5.6. The scheme always involves the cantilevers in groups of two but in random order or arrangement across the array. An ideal array hence would contain four probes and four references.

5.4.2 Experimental details and protocol

All the general experimental pre-checks and protocols were followed as discussed previously in this chapter. Gold coated cantilever array was functionalized using capillary solutions of the Probe molecule BioB2 and reference Unspec12 sequences in 50 mM TEAA buffer by incubating the respective cantilevers in the solution for 20 mins and stored thereafter in the appropriate buffer. For the buffer SSC 1X, 1M NaCl the sensors were exposed to a target solution with 10 pM and 50 pM of BioB2-C for comparison with previously exhibited lowest concentration detected in this buffer[6]. For the Gibco PBS buffer a concentration dependence of the sensor response was obtained for target BioB2-C concentration from 10 pM down to 1 fM (sensors were regenerated using 4M Urea for most experiments or a new functionalised sensor was used if there was no regeneration performed). After the chamber was allowed to reach the temperature set-point, the following injection cycle was executed. A pre-experiment peltier Test (0.7 V for 10 sec ~ 2 ^{o}C rise in temperature) was performed for normalization purposes. After the temperature was restabilized in the sensor chamber a baseline was obtained. This was followed by inject of target solution BioB2-C in appropriate buffer and then equilibration for 15-30 mins. A buffer wash 800 µl at 150 µl/min was executed after the assay and was let to equilibrate for 15 mins. The post-experiment Peltier Test (0.7 V for 10 sec) was finally performed.

For some assays performed in the Gibco PBS buffer, in addition to the above steps, multiple target injections were also performed with intermediate regeneration of the sensor with 4M Urea solution for at least 30 mins. The Urea based regeneration is effective because of its strong affinity for hydrogen bonding to DNA base pairs hence

interfering and de-hybridizing the dsDNA strands[17-19]. Other regeneration agent NaOH was also tried but did not yield an effective regeneration. Urea based regeneration was also found to be effective when used by our collaborators in Hoffman La Roche Ltd., Basel for regeneration of both surface plasmon resonance (SPR) chip and microcantilever surfaces. Between each target injection cycle and the sensor regeneration, the chamber was flushed with at least 1.5 to 2 ml for at least 30 mins of the PBS buffer solution before the next target injection is executed.

5.4.3 Results

5.4.3.1 BioB2-C detection in SSC 1X, 1 M NaCl buffer

Assays with two different target solution concentrations viz. 10 pM and 50 pM BioB2-C are detailed below. A full representation of a typical experiment is shown in Fig 5.7 along with a Peltier test which was used for normalization.

After baseline correction was performed, the sensor responses were normalized and then averaged. The averaged response of the reference Unspec12 cantilevers was subtracted from the averaged response of the probe cantilevers BioB2 to obtain a differential assay as shown in Fig. 5.8 (A and B).

The sensor response to a 10 pM target in the first injection after a differential analysis is around 40 nm at the 20 min point. This is a fourfold higher signal in comparison to literature values for BioB2-C assays carried out in the same buffer with the same set of 500 nm thin cantilever sensors[6]. This can be attributed to the improved process we applied for the cantilever sensor surface preparation, functional Au coating and bio functionalization thereby establishing it as an enhanced method. After the first injection cycle, the sensor was regenerated with a buffer wash for 15 mins for a second target injection thereafter. The second injection cycle consists of the target BioB2-C at 50 pM concentration (data analysis and discussion for this assay is show in Appendix A6).

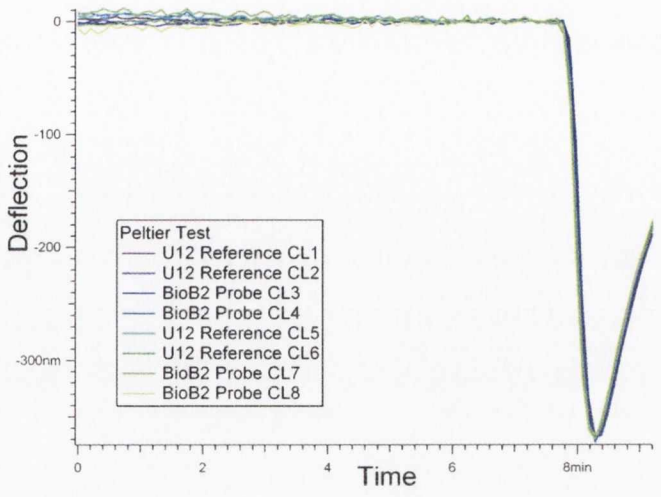

(a)

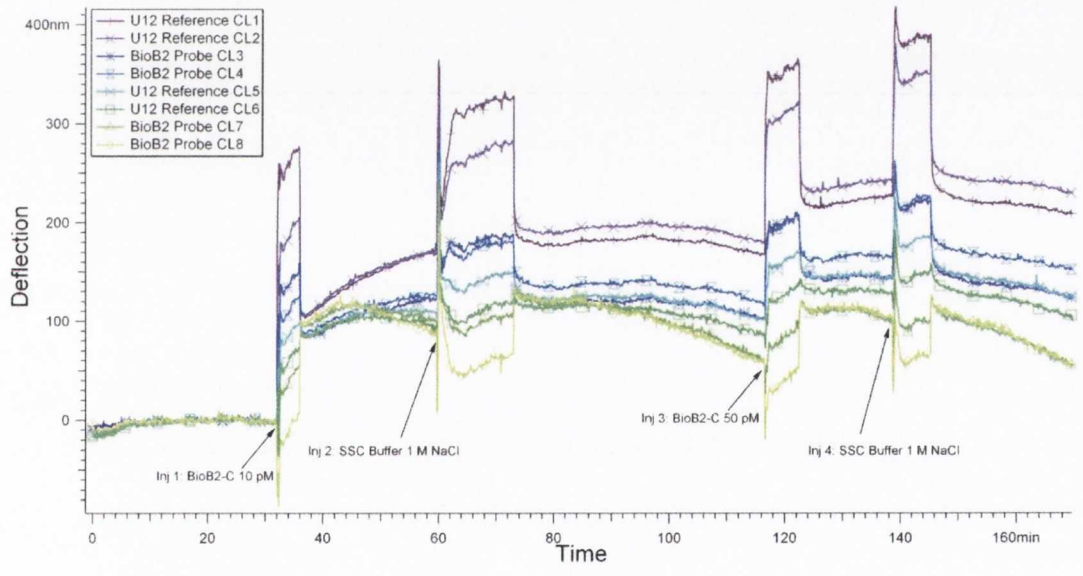

(b)

Fig. 5.7: Bioassay for BioB2-C detection in SSC 1X, 1 M NaCl buffer (a) Peltier test (0.7 V for 10 sec leading to rise of ~2°C) for eventual data normalization. After equilibration in buffer, the heat test is carried out causing the cantilevers to bend due to the bi-metallic effect. The individual values are then normalized (b) Raw data from the experiment before normalization and baseline correction with injection time points. The spikes in the data points are because of the fluid flow.

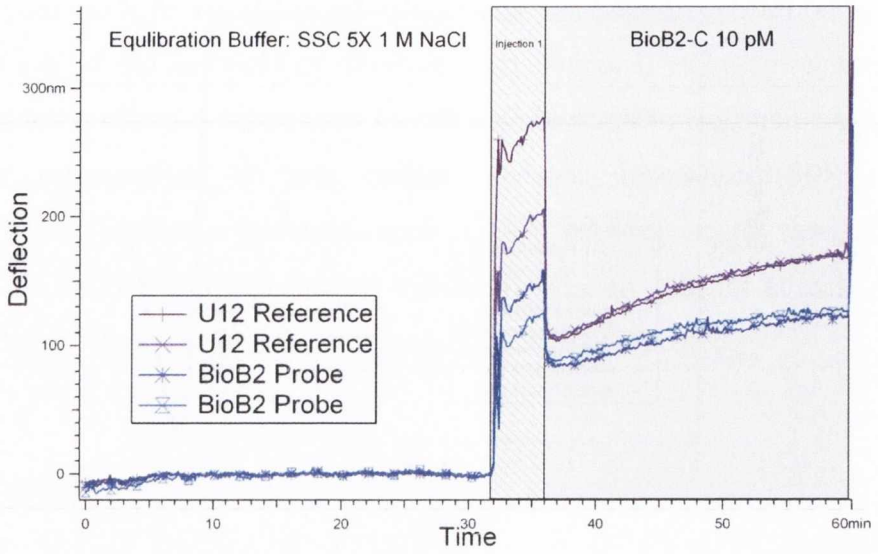

(i)

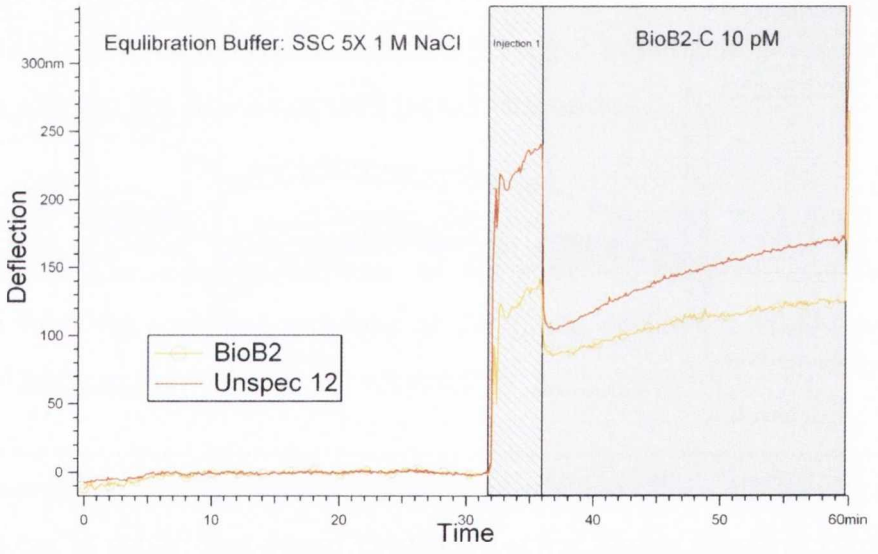

(ii)

Fig. 5.8 (A): Bioassay for 10 pM BioB2-C detection in SSC 1X, 1 M NaCl buffer using Unspec12 probe as reference. After equilibration in buffer, the sensor is exposed to 800 µl of BioB2-C at 10 pM concentration (i) Normalized and Baseline corrected raw data for Injection 1 (ii) Averaged cantilever response for the probe BioB2 and reference Unspec12. The results indicate two clear sets of cantilever response before the differential analysis.

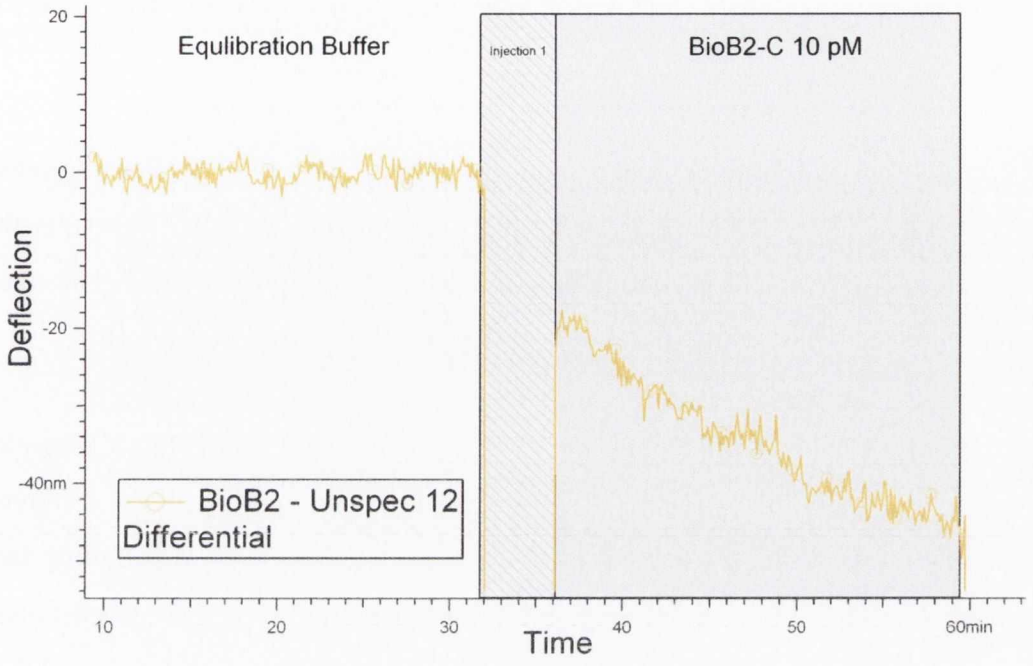

(c)

Fig. 5.8 (B): Bioassay for target BioB2-C in SSC 1X 1M NaCl buffer at 10 pM concentration. Differential response (followed on from the data analysis in Fig 5.8A) for the BioB2-C assay with Unspec 12 probe as the reference is shown. After subtraction from averaged references, the averaged differential signal for the BioB2 probe cantilevers is ~40 nm after 20 mins of sample injection.

5.4.3.2 BioB2-C detection in Gibco PBS buffer

The Gibco PBS buffer was chosen as an alternative due to its unique composition of salts (details in Appendix A5) which provides an optimal environment for the hybridization of ssDNA targets to the probes on the sensor surface after a recommendation from our collaborator P.Noy at Hoffman La Roche Ltd. To observe the lower detection limits of the sensor in this medium, this study evaluated the response of the sensors to a series of drops in target concentration from 10 pM to 1 fM.

The experimental protocol from the previous BioB2-C assays was followed with the sensors being regenerated using 4M Urea. The data was gathered using two different

sets of cantilever sensor array chips which were regenerated using 4M urea in between the different assays.

From this data set, a differential analysis for the assay of 0.01 pM BioB2-C reproduced thrice with intermediate 4M Urea regeneration is presented in Fig.5.9. The results show reproducible assays for 0.01 pM BioB2-C (average deflection of 69 nm). The overall results from the BioB2-C assay in the PBS buffer are summarized in Fig.5.10.

A summary of the concentration dependence of the differential signal (Fig.5.10) follows a power law[20,21] under the condition that when the concentration is zero the differential signal is also null. A sharp decrease in sensor response was seen with falling target concentration following a power law, $y = ax^b$ where "a" is the proportionality constant and "b" is the scaling exponent. The Power law constants were a = 122.9, b = 0.13. From this analysis, a physical significance of the sensor behaviour cannot be clearly established since it is not a steady state analysis.

5.4.4 Conclusions

Detecting rare target concentrations of Oligonucleotides (10 pM and below) has been accomplished using cantilever sensors both in the SSC 1X, 1M NaCl buffer and a new PBS buffer. The differential sensor response in the PBS buffer is significantly higher compared to the sensor response from the SSC buffer indicating an overall improvisation in the sensor preparation process and PBS buffer as the right choice of buffer for DNA/RNA hybridization events on cantilever sensors.

We are able to detect oligonucleotide segments to concentrations as low as 1 fM which is a new lower limit for such label-free nanomechanical systems when no competitive molecules were present. This indicates the suitability of the sensors to be used in detection of low abundance transcripts that often are early stage disease markers and

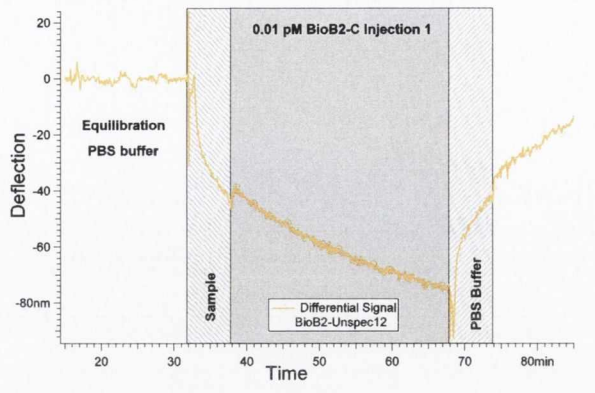

(a)

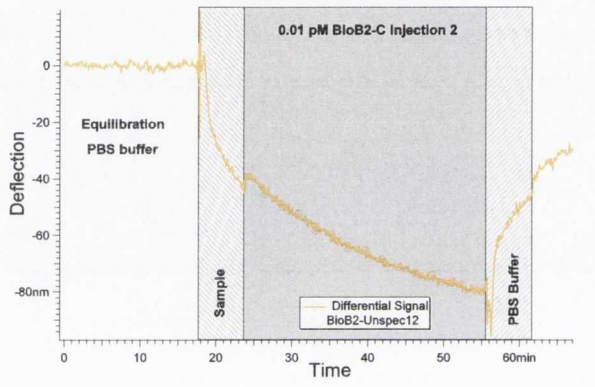

(b)

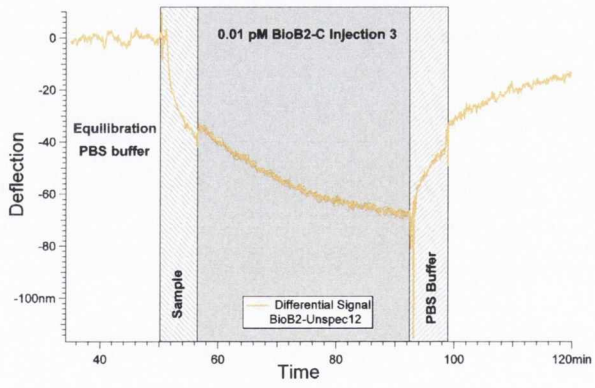

(c)

*hatched areas indicate flow

Fig. 5.9: Bioassay for 0.01 pM BioB2-C in PBS buffer showing the regeneration efficiency of using 4M urea for 30 mins between cycles. The three graphs show a final differential analysis for assay performed on the same chip with 4M urea regeneration in between. The differential signals for the assays (a) ~71nm, (b) 75nm and (c) 62nm, are 69 nm on the average for the three injections. This establishes not only an assay for BioB2-C at 0.01 pM but also the regeneration capability of 4M Urea for the sensors.

assays for their detection pave way in drug discovery and gene therapies such as RNA interference (RNAi) when measured in a competitive background.

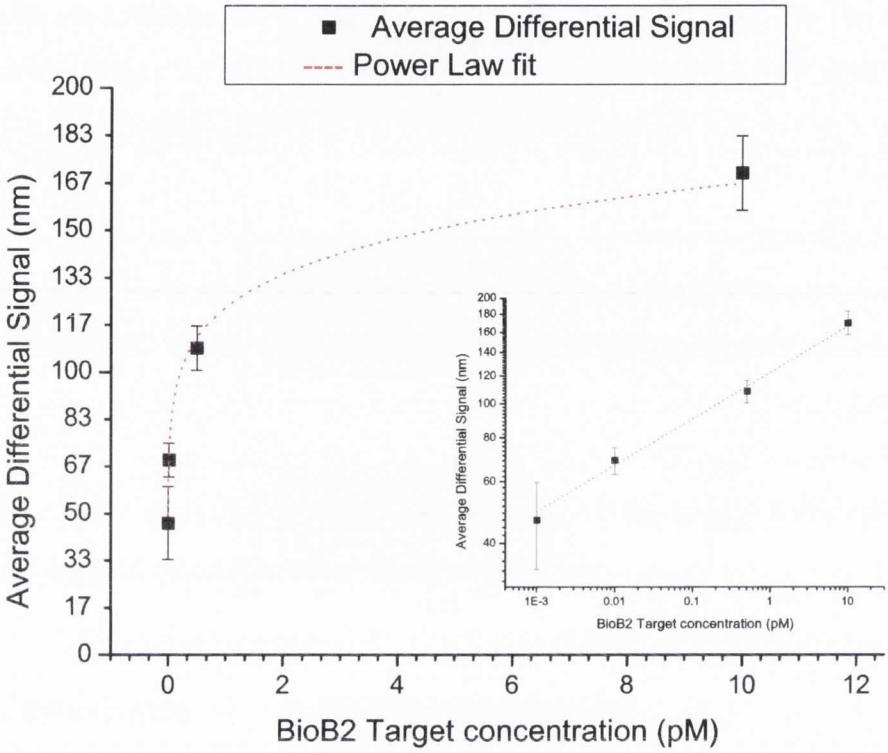

Fig. 5.10: Differential Sensor response (inset is log-scaled) to BioB2-C targets at concentrations ranging from 1 fM to 10 pM in Gibco PBS buffer. The Power law, $y = ax^b$ constants; a = 122.9, b = 0.13. The response might be an indication that in such low target regimes where the sensor response is not completely chartered, the processes governing the hybridization stress on the microcantilever may not be linear. The current data is gathered from two different sets of cantilever arrays (both regenerated) ranging from three data points for 1 fM assay to a maximum of twelve points for 0.01 pM assay.

References

1 Rahman, A.-u., Choudhary, M. I. & Thomsen, W. J. *Bioassay techniques for drug development*. (Harwood Academic Publishers, 2001).

2 Johnson, P. H. *RNA interference : application to drug discovery and challenges to pharmaceutical development*. (Wiley, 2011).

3 Ju, H., Zhang, X. & Wang, J. *NanoBiosensing principles, development and application*, <http://dx.doi.org/10.1007/978-1-4419-9622-0> (2011).

4 Schneewind, O., Friedrich, K. & Lutticken, R. Cloning and Expression of the Camp Factor of Group-B Streptococci in Escherichia-Coli. *Infect Immun* **56**, 2174-2179 (1988).

5 McKendry, R. *et al.* Multiple label-free biodetection and quantitative DNA-binding assays on a nanomechanical cantilever array. *P Natl Acad Sci USA* **99**, 9783-9788, doi:DOI 10.1073/pnas.152330199 (2002).

6 Zhang, J. *et al.* Rapid and label-free nanomechanical detection of biomarker transcripts in human RNA. *Nat Nanotechnol* **1**, 214-220, doi:DOI 10.1038/nnano.2006.134 (2006).

7 Tan, C. W. *et al.* Severe FX deficiency caused by a previously unidentified 4-bp deletion compound heterozygous with a large deletion involving FVII and FX genes. *Haemophilia* **18**, e55-e58, doi:DOI 10.1111/j.1365-2516.2011.02707.x (2012).

8 Raobaikady, R., Redman, J., Ball, J. A. S., Maloney, G. & Grounds, R. M. Use of activated recombinant coagulation factor VII in patients undergoing reconstruction surgery for traumatic fracture of pelvis or pelvis and acetabulum: a double-blind, randomized, placebo-controlled trial. *Brit J Anaesth* **94**, 586-591, doi:Doi 10.1093/Bja/Aei102 (2005).

9 Alshinawi, C., Scerri, C., Galdies, R., Aquilina, A. & Felice, A. E. Two new missense mutations (P134T and A244V) in the coagulation factor VII gene. *Human Mutation* **11**, S189-S191, doi:10.1002/humu.1380110161 (1998).

10 Lagos-Quintana, M., Rauhut, R., Lendeckel, W. & Tuschl, T. Identification of novel genes coding for small expressed RNAs. *Science* **294**, 853-858 (2001).

11 Krek, A. *et al.* Combinatorial microRNA target predictions. *Nat Genet* **37**, 495-500, doi:Doi 10.1038/Ng1536 (2005).

12 Shell, S. *et al.* Let-7 expression defines two differentiation stages of cancer. *P Natl Acad Sci USA* **104**, 11400-11405, doi:DOI 10.1073/pnas.0704372104 (2007).

13 Williams, A. E. Functional aspects of animal microRNAs. *Cell Mol Life Sci* **65**, 545-562, doi:DOI 10.1007/s00018-007-7355-9 (2008).

14 Rahman, M. M. *et al.* Frequent overexpression of HMGA1 and 2 in gastroenteropancreatic neuroendocrine tumours and its relationship to let-7 downregulation. *Brit J Cancer* **100**, 501-510, doi:DOI 10.1038/sj.bjc.6604883 (2009).

15 Chang, S. S. *et al.* MicroRNA alterations in head and neck squamous cell carcinoma. *International Journal of Cancer* **123**, 2791-2797, doi:10.1002/ijc.23831 (2008).

16 Cleland, W. W. Citation Classic - Dithiothreitol, a New Protective Reagent for Sh-Groups. *Cc/Life Sci*, 20-20 (1982).

17 Yang, A. Y., Rawle, R. J., Selassie, C. R. D. & Johal, M. S. A Quartz Crystal Microbalance Study of Polycation-Supported Single and Double Stranded DNA Surfaces. *Biomacromolecules* **9**, 3416-3421, doi:Doi 10.1021/Bm801060w (2008).

18 Bin, W., Fengliang, H., ThaiHuu, N. & Qiao, L. in *Micro Electro Mechanical Systems (MEMS), 2010 IEEE 23rd International Conference on.* 855-858.

19 Savran, C. A., Knudsen, S. M., Ellington, A. D. & Manalis, S. R. Micromechanical detection of proteins using aptamer-based receptor molecules. *Anal Chem* **76**, 3194-3198, doi:Doi 10.1021/Ac049859f (2004).

20 Clauset, A., Shalizi, C. R. & Newman, M. E. J. Power-Law Distributions in Empirical Data. *Siam Rev* **51**, 661-703, doi:Doi 10.1137/070710111 (2009).

21 Newman, M. E. J. Power laws, Pareto distributions and Zipf's law. *Contemporary Physics* **46**, 323-351 (2005).

Chapter VI

Gene detection in total cellular RNA extracts

We investigate here the response of cantilever sensors in detecting a range of ultra-low concentrations of short oligonucleotides in a complex background of Total Cellular RNA extracts from cell lines without labelling or amplification. Cantilever sensor arrays functionalized with probe ssDNA and reference ssDNA, to obtain differential signal, were exposed to complementary target ssDNA strands that were spiked in a fragmented total cellular RNA background.

6.1 Introduction

Detection of regulatory RNA species such as Antisense RNA (aRNA)[1], short interfering RNA(siRNA)[2], micro RNA(miRNA)[3] etc. in cellular extracts is widely carried out using various techniques mainly for understanding their role in disease[4-7] and cellular regulation (e.g.: biomarkers in cancer[8]). Species like miRNA can be detected in serum

since they can be protected either by RISC or packaged into exosomes. Several methods are currently available for detection of such species with microarray approaches[9], PCR based detection[10] and DNA ELISA being the most widely used methods. However these methods use amplification or tagging methods that prove ineffective in the detection of most regulatory short RNA species (siRNA, miRNA) due to inability of the primers to bind to the small RNA species and inefficient labelling and optical detection[11]. Recently microcantilever sensors have been used to detect mRNA species in total cellular RNA and track differential gene expression of cancer progression markers[12].

We have demonstrated the use of cantilever sensors for detection of a target oligonucleotide in low concentrations and also established their sensitivity and ability to distinguish mutations. Understanding sensor response in a diverse background where various other species of RNA compete with the small target RNA's is crucial to ascertain the robustness of the sensors in high noise environments and make it comparable to current technologies. We study here the sensor response to the variation in concentration of the HSf71 gene in fragmented universal human reference RNA.

6.2 Materials and methods

6.2.1 Probe and target preparation

For complementary oligonucleotide capture, the thiolated probe molecules were designed with a thiolated 5' end of the single stranded DNA and obtained from Microsynth (Balgach, CH). The extraction and storage procedure is as described in Section 5.2.1 in Chapter V. Table 6.1 enlists the thiolated probe ssDNA, their respective targets and references.

6.2.2 Sensor functionalization

Cantilever arrays chips with eight cantilevers each 500 µm long, 100 µm width, 500 nm thick manufactured at IBM Research Lab, Zurich, were used. The cantilevers were prepared for bio-functionalization using the protocols described in Section 5.2.2 in Chapter V. Probe oligonucleotides obtained from the stock desalted probe solutions were suspended at a concentration of 20 µM in 50 mM Triethylammonium acetate buffer (TEAA, Sigma Aldrich). The cantilever sensors were functionalized for 30 mins in the respective solutions. Thereafter the chip was washed in 50 mM TEAA for 5 mins to remove unbound probe molecules followed by storage in the hybridization buffer (Invitrogen Gibco PBS 1X buffer) at 4 ^{o}C until experimental use.

Table 6.1: Probes, target oligonucleotides and their roles in the assay.

Oligos	**Sequence**	**Function**
HSf71 match (Probe)	*SH* – $(CH_2)_6$- 5' ATG TGG AAA AAT ACC TAT TCT -3'	Match target gene HSf71 match
Unspec24	*SH* – $(CH_2)_6$- 5' ACA CAC ACA CAC ACA CAC ACA CAC -3'	Reference
Bio-B2 (Probe)	*SH* - $(CH_2)_6$- 5'-TGC TGT TTG AAG-3'	Positive control
HSf71 match (Target)	5'– AGA ATA GGT ATT TTT CCA CAT -3'	Target sequence for HSf71 match
BioB2- C (Target)	5'– CTT CAA ACA GCA– 3'	Complementary sequence for BioB2

6.2.3 Fragmentation of Universal Human Reference RNA (UHRR)

Different RNA transcripts can differ in abundance between cell lines and hence assays carried out in total RNA from a single cell line can lead to variability when comparing with other data for the same target genes but in a different cell line. An ideal reference would hence represent a wider collection of different RNAs[13]. We chose here the Stratagene Universal Human Reference RNA (Agilent Technologies, USA) since it is composed of total (DNase-treated) RNA from 10 human cell lines (Details in Appendix A9). Since the target molecules are 21 nucleotide sequences long, the UHRR was fragmented in order to better match this length so as to test the robustness of the sensors.

The total RNA (UHRR) obtained is provided in a solution of 70 % ethanol and 0.1 M sodium acetate suspended in RNAase free water. Prior to fragmentation, the UHRR was extracted from this solution using the following protocol. The required amount of UHRR (usually 200 µl from the stock solution) was centrifuged (Hettich, DE) at 12,000 g for 15 minutes at 4 °C. After carefully removing the supernatant, the pellet was washed with 70 % HPLC grade ethanol (Sigma, DE). The solution was centrifuged at 12,000 g for 15 minutes at 4 °C. The supernatant was then removed and the pellet was dried at room temperature for 30 minutes to remove retained ethanol. The pellet was then resuspended in RNAase free Diethylpyrocarbonate (DEPC) treated water (Ambion, USA) to the desired concentration (at least 1µg/µl). The absorbance was checked with ND-1000 UV-VIS spectrophotometer (Nanodrop, USA). The A_{260}/A_{280} ratio must be between 1.9 and 2.1 before proceeding to fragmentation.

Fragmentation of the UHRR was carried out using the Bauer Core Protocol used for microarray and genechip assays[14]. The following components are required as per the protocol: 5X Tris-acetate fragmentation buffer (details of fragmentation buffer are provided in Appendix A10), DEPC treated water and UHRR extracted and resuspended in water as per previous protocol. In order to maintain proper temperature, a Thermal Cycler was used (Techgene, Witeg, DE).

The fragmentation protocol proceeds as follows. The 5X fragmentation buffer and the UHRR plus DEPC water were combined in the ratio 1:4. (Ensuring that the final concentration of the RNA in solution is no less than 0.5 μg/μl. E.g.: For UHRR at a concentration of 1 μg/μl and final solution of 40 μl mix: 20 μl of UHRR (1 μg/μl), 12 μl of DEPC water and 8 μl of 5X fragmentation buffer). After incubation at 94 °C for 35 mins, the solution was cooled to 4 °C and placed on ice. The now fragmented UHRR solution was mixed with 3 M Sodium Acetate (Sigma Aldrich, DE) and 100% HPLC grade Ethanol in the ratio of 10: 1: 32.5 by volume respectively and placed at -80 °C for at least 30 mins. The solution was then centrifuged at 14,000 g for at least 30 mins at 4 °C. After removing the supernatant and washing the pellet with ~3 times by volume of 80 % HPLC grade Ethanol, the final solution was centrifuged at 14,000 g for 5 mins. The Ethanol was carefully drained from the tube and the pellet was air dried for 30 mins or by using the vacuum concentrator (Savant DNA Speedvac, USA) for 3 mins without heating. The pellet was resuspended in DEPC water to a suitable concentration (generally higher than 1 μg/μl) and immediately stored at -80 °C for further use.

6.2.4 Experimental protocol

All the general experimental pre-checks and protocols were followed as discussed in Section 5.2.3 of Chapter V. Gold coated cantilever array was functionalized using 20 μM capillary solutions of the probe molecules HSf71 match and reference Unspec24 with some experiments having positive control BioB2 sequences in 50 mM TEAA buffer by incubating the respective cantilevers in the solution for 30 mins. The probe and reference arrangement on the cantilevers was randomized between different experiments. HSf71 match (Target) concentrations (10 pM, 100 pM and 500 pM) were prepared for injection in the Invitrogen Gibco PBS 1X buffer with different fragmented UHRR concentrations (0 nM, 1, nM, 10 nM, 100 nM and 500 nM; calculation details in Appendix A11).

After the chamber was allowed to reach the temperature set-point, the following injection cycle was executed. A pre-experiment peltier test (0.7 V for 10 sec ~ 2 °C rise

in temperature) was performed for normalization purposes. The temperature was restabilized in the sensor chamber thereafter. A stable baseline (for at least 10 mins) was obtained. The sample solution was then injected at 150 µl/min for a total of 800 µl. After exposing the sensors for at least 30 mins to the sample, a buffer wash (800 µl) was performed. The system was equilibrated for at least 15 mins in the buffer. An injection of 4 M Urea injection (800 µl) was used for regeneration when required and the sensor was left to equilibrate in the urea for at least 30 mins. To fully recover the sensor, a buffer wash of at least 1000 µl was performed followed by equilibration for at least 40 mins in the buffer. Secondary injections after the regeneration were performed as per the first injection. A post-experiment peltier test was performed at the end to establish the mechanical stability of the sensors.

Three experiments in this series were performed on two distinct sets of cantilever array chips while the rest were performed on distinct single cantilever arrays with all of them having a minimum of three probe cantilever sensors per experiment.

6.3 Results

The sensor response to varying background and target concentrations was mapped as to understand how it affected the lower range of detection and change in target availability. All data points were taken at 30 mins from sample injection time point and do not represent equilibrium values. An instance from the present set of experiments is shown in Fig. 6.1. A detailed plot of the differential deflection vs. the increasing background concentration for varying values of target concentration is shown in Fig. 6.2. The inset shows the same dataset but with a log scaled x-axis for the fragmented background total RNA for clearer representation.

Assuming the bending signal (y) is proportional to the surface coverage of hybridized molecules[15], the data was fitted using the following logistic function similar to a dose response curve as shown below[16].

$$y = \frac{A1 - A2}{1 + (x/x_0)^p} + A2 \tag{6.1}$$

Parameters: *A1* - Initial Value, *A2* - Final Value, p – power exponent , x_0 – value of x when y is halfway between limiting values *A1* and *A2*. The initial limiting value *A1* is evident at zero background concentration while the limiting final value *A2* was fixed at 4.5 nm which is three times the inherent noise levels of detection (~1.5 nm). The model does not, in any way, represent a detailed kinetics based viewpoint of the system which is far more complex for such systems[17-20]. All parameters excluding *A2* were allowed for the fitting. The final *A1* values predicted with the model were in good agreement with the experimental data. The various values of the fitting parameters are listed in Table 6.2.

The value of x_0 is a strong indicator of the limits of the detection in background. For the 10 pM target concentration where x_0 is 1.37 nM, it indicates that the loss in signal at such low target concentrations is very rapid with increasing background when compared to higher concentrations (x_0 = 49.88 nM at 500 pM target level).

Table 6.2: Fitting parameters from Equation 6.1 for background response of sensors. Values in the brackets indicate standard error.

Target	**Fitting Parameters**			
Concentration	***A1***	***A2***	***p***	***x_0***
(pM)	**(nm)**	**(nm)**		**(nM)**
10	130 (1.12)	4.5	0.30 (0.00)	1.37 (0.17)
100	155.42 (8.64)	4.5	0.23 (0.06)	26.54 (23.76)
500	201.87 (27.85)	4.5	0.35 (0.11)	49.88 (47.52)

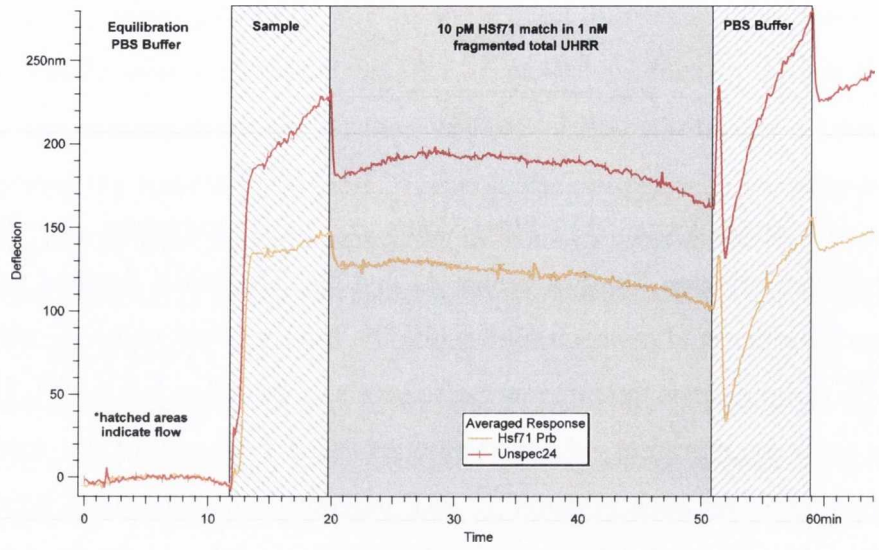

(a)

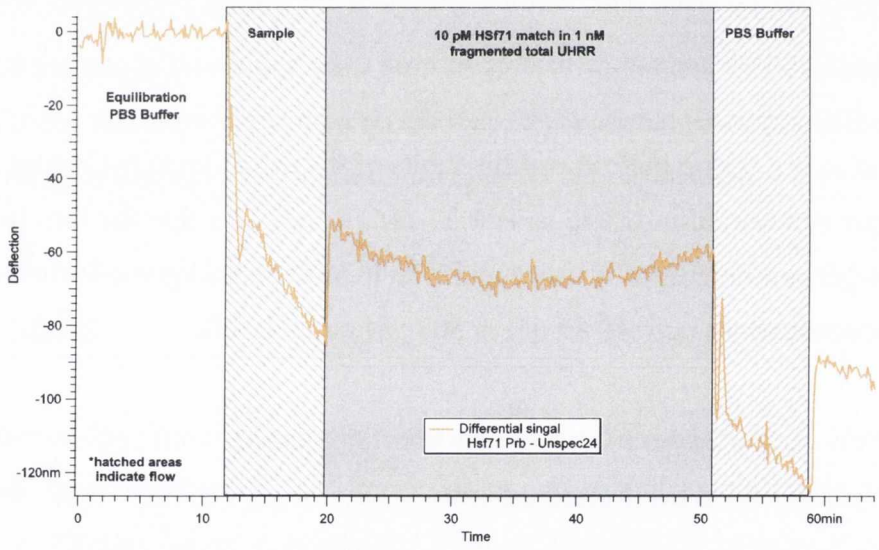

(b)

Fig. 6.1: Detection of Hsf71 match sequence (800 µl injection, 10 pM) in fragmented total UHRR background (1 nM) in Invitrogen Gibco PBS 1X. (a) After equilibration in buffer, the sensor is exposed to the injection (hatched areas). Baseline corrected and normalized data shown are then obtained after analysis in the NOSETools (b) Differential analysis of the data (see Table 6.1 for probe and reference details) yields a total deflection of ~70 nm for the probe cantilever at the time point of 30 mins from the injection of the sample. All other measurements are made at this time point to keep the results comparable.

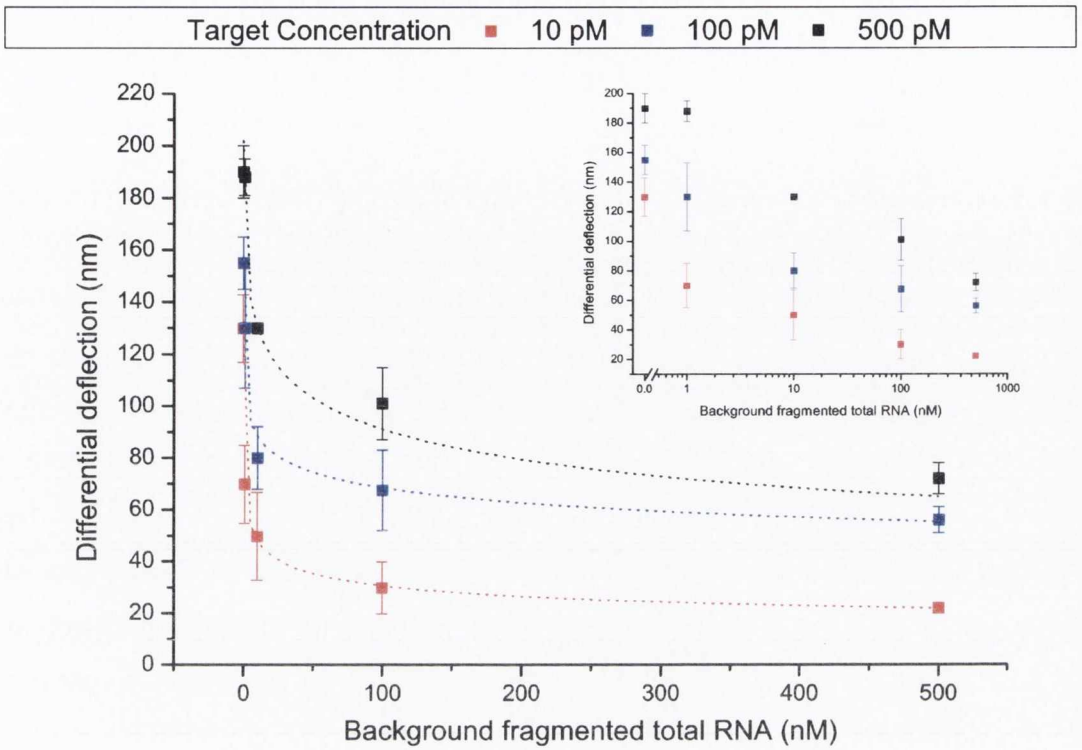

Fig. 6.2 : Detection of target HS71 match sequence at varying concentrations vs. fragmented Universal Human Reference RNA (total RNA) concentration (from no background to 500 nM fragmented UHRR concentration). The data was fit using Eq.6.1. Inset shows the same plot with a log x-axis for better representation. The graph indicates, as expected a drop in signal with a drop in the target concentration at any given value of background concentration. The analysis was based on average calculation of the differrential signals after subtraction of individual cantilevers from an averaged reference. Three experiments were performed on two distinct sets of cantilever array chips. The rest of the data was gathered from distinct cantilever arrays with all having a minimum of three probe cantilever sensors per experiment each.

6.4 Conclusion

From the graph, it can be inferred that the deflection signal depends heavily not only on the target concentration but also on the background competition from other

oligonucleotides of the total cellular RNA. The nature of the curve fitted to current data is asymptotic predicting a rather gradual loss of signal as the background concentration rises. There is however a limitation from experimental point of view since the detection limit set for 4.5 nm will not be reached till the background reaches tens of micromolar in concentration. Since this is not a steady state analysis and more importantly the mechanisms behind the cantilever deflection in competitive environments is barely known, it is not possible to accurately quantify the range of operation at steady state. There are practical considerations such as limitations of extracting total RNA from cell lines since amounts available for an assay are only limited due to cell culture and extraction methods. Also an increase in noise levels in the optical deflection based detection is observed with rise in background concentration[12]. Considering such limitations, it is possible that the sensors can be used for qualitative detection of oligonucleotides in as high as 5 μM background for a 10 pM target concentration (predicted sensor response of ~13 nm).

The current study is crucial so as to establish sensor behaviour for the application of microcantilevers as a label-free detection technique for oligonucleotide detection in total RNA. This provides some first insights into the effect of competing molecules on the differential deflection signals of microcantilever bioassays. It is not possible to extract kinetics information from these data since it is not a steady-state analysis. However the plot fitting provides information as to the range of detection in different target concentrations for the low range of target availability and the effect of background competition on the signal.

References

1 Brantl, S. Antisense-RNA regulation and RNA interference. *Bba-Gene Struct Expr* **1575**, 15-25 (2002).

2 Kittler, R. *et al.* An endoribonuclease-prepared siRNA screen in human cells identifies genes essential for cell division. *Nature* **432**, 1036-1040, doi:Doi 10.1038/Nature03159 (2004).

3 Nunez-Iglesias, J., Liu, C. C., Morgan, T. E., Finch, C. E. & Zhou, X. J. Joint Genome-Wide Profiling of miRNA and mRNA Expression in Alzheimer's Disease Cortex Reveals Altered miRNA Regulation. *Plos One* **5**, doi:Artn E8898
Doi 10.1371/Journal.Pone.0008898 (2010).

4 Calin, G. A. *et al.* Frequent deletions and down-regulation of micro-RNA genes miR15 and miR16 at 13q14 in chronic lymphocytic leukemia. *Proceedings of the National Academy of Sciences of the United States of America* **99**, 15524-15529, doi:DOI 10.1073/pnas.242606799 (2002).

5 McKinsey, T. A. & Olson, E. N. Toward transcriptional therapies for the failing heart: chemical screens to modulate genes. *J Clin Invest* **115**, 538-546, doi:Doi 10.1172/Jci200524144 (2005).

6 Perkins, D. O. *et al.* microRNA expression in the prefrontal cortex of individuals with schizophrenia and schizoaffective disorder. *Genome Biol* **8**, doi:Artn R27
Doi 10.1186/Gb-2007-8-2-R27 (2007).

7 Ura, S. *et al.* Differential MicroRNA Expression Between Hepatitis B and Hepatitis C Leading Disease Progression to Hepatocellular Carcinoma. *Hepatology* **49**, 1098-1112, doi:Doi 10.1002/Hep.22749 (2009).

8 Lu, J. *et al.* MicroRNA expression profiles classify human cancers. *Nature* **435**, 834-838, doi:Doi 10.1038/Nature03702 (2005).

9 Chen, C. F. *et al.* Real-time quantification of microRNAs by stem-loop RT-PCR. *Nucleic Acids Res* **33**, doi:ARTN e179
DOI 10.1093/nar/gni178 (2005).

10 Thomson, J. M., Parker, J. S. & Hammond, S. M. Microarray Analysis of Mirna Gene Expression. *Method Enzymol* **427**, 107-122, doi:Doi 10.1016/S0076-6879(07)27006-5 (2007).

11 Wark, A. W., Lee, H. J. & Corn, R. M. Multiplexed detection methods for profiling microRNA expression in biological samples. *Angew Chem Int Edit* **47**, 644-652, doi:DOI 10.1002/anie.200702450 (2008).

12 Zhang, J. *et al.* Rapid and label-free nanomechanical detection of biomarker transcripts in human RNA. *Nat Nanotechnol* **1**, 214-220, doi:DOI 10.1038/nnano.2006.134 (2006).

13 Novoradovskaya, N. *et al.* Universal Reference RNA as a standard for microarray experiments. *Bmc Genomics* **5** (2004).

14 Couget, J. A. Fragmentation of cRNA for Affymetrix GeneChips: Bauer Core Standard Protocol. *The Bauer Center for Genomics Research*, http://sysbio.harvard.edu/csb/resources/downloads/Bauer_Core_GeneChip_Fragmentation_Protocol.doc (2003).

15 McKendry, R. *et al.* Multiple label-free biodetection and quantitative DNA-binding assays on a nanomechanical cantilever array. *P Natl Acad Sci USA* **99**, 9783-9788, doi:DOI 10.1073/pnas.152330199 (2002).

16 Dudley, R. A. *et al.* Guidelines for Immunoassay Data-Processing. *Clin Chem* **31**, 1264-1271 (1985).

17 Chan, V., Graves, D. J. & McKenzie, S. E. The biophysics of DNA hybridization with immobilized oligonucleotide probes. *Biophys J* **69**, 2243-2255 (1995).

18 Erickson, D., Li, D. Q. & Krull, U. J. Modeling of DNA hybridization kinetics for spatially resolved biochips. *Anal Biochem* **317**, 186-200, doi:Doi 10.1016/S0003-2697(03)00090-3 (2003).

19 Held, G. A., Grinstein, G. & Tu, Y. Modeling of DNA microarray data by using physical properties of hybridization. *P Natl Acad Sci USA* **100**, 7575-7580, doi:DOI 10.1073/pnas.0832500100 (2003).

20 Pappaert, K., Van Hummelen, P., Vanderhoeven, J., Baron, G. V. & Desmet, G. Diffusion-reaction modelling of DNA hybridization kinetics on biochips. *Chem Eng Sci* **58**, 4921-4930, doi:DOI 10.1016/j.ces.2002.12.007 (2003).

Chapter VII

Insights into siRNA strand lifetimes in RNAi studies

We investigate the applications of microcantilever sensors for rapid and label-free detection of individual strands of the siRNA (21 base pairs) directed for a sequence specific cleavage of mRNA and its subsequent degradation in cells and knockdown of gene expression. The siRNA in focus was designed to temporarily knockdown the expression of the Claudin-5 protein from the family of tight junction proteins that control the blood-brain barrier (BBB) in mouse brain endothelial cells. For different time points, after transfection of the mouse brain endothelial cells with siRNA, we extracted the total RNA from the cells to detect the individual strands of the siRNA and assess their lifetimes inside the cell. The microcantilevers were able to detect these strands in the extracts thus providing a rapid label-free technique for detection of such species to understand their role in RNAi. The study was carried out in collaboration with the Ocular Genetics Department, TCD who performed the RNAi based BBB modulation and total cellular RNA extraction.

7.1 Introduction

7.1.1 Targeting the Blood-Brain barrier

The blood-brain barrier is a highly regulated bio-physical interface between the peripheral circulation and the central nervous system (CNS) allowing a selective and restricted transport of several molecules (most drugs, neurotrophic factors, peptides, bacteria and viruses) into the brain from the blood stream[1-4]. Anatomically, the majority of this barrier is composed of tight junctions (TJs) connecting the cerebral endothelial cells (Fig. 7.1) which are maintained by a complex network of 30 identified proteins that form a seal between adjacent endothelial cells.

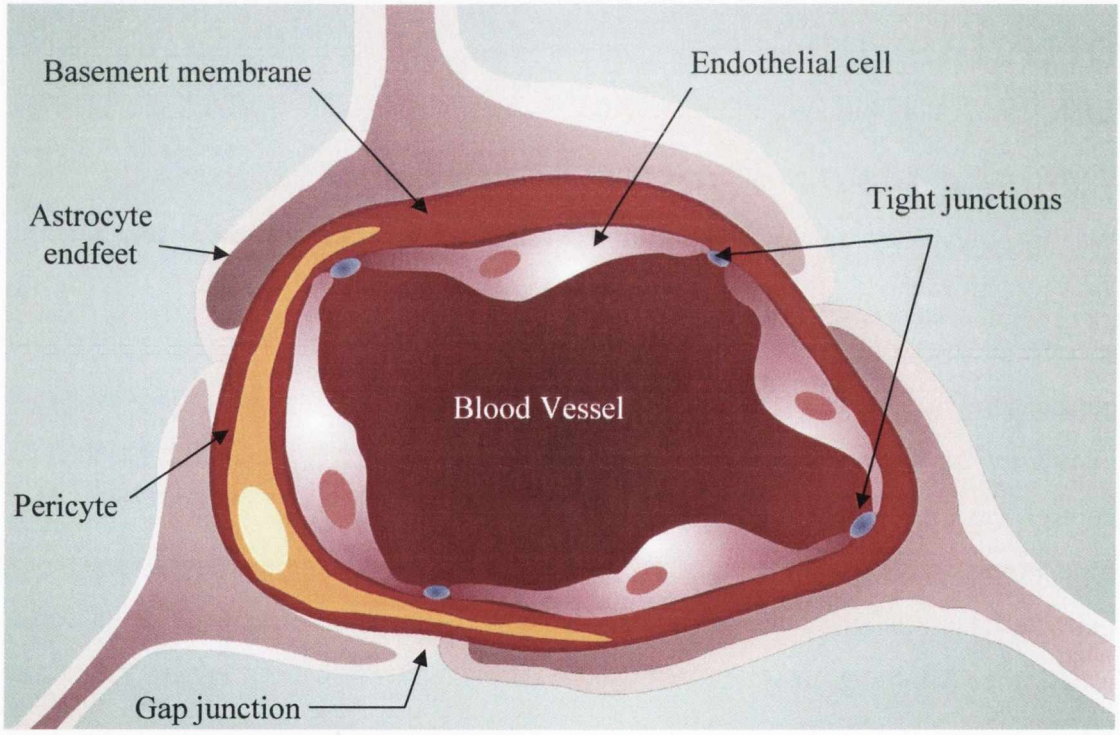

Fig. 7.1: Blood-Brain barrier. The tight junctions between endothelial cells in the vessel lining form the selective barrier between and the blood vessel and the brain allowing the controlled movement of nutrients and several other molecules. Various diseases are known to involve the critical failure of these junctions and the very mechanism that protects the brain from external molecules then acts as a hindrance to drug delivery.

The development and progression of several diseases affecting the CNS involve the critical failure of BBB and the very selective nature of the barrier impedes delivery of many systemically-deliverable small-molecule therapeutic drugs[5-8]. Hence the purpose specific and transient targeting of the BBB is critical for the treatment of such diseases.

The trans-membrane junction protein families that are fundamental to the TJs are Junction adhesion molecules (JAM), Occludin and the Claudins[9]. These proteins physically connect with their corresponding counterparts on the plasma membrane of adjacent endothelial cells, with each performing a specific set of functions. The JAMs are believed to arbitrate the early attachment of the adjoining membranes by homophilic interactions followed by the Claudins forming the principal barrier of the junction structurally assisted by Occludin[10-12]. Several methods have been used for the targeting of the barrier for drug-delivery[13-15] with recent advances that have achieved transient modulation of the barrier by targeting the junction proteins[16,17].

7.1.2 RNAi mediated BBB modulation

The Ocular Genetics group at Trinity College Dublin has recently successfully developed the use of RNAi for the reversible opening of the BBB[17] in mouse models. The technology uses a hydrodynamic approach for the delivery of siRNA (short-interfering RNA, usually ~21-23 base pairs)[18] to the mouse brain endothelial cells for the specific and transient targeting of Claudin-5 (sequence details in Appendix A12) from the Claudin family of tight junction proteins. They have observed highly increased permeability of molecules (742 Da, but not 4400 Da) across the BBB hence paving way for drug delivery using RNAi[17].

The design of the siRNA is based on the specific targeting and cleavage of the mRNA that leads to the expression of the Claudin-5 protein (Fig. 7.2). Due to the relatively short half-life of the protein[19], the expression of Claudin-5 in the endothelial cells sustains the continuous process for replenishment of the proteins in the tight junctions.

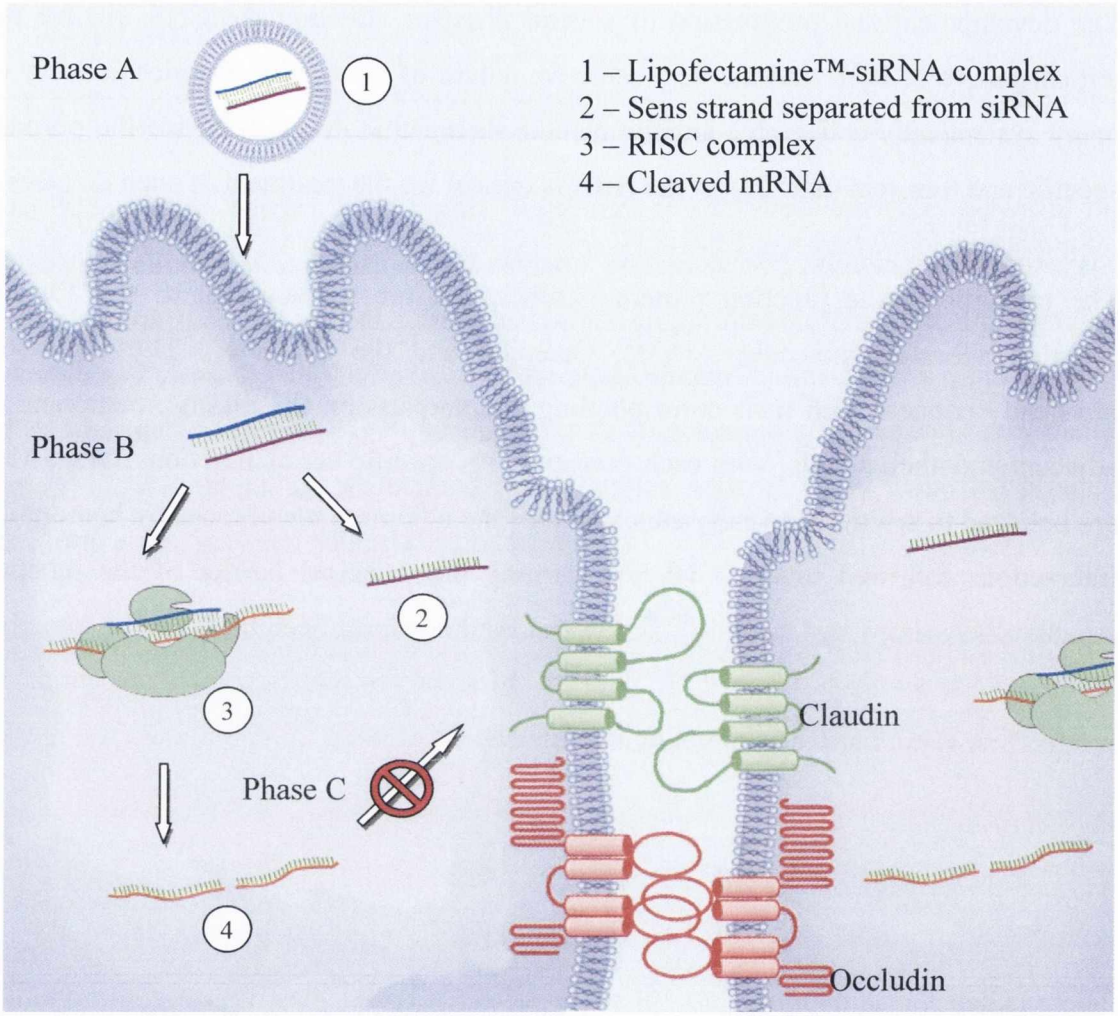

Fig. 7.2: siRNA based targeting of the tight-junction protein Claudin-5 in mouse brain endothelial cells for transient opening of the BBB. Phase A- Transfection of the Mouse brain endothelial (bEnd.3) cells with Lipofectamine™-siRNA complex. Phase B- Incorporation of the Antisense strand into the RISC complex after separation from the Sense strand. Phase C- Specific cleavage and consequent transient inhibition of the translation of mRNA responsible for Claudin-5 production. The efficiency of the transfected siRNA for gene silencing in the cell depends on a host of factors including RISC activity and lifetime of the siRNA strands.

The post-transcription targeting of the expression of this protein hence leads to a reversible and transient control over the BBB[17] and the Blood Retinal barrier[20].

	Sense sequence:
	5'- CGU UGG AAA UUC UGG GUC UUU -3'
Mouse Claudin-5 siRNA:	Antisense sequence:
	5'- AGA CCC AGA AUU UCC AAC GUU -3'

7.1.3 Microcantilever based bioassay for siRNA

Due to potential side effects[21-23], it is essential that the design and dosage of the siRNA be highly specific and optimal. A lack of detailed direct pharmacokinetic studies (dosage, elimination rate, half-life etc.) of siRNA has hindered the translation of the RNAi therapies to human subjects. Most current methods for siRNA detection are limited owing to the short length of siRNAs which are usually too small to anneal primers and generate amplicons[24,25] or due to requirement of extensive time and material intensive routines[26,27]. We employ 500 nm thin microcantilever based sensors for the detection of the individual siRNA strands in total RNA extracted from cell lines without labelling or other tedious procedures.

7.2 Materials and methods

Please note that the procedures in sections 7.2.3-7.2.8 were performed by Mr James Keaney, our collaborating postgraduate student in the Ocular Genetics Unit, Smurfit Institute of Genetics, TCD. The detailed protocols are included here for the purpose of continuity and clarity.

7.2.1 Sensor probe preparation

Probes for the detection of the siRNA were designed for complete complementarities to the individual strands of the siRNA. It is important to note that the siRNA individual strands (Sense and Antisense) are completely complementary except for the 3' ends which have a UU overhang that has been shown to be the most efficient trigger of

mRNA degradation[28,29]. Thiolated ssDNA probes were obtained from Microsynth (Balgach, CH). The extraction and storage procedure is as described in Section 5.2.1 in Chapter V. Table 7.1 enlists the thiolated probe ssDNA and the reference. The targets (the Sense and Antisense strands of the siRNA) are enlisted in Section 7.1.2 (Mouse Claudin-5 siRNA).

Table 7.1: ssDNA Probes and their roles in the siRNA assay.

ssDNA probe	**Sequence**	**Function**
Probe_SENS	*SH*- $(CH_2)_6$- 5' AAA GAC CCA GAA TTT CCA ACG 3'	Detect Sense Strand
Probe_ASENS	*SH*- $(CH_2)_6$- 5' AAC GTT GGA AAT TCT GGG TCT 3'	Detect Antisense Strand
Unspec_21	*SH*- $(CH_2)_6$- 5' ACA CAC ACA CAC ACA CAC ACA 3'	Reference

7.2.2 Sensor functionalization

Cantilever array sensors with eight cantilevers each (individual cantilever 500 µm long, 100 µm wide, 500 nm thin) were used. The detailed functionalization protocols for the sensors are described in Section 5.2.2 in Chapter V. Probe ssDNA obtained from the stock desalted probe solutions were suspended at a concentration of 20 µM in 50 mM Triethylammonium acetate buffer (TEAA, Sigma Aldrich). The cantilever sensors were functionalized with the two ssDNA probes and the reference, for 30 mins in the respective solutions. Thereafter the chip was washed in 50 mM TEAA for 5 mins to remove unbound thiolated ssDNA molecules followed by storage in the hybridization buffer (Invitrogen Gibco PBS 1X buffer) at 4 ^{o}C until experimental use.

7.2.3 bEnd.3 cell culture

Mouse brain endothelial (bEnd.3) cells (ATCC, CRL-2299) were cultured in 25 ml of Dulbecco's modified Eagle medium (DMEM, BioWhittaker) supplemented with 20% fetal calf serum (FCS) and 100 ml sodium pyruvate (2 mM) per 500 ml bottle, in T175 filter-capped flasks (Sarstedt, DE). The flasks were stored in a 5% CO_2 incubator (Hepa Class 100, Thermo Scientific) at 37 °C. The cell culture was passaged to maintain exponential cell growth and to minimise cell death. Thereafter the DMEM medium was aspirated off and cells were washed gently with 10 ml of phosphate buffered saline (PBS) at pH 7.2 for 1-2 mins. The PBS was removed and 3 ml of trypsin-EDTA (Gibco-BRL) was added to the flasks to dissociate cells. The flasks were incubated for 5 mins at 37 °C to allow for the trypsinization and the cells were then visualised under the light microscope to ensure proper suspension. The trypsinization was terminated using 12 ml of supplemented DMEM per flask and the cell suspension was then transferred to a sterile universal tube. The cell solution was then centrifuged for 5 mins at 1,000 rpm, the supernatant removed and the pellets re-suspended in 2 ml of supplemented DMEM. 1 ml of the cell culture was transferred to each of two T175 flasks containing 25 ml of supplemented DMEM and the flasks were placed in the 37 °C incubator.

7.2.4 Haemocytometer cell counting and bEnd.3 cell preservation

The cells were trypsinized as described previously, centrifuged for 5 mins at 1,000 rpm and the pellets were resuspended in 1 ml of DMEM. Make sure the haemocytometer is pre-cleaned with Ethanol. After a 1:10 dilution in DMEM was made, 20 µl of the diluted cell suspension was pipetted along the edge of a glass coverslip on top of the haemocytometer. Cells present within the four 16-square corner areas were counted. The total number of cells in the original bEnd.3 stock was calculated as follows:

bEnd.3 Stock No. = Average no. of cells from the corner grids x $10_{(\text{dilution})}$ x 10^4

Each corner volume is 0.1 mm^3 (1 mm x 1 mm x 0.1 mm). Hence, for the number of cells per ml (or cm^3), the factor 10^4 is used. For freezing the cells, the cell stock was added to 10 ml of DMEM followed by centrifugation and pellet resuspension in 2 ml of freezing media (80% FCS, 10% dimethyl sulfoxide and 10% DMEM) in CryoTubes (Nunc). bEnd.3 cells were stored in a -80 °C freezer for future use.

7.2.5 siRNA transfection of bEnd.3 cells using Lipofectamine 2000

The bEend.3 cells were transfected with the siRNA for RNAi based Claudin-5 knockdown using Lipofectamine LF2000 (Life technologies, USA). Lipofectamine reagent essentially forms vesicles of phospholipid bi-layer that mimic cell walls in an aqueous environment, entrapping and delivering siRNA to the cells. The bEnd.3 cells were firstly isolated from a T175 flask and counted using the haemocytometer. Each well from a 24-well plate was then seeded at a cell density of $1x10^5$ cells in 500 ml of DMEM. For each well of cells to be transfected: 20 picomoles of targeting or non-targeting siRNA was diluted in 50 µl of Opti-MEM (Gibco-Invitrogen). 1 µl of LF2000 was diluted in 50 µl of Opti-MEM in a 1.5 ml Eppendorf tube and incubated for 5 mins at room temperature. The diluted LF2000 was then combined with the siRNA and incubated for 20 mins at room temperature. Finally, 100 µl of the siRNA-LF2000 mixture was added to each well and mixed well. The plates were then swirled gently and placed in the 37 °C incubator for the required length of time (1, 2, 12, 24, 48, 72 and 96 hours time-points). All transfections were performed in triplicate and repeated two more times.

7.2.6 Total cellular RNA extraction from transfected cells

The total cellular RNA was extracted from the bEnd.3 cell line at the stated time points using reagents and instructions supplied in the Qiagen RNeasy© Mini Kit. After measuring the RNA concentration using the Nanodrop ND-1000 UV- Vis (Thermo Fischer, USA), the samples were aliquoted and stored at -80 °C.

7.2.7 Reverse transcriptase polymerase chain reaction (RT-PCR)

RT-PCR is an specialized polymerase chain reaction using the enzyme reverse transcriptase[30]. Isolated RNA from bEnd.3 cells samples was quantified using one-step real-time reverse transcriptase-PCR (RT-PCR) on a 7300 Real Time PCR System (Applied Biosystems) with Quantitect SYBR Green I as fluorescent dye (Qiagen). Quantitect One-Step RT-PCR Kit and standard protocol was used (Appendix A14 for full details). Post RT-PCR analysis was carried out on the 7300 System Software and relative gene expression levels were measured using the comparative C_t method ($\Delta\Delta C_T$). For all RT-PCR experiments, expression levels of target genes were standardized to the housekeeping gene, β-actin. To assess levels of RNAi-mediated tight junction suppression (suppression of the normal right junctions protein Claudin-5 functions using siRNA targeting of its mRNA expression levels), results were also expressed as a percentage of the non-targeting siRNA control (normalized to β-actin), where applicable.

7.2.8 Western blot analysis

Western blot is an analytical technique used to identify proteins by segregating them by molecular weight using denaturing sodium dodecyl sulphate-polyacrylamide gel electrophoresis and hence resolving them from the extract[31]. The separated proteins are then identified using specific antibodies and secondary detection antibodies (detailed protocol in Appendix A15).

7.2.9 Microcantilever assay: experimental protocol

The total RNA extracts obtained from the RNAi studies varied in their concentrations with different time points of extraction. Hence, the sample for the cantilever assay was normalized to a fixed total RNA concentration in order to keep the assay results comparable since it is evident from the previous studies that the background

competition does influence the deflection based assay. The total RNA concentration at time point 72 hours (80.4 ng/µl) was chosen as the base and all samples injected for assay were normalized to a total of 804 ng of total RNA per assay. Details of the calculations are available in the Appendix A16. Invitrogen Gibco PBS 1X was used as the buffer for all assays.

The instrumental setup was modified for the injection of the sample volume into the chamber using an analytical injection loop valve D UNI (ECOM, CZ). This is to accommodate the injection of the sample immediately after the denaturing step. Since a small sample volume of 11.11 µl was available in the loop, the time required for the entire sample from the loop to be emptied into the sensor chamber at the flow rate of the injection (60 µl/min) had to be pre-determined. One could calculate this time by determining the volume of the tubing. However this method is bound to introduce errors since the tubing volume and the volumes of the injection loops and valve are not definitely quantifiable. Hence, this time was calculated by emptying the loop (introducing air bubble) and then determining the time required for the bubble to empty into the chamber. The chamber volume is ~ 14 µl in comparison to the total of 11.11 µl of sample and it is assumed that the sample volume will mix into the flow cell. This is a limitation of the device for handling small volumes. However for the given sample (804 ng of total RNA) the effect of this dilution should be negligible.

All the general experimental pre-checks and protocols were followed as discussed in Section 5.2.3 of Chapter V. Cantilever sensors were prepared as per the protocol in Section 7.2.2. After the chamber was allowed to reach the temperature set-point, the following injection cycle was executed. A pre-experiment peltier test (0.7 V for 10 sec ~ 2 ^{o}C rise in temperature) was performed for normalization. After the chamber temperature restabilized (22.5 ^{o}C), a baseline was obtained for at least 10 mins. In order to separate the strands, the sample solution was denatured in a PCR tube at 80 ^{o}C for 4 mins and immediately transferred to an ice bath for 30 seconds followed by immediate injection into the chamber (injection of sample at 60 µl/min for a total loop-volume of 11.11 µl). The sensor was exposed to the sample for at least 30 mins to obtain an assay. Thereafter a buffer wash (800 µl at 150 µl/min) was executed followed by equilibration

for at least 15 mins in the buffer. A 4 M Urea injection (800 µl at 150 µl/min) was performed on the sensor for regeneration of the cantilever sensors. The sensors were left exposed to the 4 M Urea for at least 30 mins. The regeneration was completed with a buffer wash of at least 1000 µl followed by equilibration for at least 40 mins. For second sample injection, the same procedure was repeated. The sensors were always regenerated at the end using the 4M urea and buffer wash steps as before. A post-experiment peltier test was performed to ensure mechanical stability of the sensors.

7.3 Results and conclusions

The detection of siRNA in total RNA extracts from bEnd.3 cells exposed for different periods to Claudin-5 targeting was achieved using microcantilever sensors. Figure 7.3 shows the results of the differential nanomechanical response of the probe sensors, Sense and Antisense, to different times after transfection. It can be seen that the response is different for the two probes with the Antisense peaking at 24 hours as compared to the Sense that peaks later at 72 hours. Since the sample was denatured before injection, it is important to note that the strands detected by the individual probes could be a combination two different sources of the strands. One source are the individual strands that have been separated after RISC incorporation and the other are the strands separated due to the denaturation from delivered and intact intra-cellular siRNA that have not been processed by the RISC complex or degraded yet. It is important to note that that the cells were thoroughly washed with appropriate buffer before total RNA extraction and therefore the assay represents the intra-cellular siRNA which was transfected by Lipofectamine™ successfully into the cells.

The result indicates that the two different strands, although entering the cell as a double stranded siRNA (and must hence be in the same proportion when separated) do not seem to follow the same half life. The concentration of the Antisense strand (which after RISC incorporation cleaves mRNA) seems to begin to diminish after 24 hours. The RT-PCR and Western Blot results (from James Keaney, the Ocular Genetic Unit) also confirm the gradual loss of effective Claudin-5 silencing with time (Fig.7.4). The

passenger stand (Sense) concentration however peaks at a different time point. According to recent literature, the Sense strand degradation is rapid and may not take more than a few hours depending on the cell type[32,33]. The Antisense strand has been show to exhibit higher resistance to nuclease degradation probably because it is incorporated in the RISC[34]. In light of the literature one might want to draw a conclusion from the present results that the rate of degradation of the Sense strand is not constant throughout the period of the transfection leading to varying degree of available Sense strand in the total RNA extracts. The results are hence preliminary and more controlled experiments and assays will be required to have a detailed picture of the siRNA strand lifetime in the cells.

It could also be argued that the result might indicate an overwhelming of the cellular machinery by the large amounts of artificially introduced siRNA since the processes governing the siRNA strands inside a cell are not very well understood. The results hence demonstrate that the microcantilevers can be employed in concurrence with other current technologies to understand and elucidate broader open questions in the application of siRNA for gene silencing.

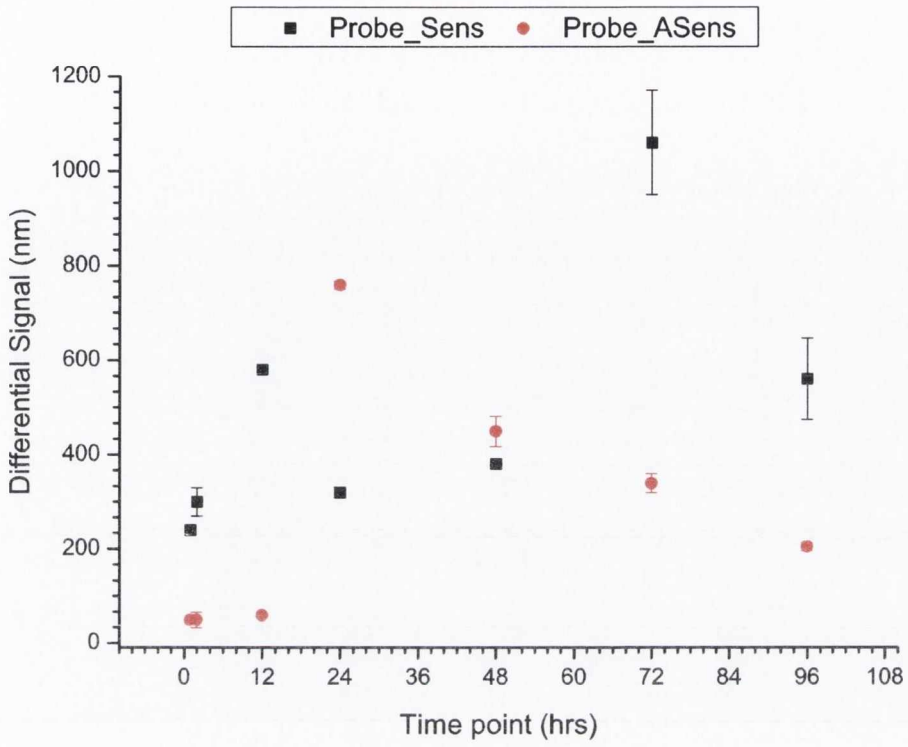

Fig. 7.3: Differential nanomechanical response of Sense and Antisense probes on exposure to total RNA extracts from siRNA transfected bEnd.3 cells at different time points after transfection (all points are for a normalized background of 804 ng of total RNA extracts) from 1 hour to 96 hours. The responses for the two probes are distinct with each showing a different time of peak concentration. It is unclear at this point why the Sense strand seems to be detected in higher proportions at certain time points late in the RNAi. The results are from three distinct sets of microcantilevers that have been regenerated using 4M Urea throughout the study and each point represents an experiment with one cantilever array with a minimum of three probe sensors (for both Sense and Antisense) each.

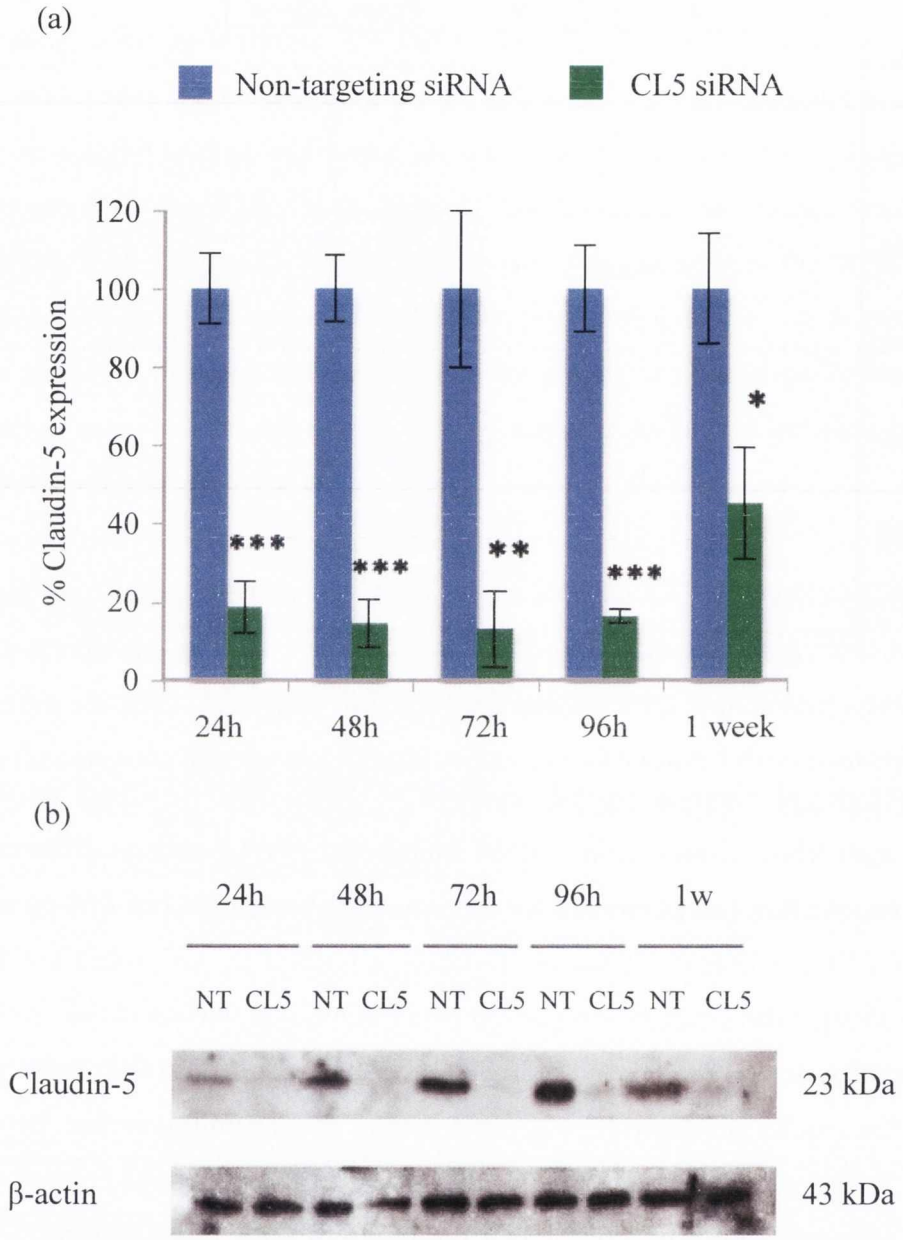

Fig. 7.4: Expression analysis (a) RT-PCR analysis of Claudin-5 mRNA expression. It clearly shows effective suppression as compared to a non-targeting siRNA (NT) with eventually a slow resurgence of the expression after 1 week of transfection (b) Western blot analysis of Claudin-5 protein expression. The β-actin provides a control for the analysis. From the analysis, it is clear that the siRNA was very effective in Claudin-5 suppression. (Results from James Keaney, Ocular Genetics Unit, TCD)

References

1 Rapoport, S. I. *Blood-brain barrier in physiology and medicine*. (Raven, 1976).

2 Bradbury, M. W. B. *The concept of a blood-brain barrier*. (Wiley, 1979).

3 Rubin, L. L. & Staddon, J. M. THE CELL BIOLOGY OF THE BLOOD-BRAIN BARRIER. *Annual Review of Neuroscience* **22**, 11-28, doi:doi:10.1146/annurev.neuro.22.1.11 (1999).

4 Pardridge, W. M. Transport of small molecules through the blood-brain barrier: biology and methodology. *Advanced Drug Delivery Reviews* **15**, 5-36, doi:10.1016/0169-409x(95)00003-p (1995).

5 Morganti-Kossmann, M. C. P., Rancan, M. M. D., Stahel, P. F. M. D. & Kossmann, T. M. D. Inflammatory response in acute traumatic brain injury: a double-edged sword. *Current Opinion in Critical Care* **8**, 101-105 (2002).

6 Yamamoto, T., Harada, N., Kawano, Y., Taya, S. & Kaibuchi, K. In VivoInteraction of AF-6 with Activated Ras and ZO-1. *Biochemical and Biophysical Research Communications* **259**, 103-107, doi:10.1006/bbrc.1999.0731 (1999).

7 Petty, M. A. & Lo, E. H. Junctional complexes of the blood–brain barrier: permeability changes in neuroinflammation. *Progress in Neurobiology* **68**, 311-323, doi:10.1016/s0301-0082(02)00128-4 (2002).

8 Kempski, O. Cerebral edema. *Semin Nephrol* **21**, 303-307, doi:DOI 10.1053/snep.2001.21665 (2001).

9 Del Maschio, A. *et al.* Leukocyte recruitment in the cerebrospinal fluid of mice with experimental meningitis is inhibited by an antibody to junctional adhesion molecule (JAM). *J Exp Med* **190**, 1351-1356 (1999).

10 Kubota, K. *et al.* Ca2+-independent cell-adhesion activity of claudins, a family of integral membrane proteins localized at tight junctions. *Curr Biol* **9**, 1035-1038 (1999).

11 Bazzoni, G. Endothelial tight junctions: permeable barriers of the vessel wall. *Thromb Haemostasis* **95**, 36-42, doi:Doi 10.1160/Th05-07-0488 (2006).

12 Comerford, K. M., Lawrence, D. W., Synnestvedt, K., Levi, B. P. & Colgan, S. P. Role of vasodilator-stimulated phosphoprotein in protein kinase A-induced changes in endothelial junctional permeability. *The FASEB Journal*, doi:10.1096/fj.01-0739fje (2002).

13 Haluska, M. & Anthony, M. Osmotic Blood-Brain Barrier Modification for the Treatment of Malignant Brain Tumors. *Clinical Journal of Oncology Nursing* **8**, 263-267, doi:10.1188/04.cjon.263-267 (2004).

14 Bartus, R. T. *et al.* Permeability of the blood brain barrier by the bradykinin agonist, RMP-7: Evidence for a sensitive, auto-regulated, receptor-mediated system. *Immunopharmacology* **33**, 270-278 (1996).

15 Vautier, S. *et al.* Interactions between the dopamine agonist, bromocriptine and the efflux protein, P-glycoprotein at the blood-brain barrier in the mouse. *Eur J Pharm Sci* **27**, 167-174, doi:DOI 10.1016/j.ejps.2005.09.009 (2006).

16 Kondoh, M., Yoshida, T., Kakutani, H. & Yagi, K. Targeting tight junction proteins-significance for drug development. *Drug Discov Today* **13**, 180-186, doi:DOI 10.1016/j.drudis.2007.11.005 (2008).

17 Campbell, M. *et al.* RNAi-mediated reversible opening of the blood-brain barrier. *J Gene Med* **10**, 930-947, doi:Doi 10.1002/Jgm.1211 (2008).

18 Echeverri, C. J. & Perrimon, N. High-throughput RNAi screening in cultured cells: a user's guide. *Nat Rev Genet* **7**, 373-384, doi:Doi 10.1038/Nrg1836 (2006).

19 Krause, G. *et al.* Structure and function of claudins. *Bba-Biomembranes* **1778**, 631-645, doi:DOI 10.1016/j.bbamem.2007.10.018 (2008).

20 Campbell, M. *et al.* An experimental platform for systemic drug delivery to the retina. *P Natl Acad Sci USA* **106**, 17817-17822, doi:DOI 10.1073/pnas.0908561106 (2009).

21 Persengiev, S. P., Zhu, X. C. & Green, M. R. Nonspecific, concentration-dependent stimulation and repression of mammalian gene expression by small interfering RNAs (siRNAs). *Rna* **10**, 12-18, doi:Doi 10.1261/Rna5160904 (2004).

22 Sledz, C. A., Holko, M., de Veer, M. J., Silverman, R. H. & Williams, B. R. G. Activation of the interferon system by short-interfering RNAs. *Nat Cell Biol* **5**, 834-839, doi:Doi 10.1038/Ncb1038 (2003).

23 Bridge, A. J., Pebernard, S., Ducraux, A., Nicoulaz, A. L. & Iggo, R. Induction of an interferon response by RNAi vectors in mammalian cells. *Nat Genet* **34**, 263-264, doi:Doi 10.1038/Ng1173 (2003).

24 Raymond, C. K., Roberts, B. S., Garrett-Engele, P., Lim, L. P. & Johnson, J. M. Simple, quantitative primer-extension PCR assay for direct monitoring of microRNAs and short-interfering RNAs. *Rna* **11**, 1737-1744, doi:Doi 10.1261/Rna.2148705 (2005).

25 Liu, W. L., Stevenson, M., Seymour, L. W. & Fisher, K. D. Quantification of siRNA using competitive qPCR. *Nucleic Acids Res* **37**, doi:ARTN e4
DOI 10.1093/nar/gkn903 (2009).

26 Hong, H., Zhang, Y. & Cai, W. B. In Vivo Imaging of RNA Interference. *J Nucl Med* **51**, 169-172, doi:DOI 10.2967/jnumed.109.066878 (2010).

27 Kim, E. J., Park, T. G., Oh, Y. K. & Shim, C. K. Assessment of siRNA pharmacokinetics using ELISA-based quantification. *J Control Release* **143**, 80-87, doi:DOI 10.1016/j.jconrel.2009.12.004 (2010).

28 Elbashir, S. M., Martinez, J., Patkaniowska, A., Lendeckel, W. & Tuschl, T. Functional anatomy of siRNAs for mediating efficient RNAi in Drosophila melanogaster embryo lysate. *Embo J* **20**, 6877-6888 (2001).

29 Ghosh, P. *et al.* Comparing 2-nt 3 ' overhangs against blunt-ended siRNAs: a systems biology based study. *Bmc Genomics* **10**, doi:Artn S17
Doi 10.1186/1471-2164-10-S1-S17 (2009).

30 Heid, C. A., Stevens, J., Livak, K. J. & Williams, P. M. Real time quantitative PCR. *Genome Res* **6**, 986-994 (1996).

31 Towbin, H., Staehelin, T. & Gordon, J. Electrophoretic Transfer of Proteins from Polyacrylamide Gels to Nitrocellulose Sheets - Procedure and Some Applications. *P Natl Acad Sci USA* **76**, 4350-4354 (1979).

32 Shin, S., Kwon, H. M., Yoon, K. S., Kim, D. E. & Hah, S. S. FRET-based probing to gain direct information on siRNA sustainability in live cells: Asymmetric degradation of siRNA strands. *Mol Biosyst* **7**, 2110-2113, doi:Doi 10.1039/C1mb05054k (2011).

33 Raemdonck, K. *et al.* In situ analysis of single-stranded and duplex siRNA integrity in living cells. *Biochemistry-Us* **45**, 10614-10623, doi:Doi 10.1021/Bi060351b (2006).

34 Kawamata, T. & Tomari, Y. Making RISC. *Trends Biochem Sci* **35**, 368-376, doi:DOI 10.1016/j.tibs.2010.03.009 (2010).

Chapter VIII

Outlook

We present here the application of the static mode detection of oligonucleotides from the initial instrumentation, highly sensitive detection of oligonucleotides in non-competitive environments, study of the effect of competition on sensor response to its eventual application in RNAi. The sensors are suitable for qualitative studies due to their ease of application and can be used for a quantitative analysis with proper references only. We have clearly demonstrated that they can compete with conventional techniques both in terms of sensitivity and selectivity. The sensors can be used in the dynamic mode (with a thickness of 1μm and higher) and have shown promising results for detecting bio-molecules[1-3] but are not capable of detection of such small strands of oligonucleotides without additional amplification of the mass using tagging methods like gold or polystyrene nanoparticles[4,5]. This method seriously affects the final assay since additional procedures for nanoparticle binding are introduced especially when detecting target molecules at very low concentrations (pico to femto moles).

As can been seen from our studies the assays are repeatable not only across a single chip but also across different sensor chips. The variation in the data can be attributed to

several aspects of the sensor manufacturing, its functionalization and the eventual experimental setups. The sensors are very delicate to handle and are extremely sensitive to functionalization techniques (functional gold layer and bio-molecules). In order to ensure repeatability across chips it is very important to control the parameters for the gold and titanium layer deposition (deposition time and rate; heat effects from the e-beam) and the thiol functionalization (surface activation, incubation time and functionalization medium). In addition to this, during experiments the stability of the temperature enclosure and laser power is essential. The difference of cantilever thickness in the sensor chip (tolerance for the 500 nm thick cantilevers within a wafer is 60 nm and within a chip is 10 nm) can attribute to variation in values of differential signal but this is avoided within a chip by data normalization and can be applied to an entire chipset from a manufacturer if a standard value of the normalization is included.

We have already taken the right steps for the application of microcantilever sensors towards direct applications for oligonucleotide sensing with a new and improved functionalization strategy, novel sensor deflection measurement setup and optimized buffer environments. For a commercial application we envisage the integration of the cantilevers with microfluidics so as to drastically reduce sample requirements. Also the passivation of the rear side of the cantilever that is exposed to the sample environment will help elucidate the complex mechanisms that affect cantilever deflection (interaction of sample and buffer with the bare silicon oxide surface). We have had preliminary success with such passivation and further more detailed studies are required.

8.1 siRNA detection in RNAi based silencing

It is a truly exciting time in RNAi research and the siRNA is a promising tool for drug discovery and understanding the fundamental processes in biology and medicine. In order to reveal the true feasibility of the siRNA based strategies for disease control, it is essential to understand its principles of administration, distribution in the organism, metabolism and its degradation in the body (intracellular fate and pharmacokinetics).

Using microcantilevers to detect the presence of the individual strands of siRNA, the current work has provided a new insight on how such nanomechanical systems could be utilised to understand the aforementioned processes.

The present detection of individual strands of siRNA was performed using a denaturing process just before the sample injection so as to detect all strands including the possibly intact double stranded siRNA that was transfected into the cells but not activated by the RISC complex. In order to track the presence of only the RISC separated Sense and Antisense strands[6,7], it is recommended an assay be performed at different time points without the denaturing step. The data from these two sets of experiments would eventually help elucidate the life times of both the RISC separated strands and the still intact double stranded siRNA which has been transfected to the cells but is not yet cleaved by endonucleases or separated by RISC. It is important to note here that one would have to determine whether the RISC bound Antisense strand is able to separate and then hybridize as efficiently to the functionalized cantilever sensor as the freed Antisense siRNA strand by denaturation. Data from such experiments could also be complimented by a more quantitative approach where the determination of the concentration of single strand oligonucleotide (either strand of the siRNA) and its sensor response (deflection) is quantified for dependence on background concentration as performed for the HSf71 oligonucleotides in Chapter VI over a wide range of background and target concentrations.

The current detection assay was performed with a considerable amount of the total cellular RNA extract for each time point per experiment (804 ng) leading to small injection volumes but a higher target concentrations leading to ease of detection. In the future, these experiments could be performed (and hence repeated) with much lower concentrations of the total cellular RNA (hence providing larger injection volumes) provided the results are all normalized to a given value of total RNA concentration to keep the deflection assays comparable.

8.2 Cantilever assays for oligonucleotides: Kinetics and the effect of competing molecules

The current work provides a robust and reproducible background for detection of oligonucleotides in buffers in complex genomics backgrounds using microcantilevers. The detection limits have been pushed further achieving new lower limits by improved sensor functionalization processes and optimised buffer systems. The behaviour of the sensor response to increasing competition in the background and the rarity of targets have also been investigated. Although the study of the kinetics was not in scope of this thesis, the current work is a first in providing information to sensor response in background which is a barely understood area in microcantilever and other surface immobilization based assays[8,9]. Various models have been posed theoretically with the aim of understanding the processes occurring on the surface where an immobilized single stranded probe hybridizes with a single stranded target in presence of other molecules but the sheer complexity of the system has made it hard to explain completely all the processes and to obtain a steady state equation[10-13]. Further, the phenomenon of hybridization leading to the stress formation in microcantilever sensors has been probed but is also not well understood and is still in its infancy since most studies do not consider the effect of the competing molecules[14-16].

The effect of the decreasing target concentration as a function of background concentration (Chapter VI, Section 6.3) was described using a logistic function Eq. 6.1. as below:

$$y = \frac{A1 - A2}{1 + (x/x_0)^p} + A2$$

From the trend in the model fitting parameters, it can be predicted that for increasing target concentration, the effect of background will diminish (increasing value of p and x_0) leading to a corresponding increasing value of the limit $A1$ for the system. It is recommended that, in order to understand the sensor response in its entirety, a similar

study but in very high target concentrations (nano to micro molar range) be carried out in background at equilibrium values. Overall, such experiments could possibly help decipher the processes governing microcantilever sensor response.

8.3 Instrumentation and sensor array functionalization

The current device is designed with a single micro-translation stage with improved focusing and scanning capability to scan the cantilever tips from an array. For a more detailed representation of the individual cantilever bending, an additional micro-translation stage could be employed for scanning along the length of the cantilever which will better help in revealing the full state of the microcantilever. The current temperature control system is robust and provides excellent control but it could use a smaller equilibration time. An improved system installed directly behind the chamber which can bring the chamber temperature to required temperature and maintain it with a lower equilibration period could be more effective. For applications that require analysis of small amounts of analyte such as in the range of a few microliters, a loop base injection system could be integrated into the main injection valve fluidics inside the equilibration chamber. It is also recommended to install a bypass line to the main suction lines coming to and from the chamber in order to deal with possible bubbles that may jeopardize the experiments.

Several sensor arrays on the main chip obtained from the manufacturer (IBM, Zurich) are contaminated with residues and particulate matter. For dealing with small amounts of contamination the new optimized protocol for cleaning and functionalization has proved to provide excellent function. However for many sensor arrays, the contamination is heavy and may be dealt with using a quick Hydrofluoric acid (HF) rinse for short times (10 - 30 seconds) in order to get rid of the contaminants with a minimal effect on the cantilever thickness. This will also need to be followed by an oxidizing process such as plasma cleaning to render the surface hydrophilic (since the HF etching leaves the surface hydrophobic) before the metal deposition. A scanning

electron microscope based visual analysis will be necessary thereafter to check for the effectiveness of the cleaning.

The activation of the gold surface on the microcantilevers is performed using the UV/Ozone cleaning method as described in Chapter III. This allows for the gold surface activation prior to the sensor bio-functionalization with thiolated probes. The current system uses cleaning (in air) with no additional oxygen provided. It is recommended that a dedicated filtered oxygen line is provided to the UV cleaner so as to increase the oxygen content in the cleaner for better and faster cleaning. Precaution will however need to be taken with high oxygen environment and the ozone produced.

References

1 Arntz, Y. *et al.* Label-free protein assay based on a nanomechanical cantilever array. *Nanotechnology* **14**, 86-90 (2003).

2 Wu, G. H. *et al.* Bioassay of prostate-specific antigen (PSA) using microcantilevers. *Nat Biotechnol* **19**, 856-860 (2001).

3 Mukhopadhyay, R. *et al.* Cantilever Sensor for Nanomechanical Detection of Specific Protein Conformations. *Nano Letters* **5**, 2385-2388, doi:10.1021/nl051449z (2005).

4 Su, M., Li, S. U. & Dravid, V. P. Microcantilever resonance-based DNA detection with nanoparticle probes. *Appl Phys Lett* **82**, 3562-3564, doi:Doi 10.1063/1.1576915 (2003).

5 Braun, T. *et al.* Micromechanical mass sensors for biomolecular detection in a physiological environment. *Phys Rev E* **72**, doi:Artn 031907
Doi 10.1103/Physreve.72.031907 (2005).

6 Meister, G. & Tuschl, T. Mechanisms of gene silencing by double-stranded RNA. *Nature* **431**, 343-349, doi:Doi 10.1038/Nature02873 (2004).

7 Sontheimer, E. J. Assembly and function of RNA silencing complexes. *Nat Rev Mol Cell Bio* **6**, 127-138, doi:Doi 10.1038/Nrm1568 (2005).

8 Okahata, Y. *et al.* Kinetic measurements of DNA hybridisation an an oligonucleotide-immobilized 27-MHz quartz crystal microbalance. *Anal Chem* **70**, 1288-1296 (1998).

9 Štěpánek, J., Vaisocherová, H. & Piliarik, M. Vol. 4 *Springer Series on Chemical Sensors and Biosensors* (ed Jiří Homola) 69-91 (Springer Berlin Heidelberg, 2006).

10 Erickson, D., Li, D. Q. & Krull, U. J. Modeling of DNA hybridization kinetics for spatially resolved biochips. *Anal Biochem* **317**, 186-200, doi:Doi 10.1016/S0003-2697(03)00090-3 (2003).

11 Weckx, S., Carlon, E., De Vuyst, L. & Van Hummelen, P. Thermodynamic behavior of short oligonucleotides in microarray hybridizations can be described using Gibbs free energy in a nearest-neighbor model. *J Phys Chem B* **111**, 13583-13590, doi:Doi 10.1021/Jp075197x (2007).

12 Ono, N. *et al.* An improved physico-chemical model of hybridization on high-density oligonucleotide microarrays. *Bioinformatics* **24**, 1278-1285, doi:10.1093/bioinformatics/btn109 (2008).

13 Georgiadis, R., Peterlinz, K. P. & Peterson, A. W. Quantitative measurements and modeling of kinetics in nucleic acid monolayer films using SPR spectroscopy. *J Am Chem Soc* **122**, 3166-3173 (2000).

14 McKendry, R. *et al.* Multiple label-free biodetection and quantitative DNA-binding assays on a nanomechanical cantilever array. *P Natl Acad Sci USA* **99**, 9783-9788, doi:DOI 10.1073/pnas.152330199 (2002).

15 Zhao, Y., Ganapathysubramanian, B. & Shrotriya, P. Cantilever deflection associated with hybridization of monomolecular DNA film. *Journal of Applied Physics* **111**, 074310-074319 (2012).

16 Hagan, M. F., Majumdar, A. & Chakraborty, A. K. Nanomechanical forces generated by surface grafted DNA. *J Phys Chem B* **106**, 10163-10173, doi:Doi 10.1021/Jp020972o (2002).

APPENDIX

A1: Piranha cleaning protocol for cantilever array

Materials:

- 2%-RBS solution
- Sulfuric acid 99.99%. Location: Under the hood in the acids drip pan. Do not take out from the glass baker.
- Hydrogen peroxide 30%. Note: Higher concentrated H_2O_2 can lead to explosions when mixing with sulfuric acid.
- Glassware:

  10 Small cups (ca. 4ml) for Piranha solution

  Work in a glass drip pan

  1L Beaker with deionized water
- Stainless steel or teflon (PTFE) tweezers
- 1M NaCl solution, 100 ml
- EtOH:H_2O (1:1), 100 ml
- Isopropanol

Precautions

Important: Piranha solutions are hot (>100°C) and produce poisonous gases. It reacts violently with all organic material. (Danger of explosions.) Other people in the lab must

be informed about the experiment. The cleaning must be performed between 0900 and 1800 on week days only. At least one other person must be present in the case of emergencies. All steps must be performed in a running fume-hood with lowered front plate. Avoid any contact with skin and inhalation. Always were *two* nitril gloves per hand and face protection. No other organic material must be stored in the hood. Only properly instructed persons are allowed to perform these experiments. Do not use any plastic material: It will be destroyed or even can lead to explosions! Keep a beaker with water to quench the solution after usage. Always make a minimal amount of Piranha-solution (e.g. 5ml). *For volumes > 20ml, additional protection is needed (additional special lab coat and gloves).*

Protocol

Phase	Treatment	Note
1	Pre cleaning in 2% RBS for 5min	
	10 sec wash in NaCl	
	30 sec wash in Nanopure water	
	Dry with filter paper	
2	Prepare Piranha -solution: H_2O_2:H_2SO_4 = 1:1 Prepare a minimal amount of solution (3x), always use glassware. Place the solutions in the glass drip pan Slowly add the hydrogen peroxide to the sulfuric acid. (H_2O_2 to sulfuric acid!)	
	Pre-bath: Holding for 30sec in Piranha solution	
	Washing in 10ml 1M NaCl for 10 sec	
	30 sec wash in Nanopure water	
3	First bath: 6ml Piranha volume for 20min	
	2 x 10ml 1M NaCl for 5min	
	10ml Nano-pure Water:EtOH = 1:1 for 5min	
	Wash in Nanopure water to remove EtOH	
4	Second bath: 2ml Piranha volume for 10min	
	5ml 1M NaCl for 5min	
	2x 5ml Nano-pure Water:ETOH 1:1 for 5min	
5	1x 5ml Isopropanol for 2 min	
	Drying on filter paper and store under Argon immediately	

(Note: Remove wash solutions with filter paper between each washing step)

Waste/Cleaning:

All chemicals must be diluted 1'000 times by water and dispose via the drain. Let the water run for 5 min. NEVER store used Piranha!

Cleaning of instruments:
Incubate all instruments/glasses in water for 15min. Rinse with EtOH and dry.

A2: New cleaning protocol for cantilever arrays

Materials: Acetone (HPLC grade), Filter paper, Ethanol (HPLC grade)

Procedure:

a. Using the Boekel UV Ozone cleaner, clean the array for 2 mins.
b. Soak in HPLC grade Acetone for at least 30 mins.
c. Dry carefully on filter paper/hot plate.
d. Using the Diener PICO Barrel Asher (Oxygen Plasma cleaner), clean array for 3 mins for the plasma operating at 0.3 mbar O_2 for 3 minutes at 160 W, 40 kHz power setting for the device using the custom made holder to ensure both sides of the cantilever sensors are cleaned.
e. Soak in HPLC Ethanol for 2 minutes.
f. Proceed immediately with Titanium–Gold functionalization in the Temescal.

A3: Modified PSD Amplification Electronics for 150 kHz PSD (G=1)

Shown below is a schematic of the modified PSD. The cut-off frequency, f_c (Hz) is defined as below.

$$f_c = \frac{1}{2\pi RC}$$

where R– Resistance (in ohms) and C– Capacitance (in Farads). For R=10K and C=100 pF, f_c = 159.134 kHz

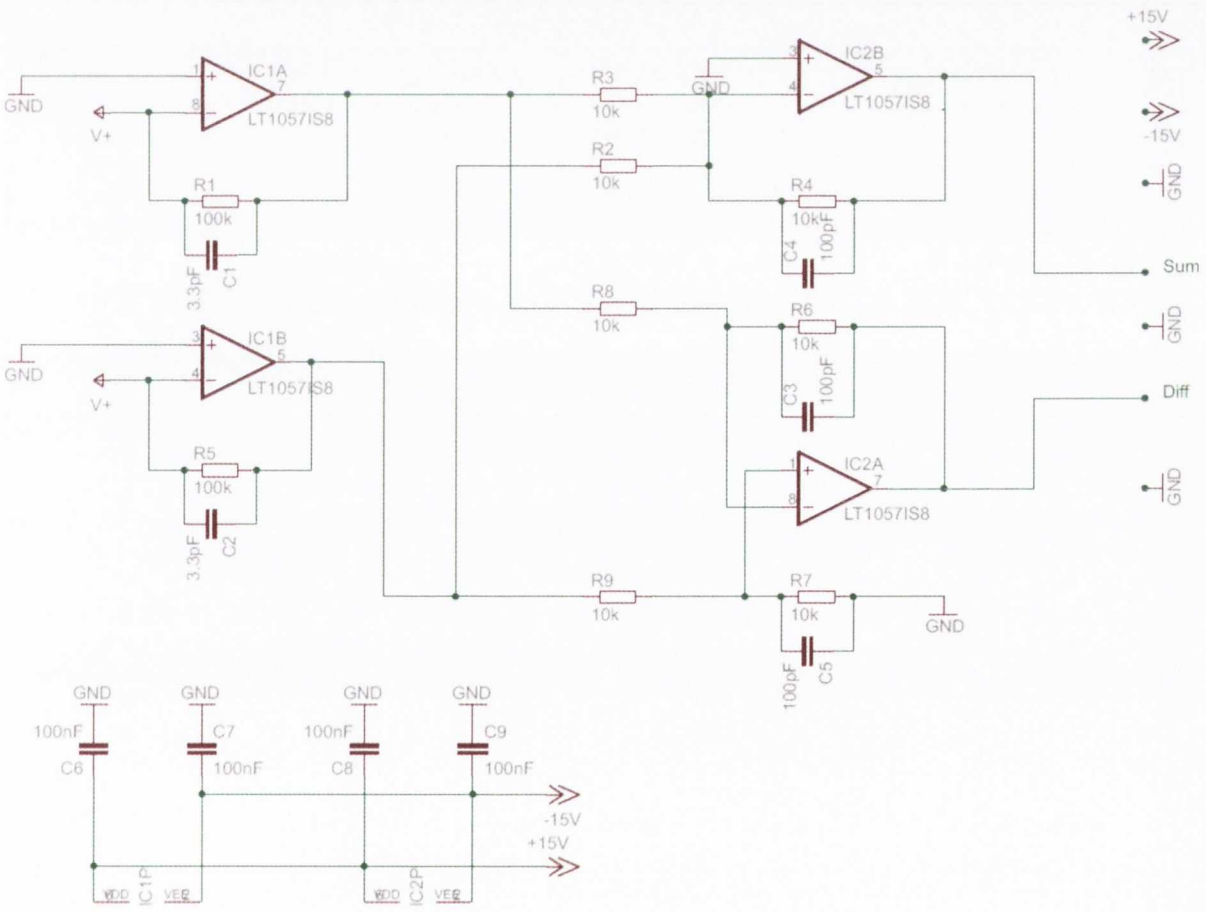

A4: Sample preparation for studies of sensitivity and specificity (Chapter V)

A4.1: Calculations for sample preparation for specificity assay with targets HSf71 match, HSf71 mismatch and let7b sequences (Section 5.3)

		Stock Concentration		
Buffer	NaCl in SSC	=	3.00E+06 uM
Oligos	HSf71 match -C	=	119 uM
	HSf71 mismatch -C	=	113 uM
	hsalet7b compl -C (DNA)	=	128 uM
Buffer	SSC	=	3.00E+05 uM

WE NEED (before changing NaCl concentration)		
Final Solution Volume for Injection in Chamber	=	5000 ul
Oligo Concentration	=	0.1 uM
NaCl SSC Concentration	=	7.50E+05 uM
SSC	=	7.50E+04 uM

	Oligo Stock (ul)	NaCl SSC (ul)	SSC	Water to top up (ul)before changing Nacl	For 1 M Nacl final concentration add (ul) from 1 M stock	Final volume of water for TOPUP (ul)
HSf71 match -C	4.201680672	1250.00	1250.00	3745.80	1250	2495.80
HSf71 mismatch -C	4.424778761			3745.58	1250	2495.58
hsalet7b compl -C (DNA)	3.90625			3746.09	1250	2496.09

↓

Only to cross check for right volume
NaCl and SSC are both the same solution

FOR 1M NaCl in the Final Solution		
Final NaCl Concentration required	=	1.00 M
Add NaCl to this Diluted Stock		
NaCl Mol wt:	=	58.44 g/mol
Moles of NaCl to be added	=	2.50E-01 M
Weight of NaCl to be added	=	14.61 gms/l
Hence for 5.00E-03 liters, weight of NaCl	=	**0.07305** gms

Final solution is		
	Volume	5000 ul
	All Oligos	0.1 uM
Buffer:	SSC	7.50E+04 uM
	NaCl	1.00 M

From a Stock of **1** M NaCl
Additional Volume of NaCl needed = **1250** ul
to get additional
2.50E-01 Moles of NaCl

The solutions prepared as above were used for the assay described in Section 5.3.3 in Chapter V.

A4.2: Calculations for sample preparation for target BioB2-C assay in SSC 1X, 1 M NaCl (Section 5.4.3.1)

		Stock Concentration			
Buffer	NaCl SSC	=	3.00E+06 uM		
Oligos	BioB2-C	=	0.00005 uM		
Buffer	SSC	=	3.00E+05 uM		

WE NEED (before changing NaCl concentration)				
Final Solution Volume for Injection in Chamber	=	5000 ul		
Oligo Concentration	=	0.00001 uM		**10pM**
NaCl SSC Concentration	=	7.50E+05 uM	5X	
SSC	=	7.50E+04 uM	5X	

		Oligo Stock	NaCl SSC	SSC	Water to top up		For 1 M Nacl final concentration add			Final volume of water for TOPUP		
		(ul)	(ul)		(ul)before changing Nacl		(ul) from	1	M stock	(ul)		
BioB2-C		1000	1250.00	1250.00	2750.00		1250			1500.00		

↓

Only to cross check for right volume
NaCl and SSC are both the same solution

FOR 1M NaCl in the Final Solution			
Final NaCl Concentration required	=	1.00 M	
Add NaCl to this Diluted Stock			
NaCl Mol wt:	=	58.44 g/mol	
Moles of NaCl to be added	=	2.50E-01 M	
Weight of NaCl to be added	=	14.61 gms/l	
Hence for 5.00E-03 liters, weight of NaCl	=	**0.07305** gms	

	Final solution is	
	Volume	5000 ul
	BioB2-C	0.00001 uM
Buffer:	SSC	7.50E+04 uM
	NaCl	1.00 M

From a Stock of **1** M NaCl
Additional Volume of NaCl needed = **1250** ul
to get additional
2.50E-01 Moles of NaCl

The solutions prepared as above were used for the assay described in Section 5.4.3.1 in Chapter V.

A4.3: Calculations for sample preparation for target BioB2-C assay in Gibco PBS buffer (Section 5.4.3.2)

	Stock Concentration		
Buffer	PBS 10 X	=	1.00E+01 X
Oligo	BioB2- C	=	1 nM

Required		
Final Volume of soln	=	1000 ul
BioB2-C Conc	=	10 pM
PBS Conc	=	1 X

Recipe	From Stock (ul)	Water to top up (ul)
PBS 10 X	100	890.00
BioB2- C	10	

The solutions prepared as above were used for the assay described in Section 5.4.3.2 in Chapter V. The stock solution for the BioB2-C (1 nM shown in the above calculation) is obtaiined after diluting the original stock.

A5: Composition of Gibco PBS Buffer

Components	**Molecular Weight**	**Concentration (mg/L)**	**mM**
Inorganic Salts			
Calcium Chloride ($CaCl_2$) (anhyd.)	111	100	0.901
Magnesium Chloride ($MgCl_2$-$6H_2O$)	203	100	0.493
Potassium Chloride (KCl)	75	200	2.67
Potassium Phosphate monobasic (KH_2PO_4)	136	200	1.47
Sodium Chloride (NaCl)	58	8000	137.93
Sodium Phosphate dibasic (Na_2HPO_4-$7H_2O$)	268	2160	8.06

Reference:

Dulbecco, R. and Vogt, M., (1954) *Plaque formation and isolation of pure lines with Poliomyelitis viruses*. J. Exp. Med., **98**:167

A6: Data analysis for 50 pM BioB2-C injection from Section 5.4.3.1

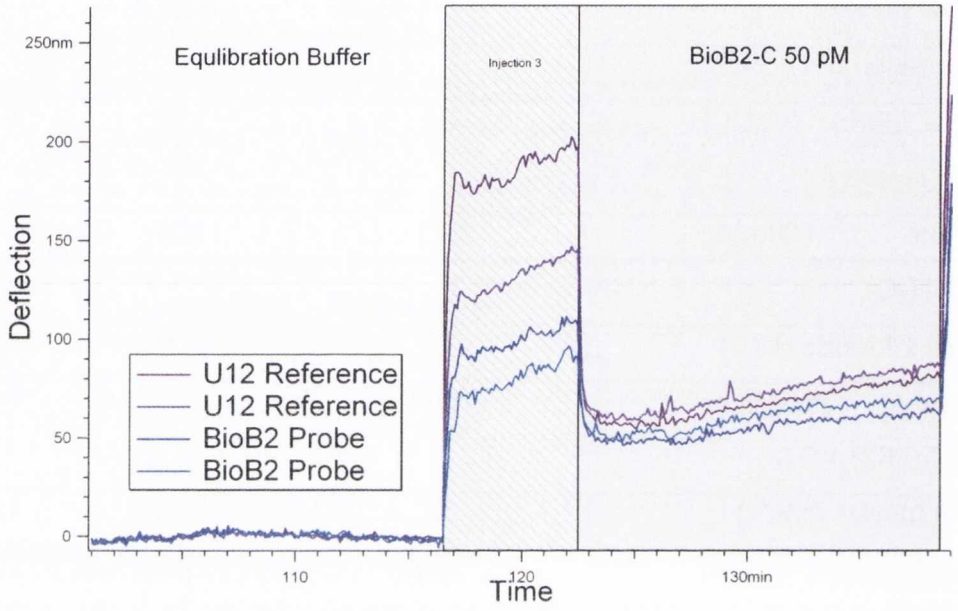

(a)

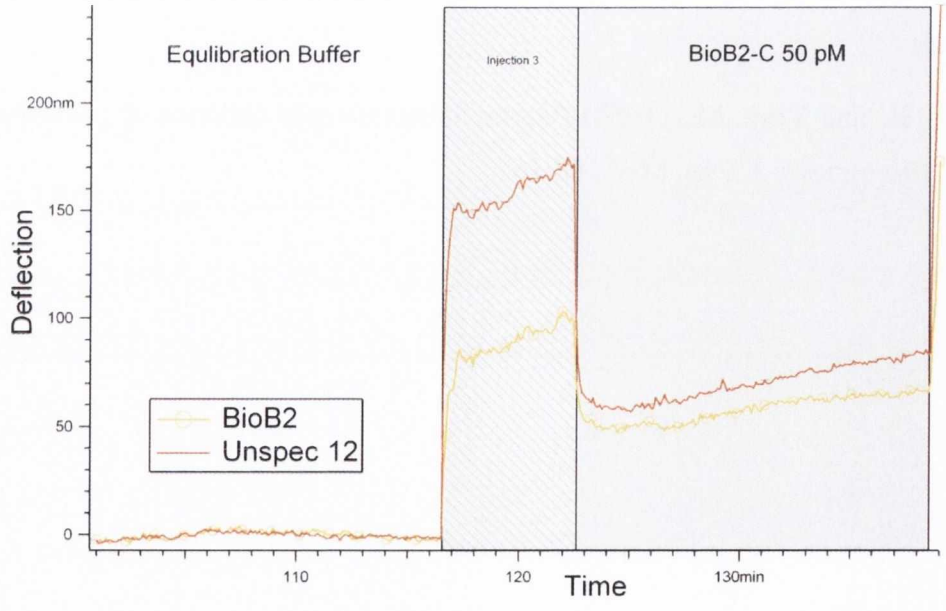

(b)

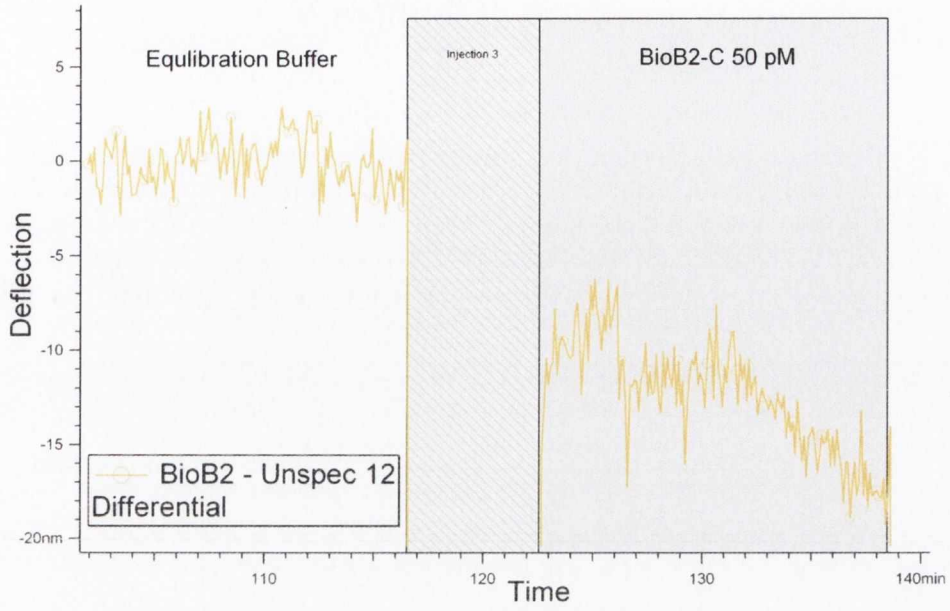

(c)

Fig. A1: Injection of target BioB2-C (50 pM) at 150µl/min for 800µl in SSC 1X 1M NaCl buffer (a) Baseline corrected and normalized raw data (b) Average sensor response for probe and reference sensors (c) Differential response for the BioB2-C assay. A smaller sensor response is seen despite a higher concentration on the target molecule.

From the differential analysis it can be seen that the sensor response is 15 nm at the time point of 20 mins which is a minor response when compared to the previous target assay at 10 pM concentration. The smaller response to a higher concentration of target after a regeneration points to the inability of the buffer wash to completely regenerate the chip by de-hybridization of target ssDNA molecule. Buffer wash does not seem to reduce stability of previously hybridized targets completely and only removes unspecific bound targets thereby leaving some binding sites 'blocked' for subsequent hybridizations in the 50pM BioB2-C injection. This can also be inferred when the time of incubation and the volume of buffer in this present regeneration is compared to literature values where the regeneration buffer volume and time both are significantly higher*.

* Zhang, J. *et al.* Rapid and label-free nanomechanical detection of biomarker transcripts in human RNA. *Nat Nanotechnol* **1**, 214-220, doi:DOI 10.1038/nnano.2006.134 (2006).

A7: Experimental protocols: Chapter V

A7.1: Experimental Protocol for Specificity of Cantilever assay (Section 5.3)

After the chamber was allowed to reach the temperature set-point, the following injection cycle was executed:

1. Pre-Experiment Peltier Test: 0.7 V for 10 sec ~ 2 °C rise in temperature
2. Baseline
3. Positive Control: 100 nM Let7b in SSC 5X, 1 M NaCl.
4. Equilibration for 15 mins.
5. Buffer SSC 5X, 1 M NaCl injection for 8 mins.
6. Equilibration for 10 mins.
7. Selectivity Control: 100 nM HSf71-mismatch in SSC 5X, 1M NaCl
8. Equilibration for 15 mins.
9. Buffer SSC 5X, 1 M NaCl injection for 8 mins.
10. Equilibration for 10 mins.
11. Target: 100 nM HSf71 in SSC 5X, 1M NaCl
12. Equilibration for 15 mins.
13. Buffer SSC 5X, 1 M NaCl injection.
14. Post-Experiment Peltier Test: 0.7 V for 10 sec ~ 2 °C rise in temperature

A7.2: Experimental Protocol: Cantilever assay for BioB2 gene sequence at rare concentrations (Section 5.4)

After the chamber was allowed to reach the temperature set-point, the following injection cycle was executed:

1. Pre-experiment Peltier Test: 0.7 V for 10 sec ~ 2 °C rise in temperature.
2. Baseline.

3. Inject target solution: BioB2-C in appropriate buffer.
4. Equilibration for 15-30 mins.
5. Buffer wash 800 μl at 150 μl/min.
6. Equilibration for 15 mins.
7. Post-experiment Peltier Test: 0.7 V for 10 sec.

A8: Experimental protocols: Chapter VI

A8.1: Extraction of UHRR prior to fragmentation

Prior to fragmentation, the UHRR was extracted from this solution using the following protocol.

1. Required amount of UHRR (usually 200 µl from the stock solution) was centrifuged (Hettich, DE) at 12,000 x g for 15 minutes at 4°C.
2. After carefully removing the supernatant, the pellet was washed with 70 % HPLC grade ethanol (Sigma, DE).
3. Solution was centrifuged at 12,000 x g for 15 minutes at 4°C.
4. The supernatant was removed and the pellet was dried at room temperature for 30 mins to remove retained ethanol.
5. The pellet was then resuspended in RNAase free Diethylpyrocarbonate (DEPC) treated water (Ambion, USA) to the desired concentration (at least 1µg/µl). The absorbance was checked with ND-1000 UV-VIS spectrophotometer (Nanodrop, USA). The A_{260}/A_{280} ratio must be between 1.9 and 2.1 before proceeding to fragmentation.

A8.2: UHRR fragmentation protocol

In order to maintain proper temperature, a Thermal Cycler was used. The protocol proceeds as below:

1. Combine the 5X fragmentation buffer and the UHRR plus DEPC water in the ratio 1:4. Also, make sure the final concentration of the RNA in solution is no less than 0.5 µg/µl. E.g.: For UHRR at a concentration of 1µg/µl and final solution of 40 µl mix: 20 µl of UHRR (1µg/µl), 12 µl of DEPC water and 8 µl of 5X fragmentation buffer.
2. Incubate at 94°C for 35 minutes. Cool to 4°C and place on ice.

3. Mix, the now fragmented UHRR solution with 3M Sodium Acetate (Sigma Aldrich, DE) and 100% HPLC grade Ethanol in the ratio of 10: 1: 32.5 by volume respectively and place on dry ice or at -80°C for at least 30 mins.
4. Centrifuge the solution at 14,000 x g for at least 30 mins at 4°C.
5. Remove the supernatant and wash the pellet with ~3 times by volume of 80 % HPLC grade Ethanol.
6. Centrifuge the solution at 14,000 x g for 5 mins.
7. Carefully drain the ethanol from the tube and air dry the pellet for 30 mins or use the vacuum concentrator (Savant DNA Speedvac, USA) for 3 mins without heating.
8. Resuspend in DEPC water to a suitable concentration generally higher than 1µg/µl.
9. Immediately store the solution at -80°C for further use.

A8.3: Experimental protocol: Cantilever assay for HSf71 target in fragmented UHRR (Section 6.2.4)

After the chamber was allowed to reach the temperature set-point, the following injection cycle was executed:

1. Pre-experiment peltier test: 0.7 V for 10 sec ~ 2 °C rise in temperature.
2. Equilibration time till temperature is restabilized in the sensor chamber.
3. Baseline for at least 10 mins.
4. Sample solution injection at 150 µl/min for a total of 800 µl.
5. Equilibration for at least 30 mins.
6. Buffer wash (800 µl).
7. Equilibration for at least 15 mins.
8. 4 M Urea injection (800 µl; for regeneration as required).
9. Equilibration in 4 M Urea for at least 30 mins.
10. Buffer wash of 1000 µl followed by equilibration for at least 40 mins.
11. Repeat steps 3 to 10 for second sample injection.
12. Post-experiment peltier test: 0.7 V for 10 sec ~ 2 °C rise in temperature.

A9: Datasheet for UHRR obtained from Agilent Tech.

Universal Human Reference RNA

Catalog #740000

Storage Store the Universal Human Reference RNA at –80°C. Store the RNase-free water at –20°C.

Introduction

Stratagene's Universal Human Reference RNA is composed of total RNA from 10 human cell lines. The reference RNA is designed to be used as a reference for microarray gene-profiling experiments. Since RNA species differ in abundance between cell lines, an ideal reference sample should represent these different RNAs. Equal quantities of DNase-treated total RNA from each cell line were pooled to make the Universal Human Reference RNA. This Universal Reference RNA is suitable for microarray experiments. Stratagene also supplies a QPCR Human Reference Total RNA, suitable for QRT-PCR, which has undergone further DNase treatment.

Materials Provided

Material Provided	Quantity
Reference RNA	2 tubes x 200 µg each
RNase-free water	1.5 ml

Cell Line Derivations	
Adenocarcinoma, mammary gland	Melanoma
Hepatoblastoma, liver	Liposarcoma
Adenocarcinoma, cervix	Histiocytic lymphoma; macrophage; histocyte
Embryonal carcinoma, testis	Lymphoblastic leukemia, T lymphoblast
Glioblastoma, brain	Plasmacytoma; myeloma; B lymphocyte

Additional Materials Required

RNase-free 70% Ethanol

Protocol

Universal Human Reference RNA is provided in a solution of 70% ethanol and 0.1 M sodium acetate. Prepare the Reference RNA for use as follows:

1. Centrifuge the tube at 12,000 × g for 15 minutes at 4°C.
2. Carefully remove the supernatant.
3. Wash the pellet in 70% ethanol.
4. Centrifuge the tube at 12,000 × g for 15 minutes at 4°C.
5. Carefully remove the supernatant and air-dry the pellet at room temperature for 30 minutes to remove retained ethanol.
6. Resuspend the pellet in RNase-free water to the desired concentration.

Proceed with the preparation of labeled cDNA and interrogate the arrays according to the manufacturer's instructions.

Quality Control Testing

The quality of the Universal Human Reference RNA is assessed by observing distinct 28S and 18S ribosomal bands on a 1× MOPS agarose gel under denaturing conditions. The purity of the RNA is assessed by spectrophotometry (A260/A280 ≥1.8). The RNA is then shown to be free of contaminating RNases by incubation in a suitable buffer at 37°C followed by gel analysis against known RNAse-free controls. The RNA is further tested functionally by synthesizing labeled cDNA, which is then hybridized to a microarray to examine gene representation and coverage.

Limited Product Warranty

This warranty limits our liability to replacement of this product. No other warranties of any kind, express or implied, including without limitation, implied warranties of merchantability or fitness for a particular purpose, are provided by Stratagene. Stratagene shall have no liability for any direct, indirect, consequential, or incidental damages arising out of the use, the results of use, or the inability to use this product.

A10: UHRR Fragmentation buffer

For 5X Fragmentation Buffer: 200mM Tris-acetate, pH 8.1; 500 mM KOAc; 150 mM MgOAc

1M Tris acetate pH 8.1	: 4 ml
MgOAc	: 0.64 g
KOAc	: 0.98 g
DEPC-water	: Top up to 20 ml

A11: Calculations for sample preparation for detection of HSf71 gene in fragmented UHRR in PBS buffer

Fragmented Total RNA (Universal Human Reference) Background Experiments

Aim: **1000** ul — Final Solution for Injection in the experiments (in 1 X PBS buffer)

Material

Stock fragmented RNA (S)		1368.4	ng/ul
Median Size of Fragmented RNA (N)		50	nucleotides
Apprx. Mol. Wt. based on Median Size		16104	daltons
M = (N x 320.5)+79	(monophosphate)		
Concentration in moles (S/M)		8.49727E-05	M

HS f71 (target molecule) stock	**1**	nM
BioB2 - C stock	**100**	nM
PBS Stock	**10**	X

Recipe

Final Frag RNA concentration (pM)	Stock Frag RNA (ul)	PBS Buffer(10X) top up (ul)	Water to top up (ul)
500000	**5.884244373**	**100**	**384.1157556**
HS f71 target (pM)	Stock HS f71 (ul)		
500	**500**		
BioB2 (pM)	Stock Bio B2 (ul)		
1000	**10**		

500 pM target **500 nM background**

The above is a sample calculation for the experiments discussed in Chapter VI, Section 6.2.4. The target HSf71 match concentrations (10 pM, 100 pM and 500 pM) were prepared for injection in the Invitrogen Gibco PBS 1X buffer with different fragmented UHRR concentrations (0 nM, 1, nM, 10 nM, 100 nM and 500 nM). When BioB2-C was used as a control the concentration was kept constant at 1nM.

A12: Sense sequence for targeting with the siRNA for Claudin-5 suppression

1 agttggtgta gttaaaacct cctcttctgc tccaggactg gaggctccag agcagaggca
61 ccagaatcaa ttcccagctc ccagcctaag cagcgcagag agcacccgga ggccccaagg
121 gccgtcgggt gagcattcag tctttagcca tggggtctgc agcgttggaa attctgggtc
181 tggtgctgtg tctggtagga tgggtgggct tgatcctggc gtgtgggctg cccatgtggc
241 aggtgactgc cttcctggac cacaacatcg tgacggcgca gacgacttgg aaggggctgt
301 ggatgtcgtg cgtggtgcag agtaccgggc acatgcagtg caaggtgtat gaatctgtgc
361 tggcgctgag tgcggaggtg caggcagctc gggcactcac cgtgggcgct gtgctgctgg
421 cgctggtggc actctttgtt accttgaccg gcgctcagtg caccacctgc gtggccccgg
481 gcccagttaa ggcacgggta gcactcacgg gaggagcgct ttacgcggtg tgcgggctgc
541 tggcactcgt gccgctctgc tggttcgcca acatcgttgt ccgcgagttc tatgatccga
601 cggtgccggt gtcacagaag tacgagctgg gcgcggcgct gtacatcggc tgggcggcct
661 ccgcactgct catgtgcggt ggcggcctcg tgtgttgcgg cgcctgggtc tgcaccgggc
721 gccctgagtt cagcttcccg gtcaagtact ctgcgccgcg gcggcccacg gccaatggcg
781 attacgacaa gaagaactat gtctaagggc gggaggcatg gcggggctct tcccgcagct
841 aagcccgcga tgggaaagac cgatgcggga agccgtgtgt ggatgacgac caccgctggg
901 ttgcgcagcg caagtcatgc tgggttcggg ccagacttgc ccgctctcag agtccgttga
961 ccatcactag ccgggccctg ctcagaacag actacaggca cttttaagaa cttgaccgac
1021 cttttcttct atgcgcagtt ggccacgacg tgggtggaac gctcagattt catcggtgaa
1081 gtaggcacca aactgccgcg aacagttcct actgagatcc tgggggcact agatgctgcc
1141 ttaatgtcca gtggcacctg ctaacctgaa agggcagctg gagaaacccc ggggctgcca
1201 gagggacgtg ttaaaaaggg cattttcttt gttagtggag aagaacctac tgaaccaaag
1261 gacttagcct ggacctggtc tcactccagc actcccccaa ggtgggggcc ctgtaggtac
1321 cagagcctta gaggggttgc cttcctcctg gaagcttggg gcttgggggg tgggccgggc
1381 aagaatttgc tcagtaaatg gtttgaacac tttcaaaaaa

Blue: CLDN5 siRNA sense sequence (followed by "gg" in mRNA sequence)

More details at: http://www.ncbi.nlm.nih.gov/gene/12741

A13: Protocol for siRNA transfection of bEnd.3 cells using Lipofectamine 2000

The following protocol was used:

- As described above, the bEnd.3 cells were firstly isolated from a T175 flask and counted using the haemocytometer.
- Each well from a 24-well plate was seeded at a cell density of $1x10^5$ cells in 500ml of DMEM.
- For each well of cells to be transfected: 20 pmoles of targeting or non-targeting siRNA was diluted in 50µl of Opti-MEM (Gibco-Invitrogen). 1µl of LF2000 was diluted in 50µl of Opti-MEM in a 1.5ml eppendorf tube and incubated for 5 min at room temperature. The diluted LF2000 was then combined with the siRNA and incubated for 20 min at room temperature.
- Finally, 100µl of the siRNA-LF2000 mixture was added to each well and mixed well. The plates were then swirled gently and placed in the 37°C incubator for the required length of time (1, 2, 12, 24, 48, 72 and 96 hours time points). All transfections were performed in triplicate and repeated two more times.

A14: Protocol for Reverse transcriptase polymerase chain reaction analysis of bEnd.3 cells

Isolated RNA from bEnd.3 cells, GFP^+ endothelial cells and capillary fractionation samples was quantified using one-step real-time reverse transcriptase-PCR (RT-PCR) on a 7300 Real Time PCR System (Applied Biosystems) with Quantitect SYBR Green I as fluorescent dye (Qiagen). The Quantitect One-Step RT-PCR Kit was able to support reverse transcription and subsequent gene-specific amplification in a single tube.

15µl of the following master mix was added to each well of a 96-well plate:

Component	**Volume**
2x Quantitect SYBR Green	10µl
Quantitect RT Mix	0.15µl
Primer Mix	1µl
RNase-free water	3.85µl
Total Volume/Well	**15µl**

Note: The reaction components of a master mix for one-step RT-PCR showing volumes for a single well/reaction are shown above. This was prepared in bulk depending on the number of wells being used

The sequences of complementary DNA PCR primers (Sigma-Aldrich) for RT-PCR experiments are provided in the appendix. Forward and reverse primers (10pmol/µl) for the sequence of interest were pooled and master mixes were then vortexed and spun down before addition to 96-well plates. 5µl of sample RNA (0.4ng/µl) or H_2O was added to each well to give a total reaction volume of 20µl. Plates were then covered with an acetate sheet, spun down and placed in the 7300 Real Time PCR machine. RT-PCR reaction conditions were as follows:

- **Stage 1** (reverse transcription): 50°C x 20 min
- **Stage 2** (activation of Taq DNA pol): 95°C x 15 min
- **Stage 3** (cDNA amplification): [95°C x 15 sec
  60°C x 1 min] X 37 times
- **Stage 4** (dissociation stage): 95°C x 15 sec
  60°C x 1 min
  95°C x 15 sec

Post RT-PCR analysis was carried out on the 7300 System Software and relative gene expression levels were measured using the comparative Ct method ($\Delta\Delta C_T$). For all RT-PCR experiments, expression levels of target genes were standardized to the housekeeping gene, β-actin. To assess levels of RNAi-mediated tight junction suppression, results were also expressed as a percentage of the non-targeting siRNA control (normalized to β-actin), where applicable.

A15: Western blot analysis of siRNA efficiency

For western blot analysis, resolving and stacking gels were prepared to separate the protein samples by sodium dodecyl sulphate-polyacrylamide (SDS-PAGE) gel electrophoresis. 10% resolving gel were prepared using 4ml distilled H_2O, 2.5ml 1.5M Tris-HCl (pH 8.8), 3.33ml 30% acrylamide, 100µl 10% SDS, 100µl ammonium persulfate (APS), and 10µl TEMED. This was mixed gently and the gel was poured between the assembled glass plates to 1cm below the comb teeth using a 10ml pipette. The gel was then overlaid with water (to provide air-free conditions for polymerization) and allowed to polymerize for 30 mins at room temperature. The overlaying ethanol was poured off and on top of this was poured a 4% stacking gel consisting of 6.1ml distilled H_2O, 2.5ml 0.5M Tris-HCl (pH 6.8), 1.3ml 30% acrylamide, 100µl 10% SDS, 100µl APS, and 10µl TEMED. The comb was then carefully inserted into the stacking gel and the gel was allowed to polymerize for 15 min. The glass plate was inserted into the Mini-Protean 3 electrophoresis module which was filled with 1X running buffer and the comb was removed prior to sample loading.

6µl of loading buffer (Thermo Scientific) was added to 30µl of protein aliquots) and heated for 5 mins at 100°C along with 10µl of a pre-stained protein ladder (New England BioLabs). Equal amounts of samples (as determined by BCA assay) were carefully loaded into the lanes and the order of sample loading recorded. The SDS-PAGE gel was run at 60mA for 1 hour in 1X running buffer.

Filter papers and polyvinylidene fluoride (PVDF) membranes were cut out to the dimensions of the gel and soaked in transfer buffer (consisting of 2.9g glycine, 5.8g Tris, 0.037g SDS, 200ml methanol and made up to 1 litre with deionised H_2O). Following SDS-PAGE electrophoresis, the gel was removed from the glass plates and transferred to a Mini Trans-Blot cell module. This cassette consisted of 4 filter papers and a PVDF membrane onto which the gel was placed and 4 more filter papers stacked on top. The transfer module was then closed and compacted tightly and an electric

current run through the cassette at 80mA for 2 hours for electrophoretic transfer of proteins onto the PVDF membrane.

The blot was removed from the transfer module and 10ml of blocking solution (5% skimmed milk in 1X TBS) was added to the blot and incubated at room temperature for 30 mins with gentle rocking. This was poured off and the membrane was washed with 1X TBS for 5 min. The blot was then probed with a 1:500 (rabbit anti-Claudin-5, Invitrogen) or 1:1000 (rabbit anti-Occludin or rabbit anti-Tricellulin, Invitrogen) dilution of the primary antibody, in 5% skimmed milk in 1X TBS. The membrane was covered and incubated overnight at 4°C on a rocker. The next morning the antibody solution was poured off and the blot was washed 3 x 15 mins in 1X TBS. This was followed by detection of primary antibody complexes using a 1:2000 dilution of horseradish peroxidase (HRP)-conjugated goat anti-rabbit secondary antibody (Abcam) in 5% skimmed milk in 1X TBS. The membrane was placed on the shaker for 2 hours and the blot then washed 3 x 15 mins in 1X TBS. To detect HRP, the immunoblot was placed in SuperSignal Chemiluminescence Substrate (Pierce) solution (1ml of reagent A and 1ml of reagent B) and agitated for 2 min. To develop images of the protein bands, the membrane was then placed between two acetate sheets in a dark room and exposed to Fugi X-ray films for 3-10 mins. The X-ray film was added to developer solution until bands became visible and transferred to H_2O to stop development and finally to fixing solution before being washed and dried.

After chemiluminescence detection, the immunoblot was washed 3 x 15 mins in 1X TBS. It was incubated in Stripping Buffer (Pierce) and agitated for 15 mins at room temperature. The membrane was then re-blocked and immunostained with rabbit anti-β-actin primary antibody (Abcam) and goat anti-rabbit secondary antibody as described above. The β-actin loading control was then exposed and visualised as described. Protein band intensities were quantified by scanning with Epson Stylus CX3200 and analysed using *ImageJ* software.

A16: Calculations for sample preparation for target Sense and Anti-Sense siRNA strands

Injection solution for Claudin 5 protein siRNA Assay

Agent: Lipofectamin 2000 complexed with siRNA. 20 pMol of siRNA in each well
Final total cellular RNA extracted 30 ul from three wells.

Time point after siRNA transfection was performed on cell lines (hrs)	Total Cellular RNA Conc (ng/ul) (T)	For injection 804 ng of total RNA (ul) A = (804/T)	Normalized to the 72 hour point, volume of water added to bring conc to 80.4 ng/ul (ul) B = 10- A	Pre Buffered Injection Volume (ul) Vi = (A+B)	PBS 10X required from stock (ul) Vs= Vi Cf/(Cs-Cf)	Final Volume (ul) Vf= Vi+Vs
1	144.1	5.58	4.42	10.00	1.11	11.11
2	114.9	7.00	3.00	10.00	1.11	11.11
12	147.4	5.45	4.55	10.00	1.11	11.11
24	92.2	8.72	1.28	10.00	1.11	11.11
48	110.2	7.30	2.70	10.00	1.11	11.11
72	80.4	10.00	0.00	10.00	1.11	11.11
96	92.3	8.71	1.29	10.00	1.11	11.11

Stock PBS bufffer (Cs) 10 X
Final PBS conc (Cf) 1 X
Final Volume(Vf)
Initial Volume (Vi)
Volume of stock to be added (Vs)
Vf= Vi+Vs

Vs Cs = Vf Cf
as Vf= Vi+Vs
Hence
Vs Cs = (Vi+Vs) Cf
Rearrange for Vs
Vs= Vi Cf/(Cs-Cf)

A17: Experimental protocol: Cantilever assay for targets Sense and Anti-Sense siRNA strands

After the chamber was allowed to reach the temperature set-point, the following injection cycle was executed:

1. Pre-experiment peltier test: 0.7 V for 10 sec ~ 2 °C rise in temperature.
2. Equilibration time till temperature is restabilized in the sensor chamber.
3. Baseline for at least 10 mins.
4. Sample solution in a PCR tube was denatured at 80°C for 4 mins and immediately transferred to an ice bath for 30 seconds followed by immediate injection into the chamber.
5. Injection of sample at 60 µl/min for a total loop-volume of 11.11 µl.
6. Equilibration for at least 30 mins.
7. Buffer wash (800 µl).
8. Equilibration for at least 15 mins.
9. 4 M Urea injection (800 µl; for regeneration as required).
10. Equilibration in 4 M Urea for at least 30 mins.
11. Buffer wash of 1000 µl followed by equilibration for at least 40 mins.
12. Repeat steps 3 to 10 for second sample injection.
13. Post-experiment peltier test: 0.7 V for 10 sec ~ 2 °C rise in temperature.